Force Guided Assembly Under Bias

Peter J. Staritz

CMU-RI-TR-03-17

Submitted in partial fulfillment of the
requirements for the degree of
Doctor of Philosophy in Robotics

The Robotics Institute
Carnegie Mellon University
Pittsburgh, Pennsylvania 15213

05/2003

Abstract

Humans are able to pump gas into a car with little or no difficulty. This task is characterized by two sources of force: that from the nozzle contacting the car and that from the hose attached to the pump. The task succeeds due to the appreciable skill of a human and a forgiveness in the connection. The robotic mating of connectors burdened by forces from sources like the gas hose is beyond the current state of art. The research presented in this dissertation develops technology for robots to mate connectors that concurrently experience appreciable forces from encumbrances, like those from hoses, cables and oscillating masses, in addition to forces from contact.

Effective force guided assembly under the influence of these bias forces, requires the differentiation of contact forces from bias forces, a task that is impossible using traditional sensing configurations.

Emulating the contribution of bias during contact allows the estimation of bias forces and, subsequently, contact forces. By measuring and modeling bias prior to contact, when the only forces on the connector are from bias, a model of the bias source can be made. This model can be used to emulate bias during contact, enabling the differentiation of contact forces and allowing gentle force guided assembly.

This thesis asserts that identification of and compensation for biasing forces will enable the robotic assembly of complex and fragile connectors that would otherwise be impossible.

Acknowledgements

I would like to say thank you to: Jesus, for your grace and for taking my yoke when I could not bear it. ● My wife, for your unfailing love, support and encouragement that have kept me on course and on schedule (mostly). ● My parents, for imparting to me a desire to understand and raising me to believe anything is possible. ● Red, for working me hard, making me think, making me laugh, ticking me off, making me take the reigns, and telling crazy stories. ● Al, for bearing with me in my confusion, helping me out of the confusion and for confusing me. ● Rob, for helping me better understand my problem, making me feel at home very far from home, and for providing the resources that have kept me alive over the last year. ● Chuck, for always keeping your door open and for providing sound advice when I walked through it. ● George, for questioning my most basic assumptions and answering my most fundamental questions. ● Ron, Bill, Mike and Mike, for dealing with the paperwork, answering all my questions, getting the arms to do something useful and getting the matrix algorithms to work. ● The saints at New Hope PCA, for your constant prayers and support ● My friends, for providing something to think about *other* than work ● My daughter, for waking me up at 1 am so that I had the opportunity to solve one of my big problems ● Chris and Bernardine for your invaluable advice on my presentation ● And last but not least, Sarjoun, for helping me understand, acting as a sounding board and acting a dart board!

Table of Contents

List of Figures

Chapter 1

Introduction

1.1 Introduction

Humans are able to pump gas into a car with little or no difficulty. This task is characterized by two sources of force: that from the nozzle contacting the car and that from the hose attached to the pump. The task succeeds due to the appreciable skill of a human and a forgiveness in the connection. The robotic mating of connectors burdened by forces from sources like the gas hose is beyond the current state of art. The research presented in this dissertation develops technology for robots to mate connectors that concurrently experience appreciable forces from encumbrances, like those from hoses, cables and oscillating masses, in addition to forces from contact.

Force guided assembly is the process of mating components using contact forces to determine correct assembly commands. It is the method of choice for

mating components that have high connection tolerances because it enables gentle assembly in the presence of position uncertainty.

This research defines “bias” as the forces acting on a connector stemming from sources other than contact. Forces due to flexure of a hose, tension in a cable or vibration of a flexible part are all examples of bias.

Traditional force guided assembly fails when bias is present. This research, force guided assembly under bias, enables the gentle and accurate assembly of components that are influenced by bias and makes possible the assembly of an expanded set of components critical to future construction tasks. This technology is useful for assemblies in which manipulator force and power are insufficient relative to the challenges of assembly. The approach is never more relevant than in the space environment where high tolerance, fragile connectors that are influenced by bias sources are prevalent.

Figure 1.1 – Artist’s rendition of robotic space facility assembly.

Current space construction relies on astronauts to perform most assembly tasks. Astronauts conduct spacewalks to attach power, fluid and data cables, deploy antennas and solar arrays and activate other sub-systems. This approach is dangerous and expensive.

Robotic construction represents the best alternative to current assembly methods in space. (Figure 1.1) Robots do not require the extensive infrastructure associated with humans, are expendable, and can be designed and optimized to operate in the harsh space environment. Whittaker et al. [29] and Staritz et al. [28] discuss the role of robots in the construction of large scale space facilities. In most cases, robots for these applications will not require expendables like fuel, reducing or eliminating the need for a resupply infrastructure. Though the loss of a robot has both financial and scheduling implications, these are minimal considerations compared to loss of life. Teams of robots can be designed such that they perform the required tasks more quickly, safely and efficiently than their human counterparts.

The realization of a capable robotic workforce for space assembly requires advances in the state of the art. Whittaker et al. [30] discuss technologies that need further advancement before robotic assembly of space facilities can become a reality. Among these technologies are the ability to manipulate gently and perform wiring, plumbing and connecting operations autonomously.

The forces and torques exerted by a robot on construction elements must be minimized. Transporting materials from earth to orbit is an expensive task, thus the mass of the components used to build space facilities is minimized wherever possible. Advances in materials and design are opening the door to new "gossamer" structures. For example, recent studies examining inflatable, rigidizable structures report wall thicknesses on the order of 0.1 mm. [8] These structures are so light and fragile that improper handling during assembly could damage or destroy them.

It was also recognized by Whittaker et al. that wiring, plumbing and connecting operations represent a significant step beyond current assembly capabilities. These operations belong to a class of assembly tasks that incorporate bias. Tethers, cables and fluid lines generate bias by creating an alternative path to

ground. This path allows forces and torques to bypass sensing and corrupts accurate measurement. Bias from flexible attachments is commonly a function of position and orientation of connectors and for the purposes of this research will be relegated to the spatial domain.

Figure 1.2 – The forces and torques from beam oscillation are an example of bias.

Component dynamics like beam oscillation represent another source of bias. In this case, bias forces and torques applied to the connector are a result of component motion as shown in figure 1.2. If the dynamics are independent of connector motion they can be modeled solely in the time domain but if they are dependent they belong to both time and spatial domains.

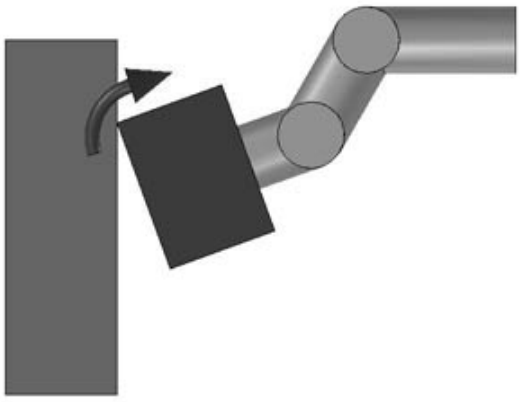

Figure 1.3 – Non-parallel contact between blocks creates a contact torque.

Traditional force guided assembly is commonly performed using a force/torque sensor to determine the forces and torques (hereafter wrenches) applied at a contact point between components. This wrench data provides information about the relative orientation of components, allowing for the determination of motions needed to perform assembly. Consider, for example, placing a block against a plane as shown in figure 1.3.

Non-parallel contact with the plane generates a torque on the block, thus providing data about the relative orientation of the two parts and the direction to turn to achieve flush contact.

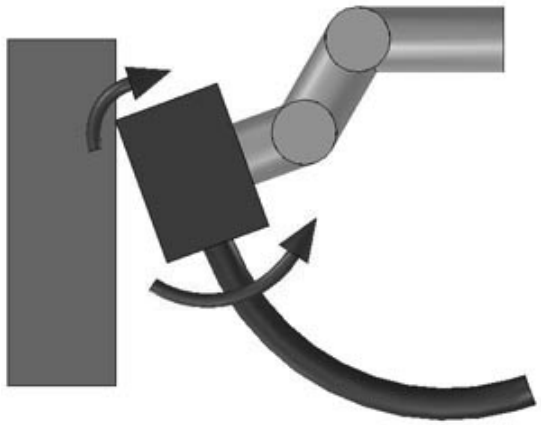

Figure 1.4 – The wrench generated by bias sources (tether) can not be distinguished from contact torques.

This approach works well as long as any other loads applied to a component are constant or vary slowly with time. In cases where the loads applied to components change as a function of position or time, traditional force guided assembly fails because it is unable to resolve contact wrenches from total wrenches sensed. Again consider the block example. The addition of a tether as shown in figure 1.4 corrupts the torque measurement. The force/torque sensor located in the wrist of the robot senses the sum of all torques applied to the block. In the example, the torque from the tether exceeds that from contact, resulting in a positive torque and incorrect motion to complete the assembly.

There are multiple approaches that may enable force guided assembly under bias. The addition of sensors to the component could provide enough data about the bias that assembly would again be possible. However this approach calls for the costly and complicated addition of sensors to each set of connectors and receptacles.

Another approach calls for assembly by robots with multiple manipulators as shown in figure 1.5. In this method the majority of the load is compensated for by one manipulator while the other performs gentle assembly. This approach is particularly useful for highly flexible elements like cables. However, as a bias

source becomes stiffer the ability of the bias compensating manipulator to isolate bias from the assembly manipulator diminishes and the approach becomes less useful.

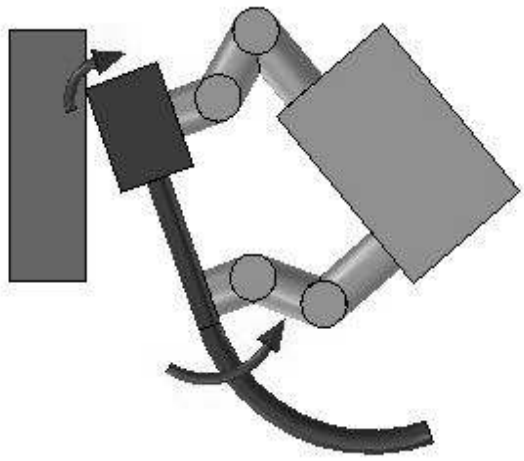

Figure 1.5 – Assembly with multiple manipulators allows the isolation of bias forces.

An alternative approach, advocated here, is the modeling of bias wrenches prior to contact, thus enabling accurate estimation of both bias and contact wrenches during assembly. This approach is implemented in software, thus succeeding with traditional robot configurations and avoiding cost.

This approach is validated by performing force guided assembly of biased connectors. Three separate sources of bias are considered: cables, bending beams and pendulums independent of the spatial domain. Also explored in this work are dependent pendulums which belong to both the spatial and time domains.

1.2 Document Outline

Chapter 2 presents the problem of force guided assembly under bias. Chapters 3 and 4 discuss the methodology and the relationship of this research to past and present work. Chapter 5 introduces the concept of the bias number and its utility and application are explained. An introduction to the experiments conducted in this research follows, outlining the common aspects of each experiment (Chapter 6). In chapters 7 through 11 five experiments are presented that illustrate the value of the approach for the spatial, temporal and spatial-temporal domains. Chapter 12 presents the contributions and conclusions of this research.

Chapter 2

Problem Statement

Force guided assembly requires the detection and interpretation of contact wrenches between connecting components. Force/torque sensors are not capable of differentiating between the wrenches generated by connector contact and the wrenches generated by bias sources because the sensor detects the sum of all applied wrenches. The inability to differentiate between these sources means that contact state can not be accurately known based on wrench data alone when bias is present.

This thesis asserts that identification of and compensation for bias will enable the robotic assembly of complex and fragile connectors that would otherwise be impossible.

Identification is the determination of the parameters and in some cases the state of a physical system. It is assumed that models of systems are known a priori and that only parameters and state are learned during the identification process. Identification is performed using manipulator state data and wrench data from

force/torque sensing; no other sensing is used for identification. In this research, identification occurs during transport, prior to contact, thus wrench data is solely from bias sources.

Bias is defined as any wrench acting on a component that is not a result of contact. Gravity is a common source of bias in many systems. Due to its constant nature, compensating the effects of gravity and other constant field effect forces is usually as simple as subtracting a constant value in the correct frame of reference. Compensating for bias becomes significantly more challenging when it is the result of D'Alembert or spring forces that change as a result of the state of the component.

The importance of dealing with bias depends on the absolute magnitude of the bias and the magnitude of change in bias as a function of time or space. Biases that are smaller in magnitude than the resolution of force/torque sensing are indiscernible and can be ignored for the purposes of this research. However, once these wrenches exceed the sensor resolution the need for bias compensation is based on the change in bias magnitude, connector characteristics, and manipulator capabilities.

If the change in bias magnitude is small, bias can be considered constant and simply subtracted from the data without the creation of a model. If the forces needed to assemble a biased component without bias compensation exceed either manipulator capabilities or connector force limits, compensation is necessary. The magnitude of bias change

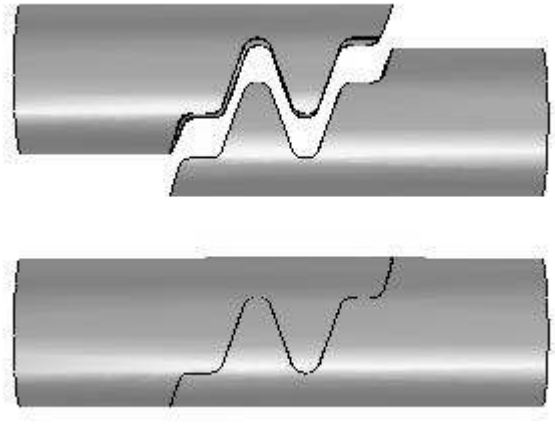

Figure 2.1 –Flush contact of connector and receptacle.

considered in this work is sufficient to ensure assembly failure if bias compensation is not performed.

For the purposes of this research, assembly is defined as the alignment of connector and receptacle such that the entire length of the contact surface is flush with the receptacle surface as shown in figure 2.1. For a connection to be considered a complete assembly the robot must achieve stable contact in the assembled position.

A complex connector is one that requires mating of high tolerance interlocking components, restricting the assembly trajectory by mandating a high accuracy docking path. Prior to assembly the connector components must be sufficiently misaligned to constitute true assembly.

Misalignment is defined as an initial position that requires translation and rotation in each available degree of freedom to achieve assembly. (Figure 2.2) The magnitudes of these offsets are sufficient to prevent accidental contact of connector and receptacle during identification. Also, the misalignment offsets must not exceed the physical constraints of the force assemblable connector as defined in Chapter 6 – Experimental Introduction.

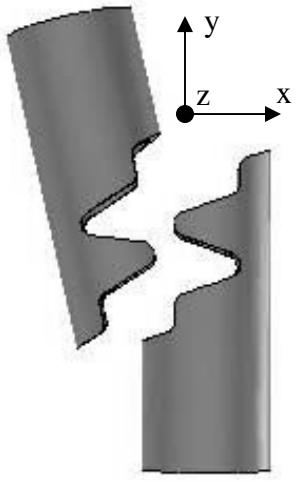

Figure 2.2 – Misalignment is error in both position and orientation.

Fragile indicates that the bias wrenches experienced during contact are the same magnitude as the wrench limits placed on the connectors. Thus a connector may be damaged if the bias wrenches are not compensated.

Chapter 3

Methodology

The methodology of force guided assembly under bias consists of parameter identification and component assembly as shown in figure 3.1. Parameter identification is performed to enable accurate emulation of bias wrenches. During contact these emulated wrenches are subtracted from the sensed wrench

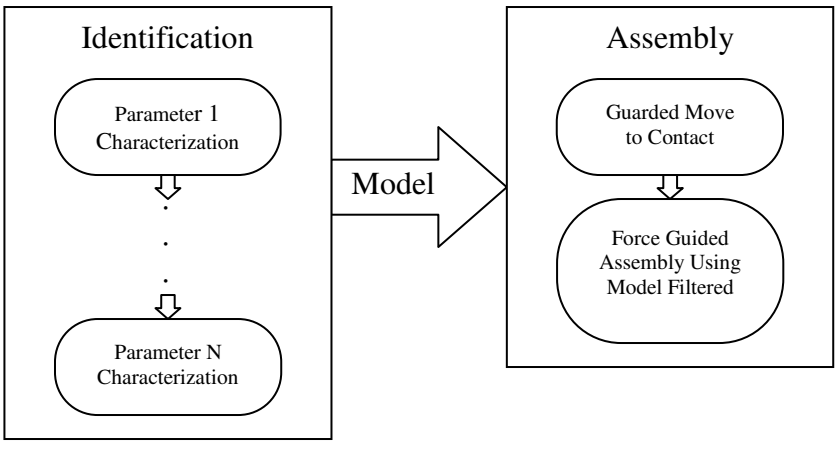

Figure 3.1 - Force Guided Assembly Under Bias Methodology

to estimate the actual contact wrenches. Thus gentle assembly can be performed under bias.

For the purposes of this research assembly refers to the process that begins after a component has been grasped by the manipulator and ends with flush alignment of connector and receptacle. This includes the transport of the component from the grasp point to the assembly point.

3.1 Parameter Identification

It is assumed that the type of payload being identified and assembled is known a priori but that the parameters of that model are not known. These assumptions are consistent with most assembly scenarios in which the class of component being assembled is known but the specific characteristics are not. For example, a database may contain information indicating that a particular component is a beam with a given length and diameter but that same database can not contain accurate parameter information due to parameter dependence on manufacture, deployment and environment.

Identification is performed during transport. The wrenches exerted on the manipulator during transport are due solely to the bias sources because contact has not yet been made. This allows the direct correlation of wrenches to the state of the system. In many cases only small changes in transport trajectories are necessary to perform identification, thus parameter characterization can be performed with little additional transport time. In all cases it is assumed that the models are linear in parameters.

The biases explored in this work are functions of the spatial and/or time domains. Identification of parameters differs for each of these domains and will be treated separately.

3.1.1 Spatial Domain

In the spatial domain bias wrenches correlate directly to the physical location and orientation of the connector. Thus by modifying the transport trajectory to include motions that isolate and modify individual model axes the parameters can be learned. A variety of approaches are sufficient for the identification of the spatial domain model parameters. Chapter 4 – Relation to Previous and Present Work, outlines the possible approaches and the method chosen.

3.1.2 Temporal Domain

Biases in the temporal domain are assumed to be independent of the spatial domain. Thus bias wrenches change only as a function of time and are not influenced by the acceleration of the connector. This is an idealized model because all real systems are influenced by acceleration. However, in the case presented, the magnitude of change is sufficiently small that the temporal domain assumption is valid. When a bias resides solely in the time domain it is unnecessary to modify the transport trajectory. Instead, identification is performed during transport directly to the assembly site.

3.1.3 Temporal-Spatial Domain

Biases in the temporal-spatial domain are a function of time and acceleration of the connector. Identification requires the determination of both model parameters and system state. An adaptive observer provides a provably stable and exponentially convergent approach to simultaneous identification of parameters and state. Fast convergence requires a persistently exciting input that can be superimposed on a transport trajectory. Thus, minimal change to a transport trajectory is necessary for identification in the temporal-spatial domain.

In all three domains, completion of identification is signaled by sufficiently low estimation error and indicates that assembly can begin.

3.2 Emulation and Assembly

During assembly bias wrenches are emulated using the predefined models and identified parameters (and in the Temporal-Spatial Domain: states). These estimated wrenches are subtracted from the wrenches sensed by the robot during assembly. Thus, accurate estimates of contact wrenches can be estimated based on sensor data and model estimates.

Chapter 4

Relation to Previous and Present Work

This research is motivated by the need for autonomous robotic assembly of large space structures. (Whittaker et. al. [29]) Whittaker advocates the use of attached mobile manipulators, robots that locomote and work on the structures they are building. This approach requires the use of the structure under assembly as a reaction platform. In the case of fragile or gossamer structures the ability to gently locomote and assemble is enabling. Whittaker et al. [31] also address the need for assembly of flexible elements like cables, tethers and hoses. Technology capable of assembling such elements is beyond prior state of art.

4.1 Force Guided Assembly

The gentle assembly of complex or high tolerance components requires the feedback of force information. The body of literature regarding force guided assembly is extensive, covering a variety of approaches that can be divided into

three general groups: search patterns, geometric interpretation and compliant motion.

4.1.1 Search Patterns

The combination of force sensing and search patterns enables the detection of changes in contact state as the pattern is performed. Such approaches systematically progress through various search patterns based on changes in contact state until all of the contact criteria are fulfilled.

By implementing virtual control points and a set of virtual springs (Figure 4.1) Newman et al. [22] realize a search pattern for transmission assembly that exploits force data. In this work a complicated set of components are mated while minimizing the forces and torques applied. Virtual control points are established and connected to the end-effector by virtual springs. By moving the virtual control points through a search pattern the manipulator is guided over the mating surface but remains subject to force constraints. When the components align properly the physical constraints are removed and the components are mated with minimal force.

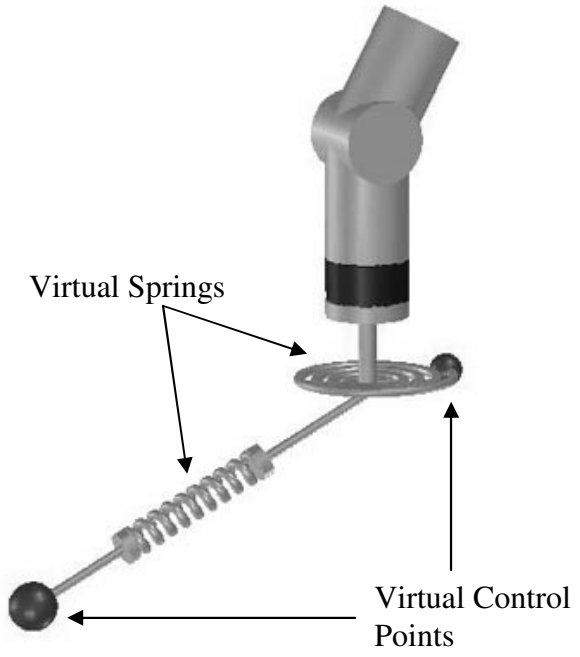

Figure 4.1 – Newman et al. implemented a search pattern using virtual control points and springs.

An alternative search pattern approach develops a set of trajectory and sensorimotor primitives to realize the assembly of complicated wire connectors.

(Morrow et al. [20]) This research focuses on the development of sense/act primitives that can be concatenated to generate useful skills. A search skill is combined with a sticking move primitive, enabling a simple search pattern with variable resolution. This relatively simple approach provides a robust method for the connection of complicated components, in this case a connector without a cable attached.

Both of these approaches rely on force guided search patterns to realize assembly. This method has proven effective for a variety of connectors and components but is most useful for connectors that do not generate useful force data when in contact. For example, the forces generated by a peg in contact with a plane reveal nothing about the location of the hole. As a result a search pattern is implemented to determine the location.

The forces generated by the connectors advocated in this research provide useful information about relative orientation if contact is established within specified error bounds. This characteristic allows the use of other forms of force guided assembly. Although the search pattern approach could be effectively applied to this research, relatively slow performance motivates an alternative solution.

4.1.2 Geometric Interpretation

The geometric interpretation approach utilizes force feedback to infer the relative orientation of connecting components in a manner similar to how a human performs assembly. This method increases reliability and can significantly decrease the time needed to complete the assembly task.

For example, by combining a search pattern with the ability to interpret the geometric meaning of force data Newman et al. [23] perform peg in hole assembly faster and more accurately than a simple search pattern. During most of the search pattern, when the peg is in contact with the plane, the information from the force/torque sensor is ambiguous, not providing any information about the location of the hole. However, when the hole is found, the tilted peg is moved laterally across the opening, enabling the detection of the distance between the hole's edges and consequently the location of the center of the hole. (Figure 4.2) Identification of the center of the hole enables the controller to bypass any more searching and move directly to the mating position.

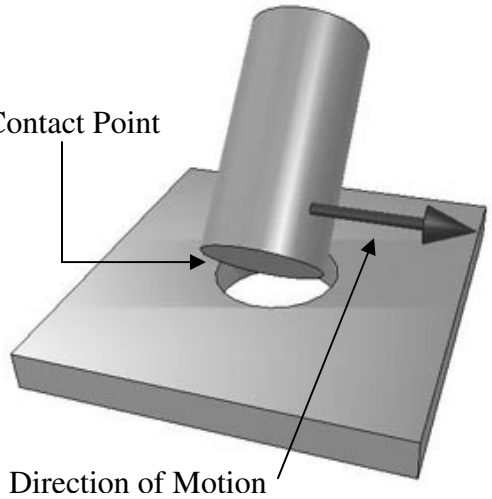

Figure 4.2 – Geometric interpretation of data can significantly reduce assembly time.

Implementing the geometric interpretation strategy with a discrete event framework enables assembly of more complex components. (Austin and McCarragher [4]) In this work each state is given a desired event to move it to the next state. The desired events are chosen such that the system constantly moves toward the goal state. For example, in one experiment a peg is brought into contact with a plane. Based on this contact state the approach calls for lateral motion until an opposing resistance is encountered. (Figure 4.3) This triggers another state and another set of motions and goals. In this way it is possible to extend the geometric approach to more complicated connectors.

Unfortunately, this method requires significant knowledge of the geometry of the connectors and relies on the enumeration of all possible contact configurations,

resulting in a complicated model of the connection process. This complexity limits the applicability of the approach for connectors with intricate shapes.

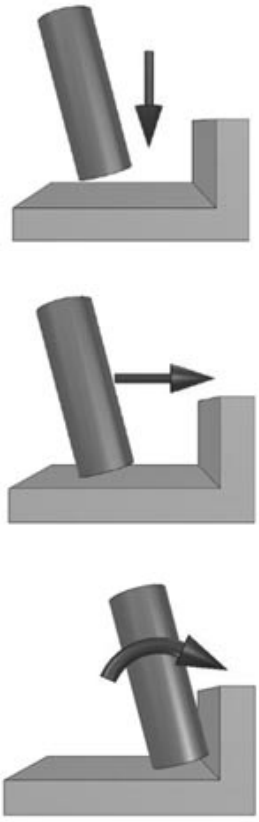

Figure 4.3 – Geometric Interpretation with a discrete event framework.

4.1.3 Compliant Motion

The final approach presented here for force guided assembly is that of compliant motion. In this approach a goal configuration is established but is subject to the constraints of force and torque. Thus if the goal state is beyond a rigid surface, the manipulator will attempt to reach the state while complying to the contact wrenches.

The correct design of manipulator admittance enables force guided assembly. (Schimmels and Peshkin [26]) In this research the authors discuss the concept of "force-assemblability". A system is said to be force-assemblable if "a single nominal velocity in conjunction with a single mapping of forces to motions … can guarantee the proper assembly of a given [connector] pair." Although this approach places significant constraints on the design of the connectors, it simplifies the control algorithms needed for assembly. The authors go on to show that, in the absence of friction, all deterministic connectors are force-assemblable. A deterministic connector is one that is constrained by N independent wrenches when mated, where N is the number of degrees of freedom of the workspace.

Adaptive accommodation control, in which the accommodation of the manipulator is modified based on the contact state, is introduced by Kang et al. [9]. The correct accommodation is achieved by modeling the assembly operation as a

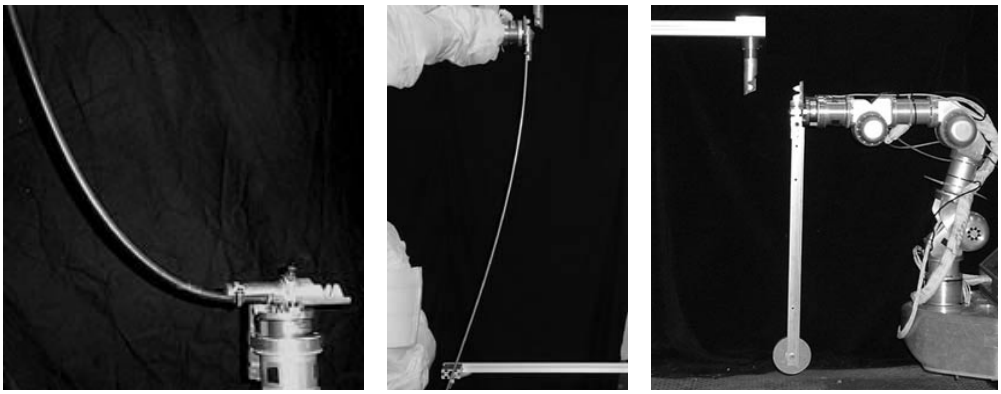

a. b. c.

Figure 4.4 – a) Cable under flexure and elongation b) Beam under bending c) Swinging pendulum

convex optimization problem. In this approach the contact forces, target location and target orientation are used to determine the correct accommodation law. This approach enables the assembly of components not addressed by Schimmels and Peshkin but adds complexity to the controller and does not represent a significant advantage over Schimmels and Peshkin for this dissertation.

Selection of a force guidance approach is based on the complexity of implementation, applicability of capabilities to the research and the anticipated speed of assembly. Based on these criteria Schimmels and Peshkin's approach serves as the basis for the work in this thesis.

4.2 Bias Source Modeling

The accurate modeling of bias sources to generate wrench estimates is critical to this research. It is necessary to emulate the wrenches generated by a given bias source as a function of changes in the spatial domain and/or time domain. For the purposes of this research three bias sources are emulated: a cable under

flexure and elongation, a beam under bending and a swinging pendulum. (Figure 4.4)

4.2.1 Cable Models

The dynamics of low tension tethers are modeled by Buckham and Nahon [5] using a lumped mass approach to emulate the motion of the umbilical of unmanned underwater vehicles. The cable is discretized and the forces on each element are calculated. Tension, internal damping, drag, buoyancy, gravity and internal bending forces are all modeled with the intention of predicting cable response to vehicle motion. Tests of the model under static conditions are conducted and errors of as little as 4% are reported.

Although a simpler cable model was sought, no literature could be found regarding spatial domain bending. Buckham and Nahon's model could be modified to reflect the less complicated case presented in this work. However, a simpler approach that does not require iterative calculation is implemented.

4.2.2 Beam Bending

Spatial domain beam bending is modeled in most elementary mechanics of solids texts using a continuous beam formulation. (Lardner and Archer [12]) Beam dimensions, modulus of elasticity, moment of inertia and end constraints relate the displacement and the associated wrench. This work is directly applicable to the modeling task addressed in this research.

4.2.3 Harmonic Motion

The modeling of the dynamics of pendulums with fixed attachment points using a time domain approach can be found in most introductory dynamics texts. Riley

and Sturges [25] provide a complete description of the modeling of a pendulum. Parameters include period of oscillation, amplitude, damping constant and phase shift. An introduction to harmonic motion and the equations that dictate damped oscillation can be found in Rao's [24] text on mechanical vibrations. These models are examined and implemented in this work.

The modeling of pendulums with movable attachment points using a dynamic model is significantly more complicated. Elmer [6] provides the equation of motion of a damped pendulum for which the attachment point may be accelerated in both x and y directions. Parameters include the damping constant, the masses of the attachment point and pendulum bob and the length of the pendulum arm. The state of the system must also be identified. The equations of motion for the connector and the pendulum bob are derived and implemented in this work.

4.3 Contact Sensing

This research will draw on previous work in transitioning from free motion to contact. Will and Grossman [34], Kazanzides et al. [10], Morrow et al. [20] and Newman et al. [22] utilize the guarded motion approach in which contact is detected by slowly moving along a vector until a force threshold is met. This approach provides accurate data regarding surface position given force readings are reliable. Utilizing this approach in an environment where spurious force signals are present jeopardizes accuracy. Despite the potential for false transition, the approach is adopted due to the simplicity of implementation.

4.4 Parameter Identification

There are many methods for identification of unknown parameters that would be sufficient for this research. The literature regarding machine learning and

adaptive approaches is voluminous. For an introduction to these fields refer to Mitchell's [19] overview of machine learning and Narendra and Annaswamy's [21] overview of adaptive systems.

For the purposes of payload parameter and state identification it is assumed that the wrenches exerted by the payload on the manipulator are available and that manipulator joint commands and responses are known. Identification for the spatial, temporal and spatial-temporal domains are addressed separately.

4.4.1 Spatial Domain

In the spatial domain it is assumed that the state of the system is entirely described by the position and orientation of the end of the payload. In such cases only the parameters and not the state need to be identified. The identification of parameters is commonly performed using a least squares approach.

Marquardt [16] presents an approach for switching between the steepest decent method and the inverse Hessian method for nonlinear least squares fitting. Using this approach the least squares algorithm will aggressively descend when far from the minima but will use the inverse Hessian method when in close proximity. Åström and Wittenmark [3] present the recursive least squares approach to parameter identification. For the spatial domain cases presented in this research both recursive least squares and batch least squares are utilized.

4.4.2 Temporal Domain

In the temporal domain bias behavior is independent of component motion. In this case it is assumed that the state of the system is well described by

undamped harmonic oscillation. The identification of parameters is commonly performed by direct calculation.

4.4.3 Spatial / Temporal Domain

This research also explores the potential for bias compensation of dependant dynamic systems. This portion of the work embarks from prior research in adaptive control. By establishing physical models of dynamic elements an adaptive observer can be created to identify both the parameters and the state of the element.

Luders and Narendra [13] present an adaptive observer that only requires a system's input and output signals. In this approach the authors design a model reference adaptive observer using Lyapunov's direct method. Thus it can be shown that the adaptive observer is globally stable and asymptotic convergence can be guaranteed. By creating an observer that does not require internal state data the authors have opened the door to real world application. This work is applicable to single input single output systems.

Kreisselmeier [11] presents a parameterized adaptive observer that is provably exponentially convergent. The author adopts the parameterized representation of the adaptive observer, an alternative but equivalent representation of the Luenberger observer [15]. This approach allows the separation of adaptation and observation and enables the independent formulation of adaptive schemes. The author exploits this freedom to demonstrate three separate adaptive schemes that are exponentially convergent. The results presented are applicable to single input single output systems.

Based on Kreisselmeier's approach Luders and Narendra [14] formulate a simpler adaptive observer that can be expanded to the multi-input multi-output case. In this work the authors present a new canonical form for the plant which

does not require the feedback of auxiliary signals to ensure convergence. Again the authors show that the observer is globally asymptotically convergent.

In Narendra and Annaswamy's [21] text, *Stable Adaptive Systems*, this approach is abandoned in favor of another parameterization. The preferred parameterization's output is a linear combination of 2n accessible signals, where n is the number of states of the system. Anderson [1] shows that this non-minimal representation of the adaptive observer can be applied to multi-input multi-output systems and that the system is globally asymptotically convergent.

Inoue et al. [7] also make use of the parameterized representation of the adaptive observer. The authors propose a method for designing multi-input multi-output adaptive observers with an exponential rate of convergence. By augmenting the filtered signals rather than the order of the plant the authors avoid direct interactions between plant outputs. This approach enables the application of single-output adaptive observer schemes to multi-output systems.

Figure 4.5 – Three degrees of freedom associated with planar pendulums.

Although this approach shows promise, in theory its application to multi-input multi-output systems is computationally prohibitive. Implementation of this approach on a 2 input 2 output system requires the integration of hundreds of intermediate signals. For this reason the application of this approach is not explored in this work.

The identification of the parameters and state of many dynamic elements, a pendulum in the planar case for example, requires the consideration of multiple degrees of freedom. (Figure 4.5) This work considers a fourth order, single-input single-output, dynamic system which can be approximated as two masses connected by a spring and damper. The identification of this system will rest on the work of Luders and Narendra which has been shown to be simple to implement.

4.5 Manipulator Control

The realization of fast and precise manipulator motion for transport and assembly tasks requires the creation of stable controllers robust to dynamic perturbations. Slotine and Li [27] present an approach to adaptive control of robot manipulators. The nonlinear nature of manipulators complicates the generation of provably stable systems. The authors show that the algorithms developed result in a globally convergent adaptive controller and demonstrate its performance on a simple two link direct drive manipulator. Performance under perturbation from unmodeled dynamics is comparable to that of a standard proportional-derivative controller but trajectory tracking is significantly better than either the proportional-derivative controller or a computed torque approach.

Although this approach works well, its applicability to manipulation for assembly is limited. The control of a manipulator conducting force sensitive assembly of rigid components is not trivial. The accurate application of wrenches and the precision tracking of a trajectory are mutually exclusive for many control techniques.

Arimoto et al. [2] propose a model based adaptive controller for simultaneous force and trajectory tracking. In this approach the authors introduce the concept of joint space orthogonalization. This design method exploits the fact that the nominal reference signal is composed of two orthogonal signals, that associated

with position trajectory tracking and that associated with force tracking. This orthogonality is a result of the physical constraints of the system in which the force vector from contact is normal to the surface but the tracking error is tangent to the surface. This approach allows the formulation of provably stable controllers with asymptotically decreasing trajectory and force errors. Whitcomb et al. [32] and [33] validate the joint space orthogonalization approach. This work compares the inverse dynamics critically damped force adaptive approach to the proportional derivative force controller. The results show that the adaptive approach is not only provably stable but delivers superior performance regardless of the proportional-derivative controller's gain.

It was anticipated that an approach similar to that presented by Arimoto et al. and validated by Whitcomb et al. would be used to perform manipulator control during the assembly process. Such an approach could be implemented over many experiments and would allow an incremental increase in performance over time until the parameters of the system had converged. However, the bandwidth and performance of the manipulators and force/torque sensors available for this work were insufficient to warrant the implementation of such an approach.

4.6 Manipulation of Flexible Objects

The accurate manipulation of flexible objects requires the ability to emulate forces as a function of time and/or space. Several researchers have examined the manipulation of flexible objects with the intent of performing assembly.

Zheng et al. [36] present a set of strategies for the insertion of flexible beams into holes. The researchers manipulate a thin beam into a hole under the effects of gravity. The resulting flexure is identified using visual sensing and the trajectory for insertion is modified depending on assembly tolerances. The researchers do not implement force guidance for these experiments, instead relying on the implied lack of force during smooth assembly.

Yukawa et al. [35] posed the problem of grasping a moving flexible object and damping its motion. In this work the authors develop a dynamic representation of the flexible object and use a visual sensing system to identify its state.

The visual sensing of flexible objects is a convenient way to emulate payload configuration and resultant forces. The visual sensing approach may be used in conjunction with the method proposed in this dissertation. However, the addition of computationally expensive sensing adds complexity to the overall system and is not necessary. Thus the visual sensing approach is not used in this work.

Meitinger and Pfeiffer [18] present the insertion of pistons with O-rings into cylinders. (Figure 4.6) The flexible nature of the O-rings generates complex non-linear forces during assembly. The authors model the force generated by the rings a priori, assuming that similar rings will have similar characteristics. During the assembly process only the rings are in contact with the cylinder so the model alone is sufficient to predict the forces encountered. Using the model developed, the authors perform insertion experiments and verify the utility of contact state prediction based on force data.

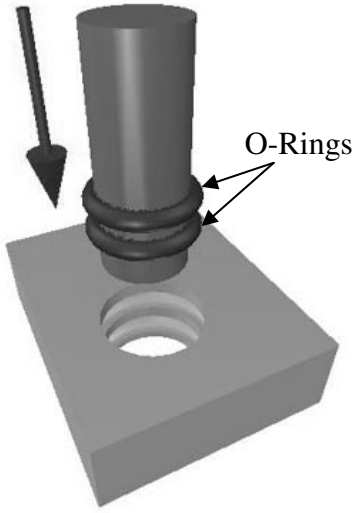

Figure 4.6 – Insertion of piston with flexible O-rings into hole.

Meitinger and Pfeiffer's research utilizes an approach similar to that presented in this thesis. By modeling the forces generated by flexible objects the anticipated forces will be predicted and used for accurate assembly of components.

However, their work is fundamentally different in that it does not address multiple sources of force, the concept of bias.

4.7 Summary

The research presented in this section is a brief introduction to the many facets of this thesis. This dissertation incorporates lessons and techniques from force guided assembly, bias source modeling, contact identification, parameter identification, manipulator control and manipulation of flexible objects. In force guided assembly a compliant assembly approach has been adopted to minimize assembly time and implementation complexity. Bias source modeling and identification for spatial domain cases is founded upon simplified physical models and a least squares approach. In the dependant dynamic case an adaptive observer that is provably globally asymptotically stable is the starting point. Manipulator control relies on fundamental lessons from proportional-derivative control due to the limitations of the experimental setup. Finally, this dissertation looks to the approach advocated by Meitinger and Pfeiffer as the most closely related research to date.

Each of the areas examined represent a critical aspect of this body of work but each is related only tangentially. There is little prior work directly related to the assembly of components under any type of bias, whether from multiple paths to ground or dynamic effects.

Chapter 5

Bias Number

Biased assemblies can be characterized by a dimensionless value called the Bias Number. This number, created in this research, has three formulations. In one formulation, the number provides a quantitative test to determine if bias compensation is necessary. In another, it enables calculation of the minimum force required for accurate assembly. In a third and final formulation, it provides an estimate of the force necessary to realize unambiguous assembly without bias compensation. Fundamental to this approach is the assumption that contact can occur at multiple locations on a connector and that connector motion is a function of the contact location.

The bias number and associated formulations are applied throughout this research (where applicable) to illustrate the need for bias compensation. The bias number is calculated for each of the experiments presented and in each case indicates the need for bias compensation. The two alternative formulations mentioned above are used to illustrate the effects of bias compensation on the "gentleness" of assembly.

The formulation of bias number presented in this chapter is applicable to planar problems. This formulation may be applied to three dimensional connectors if they can be represented as combinations of the planar case. This is described in more detail in section 5.4 of this chapter. More complicated connectors may require the formulation of the bias number for the general, three dimensional, case.

5.1 Formulation of Bias Number

The formulation of the bias number begins with the relationship between force and torque. Equation 1 shows that torque is the product of force multiplied by distance.

$$\tau = F \cdot d \qquad \text{Eq. 1}$$

This equation can be applied to the contact between connectors during force guided assembly. The force/torque sensor provides both force and torque data thus by rearranging equation 1 the distance to the contact point can be determined. Once the point of contact is known the corresponding control commands can be issued.

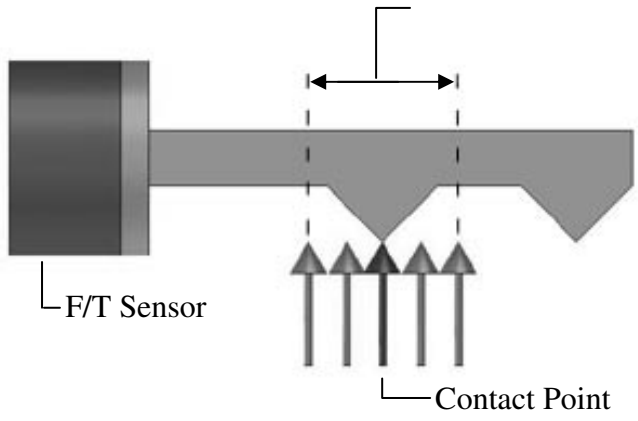

Figure 5.1 – Uncertainty of contact location due to sensor noise.

In the presence of noise, fluctuations in force and torque measurements modify the distance estimate. Figure 5.1 illustrates the uncertainty in the location of the contact point as a result of sensor noise.

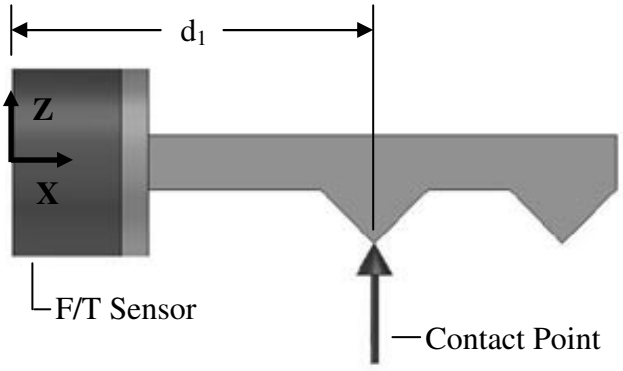

Figure 5.2 – A simple connector experiences contact at a distance d_1 from the sensor origin.

Consider the example shown in figure 5.2. A simple connector contacts the receptacle at a distance d1 from the sensor. Measurement noise in both force and torque result in a distance estimate, d_{est}, described by equation 2. In this equation it is assumed that the force and torque errors may be either positive or negative but to simplify understanding all equations will be derived based on the positive case.

$$d_{est} = d_1 + d_{er} = \frac{\tau + \tau_{er}}{F + F_{er}} \qquad \text{Eq.2}$$

Solving for d_{er}:

$$d_{er} = d_{est} - d_1 = \frac{\tau + \tau_{er}}{F + F_{er}} - \frac{\tau}{F} \qquad \text{Eq.3}$$

and after simplification:

$$d_{er+} = \frac{\tau_{er} - F_{er} \cdot d_1}{F + F_{er}} \qquad \text{Eq.4}$$

Where the + in d_{er+} will be explained shortly.

Examining the numerator of equation 4, it is clear that increasing τ_{er} or decreasing d_1F_{er} results in an increase in the distance error. The negative sign indicates that errors of opposing sign generate distance errors in the same direction. Thus it is possible that in some cases the respective errors may partially or totally cancel each other. In the denominator, the presence of F_{er} means that the largest distance error is encountered when the force error is negative and the torque error is positive. Also worth noting is that by increasing F, the magnitude of the distance error can be reduced.

The presence of force error in the denominator means that d_{er} is not symmetric and error in the negative direction is not equivalent to negative d_{er}. If the largest distance error is obtained when τ_{er} is positive and F_{er} is negative then, based on the presence of the negative sign in the numerator, the other extreme must occur when τ_{er} is negative and F_{er} is positive. This yields equation 5 that describes the negative error associated with a point.

$$d_{er-} = \frac{-\tau_{er} + F_{er} \cdot d_1}{F - F_{er}} \qquad \text{Eq.5}$$

Consequently d_{est} falls in the range described by equation 6.

$$d_1 + d_{er+} \le d_{est} \le d_1 + d_{er-} \qquad \text{Eq.6}$$

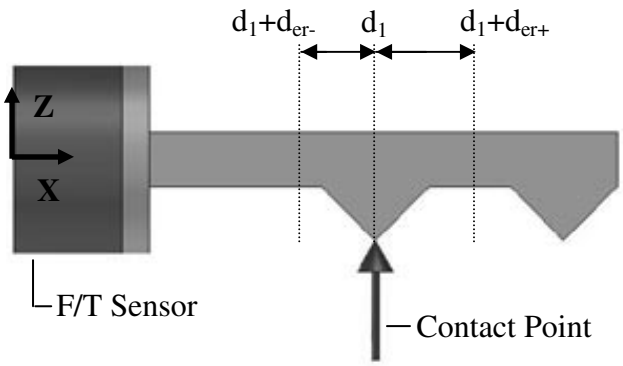

Figure 5.3 – Non-symmetric error bounds from sensor noise.

This non-symmetric error bound is illustrated in figure 5.3.

As the magnitude of the distance error on each of the contact points grows, the distance between them decreases until they overlap as shown in figure 5.4. When the errors overlap it is no longer possible to ensure correct motion based on a contact wrench. It is this indeterminacy that the bias number helps diagnose and eliminate.

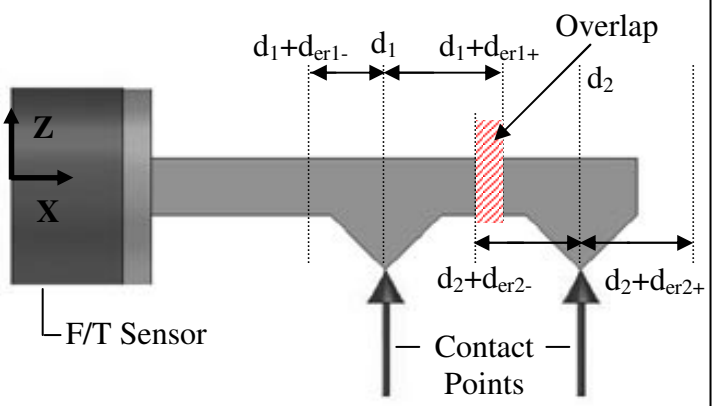

Figure 5.4 – As error magnitudes increases adjacent contact regions overlap.

Figure 5.4 shows two contact points located distances d_1 and d_2 from the force torque sensor. The distance estimate errors for these points will overlap when:

$$d_2 + d_{er2-} = d_1 + d_{er+} \qquad \text{Eq. 7}$$

Substituting equations 4 and 5 into 7 and solving for force (Appendix 1) yields equation 8.

$$F = \frac{\tau_{er} - F_{er} \cdot d_{sc}}{d_{cd}} \qquad \text{Eq. 8}$$

Where the distance from the sensor frame to the contact center, d_{sc}, is the average of d_1 and d_2 and d_{cd}, the center distance, is half the distance between d_1 and d_2. Thus, given constant values of τ_{er} and F_{er} the force at which overlap occurs can be determined.

Substituting equation 8 into equation 4 yields equation 9.

$$d_{er1+} = \frac{\tau_{er} - F_{er} \cdot d_1}{\frac{\tau_{er} - F_{er} \cdot d_{sc}}{d_{cd}} + F_{er}} = \frac{d_{cd}(\tau_{er} - F_{er} \cdot d_1)}{\tau_{er} - F_{er} \cdot d_{sd} + F_{er} \cdot d_{cd}} = d_{cd} \qquad \text{Eq. 9}$$

Thus, despite the lack of symmetry in the error equation, the intersection of the distance errors occurs at the midpoint between the contacts. In order to avoid the overlap of the error bars d_{er} must be less than d_{cd}.

Thus:

$$d_{er} < d_{cd}$$

$$d_{er} = \frac{\tau_{er} - F_{er} \cdot d_1}{F + F_{er}} \quad \text{and}$$

$$d_{sc} = \frac{d_1 + d_2}{2} = d_1 + d_{cd}$$

then,

$$\tau_{er} < F \cdot d_{cd} + F_{er} \cdot d_{sc} \quad \text{Eq. 10}$$

$$\tau_{er} - F_{er} \cdot d_{sc} < F \cdot d_{cd} \quad \text{Eq. 11}$$

or,

$$\frac{\tau_{er} - F_{er} \cdot d_{sc}}{F \cdot d_{cd}} < 1 \quad \text{Eq. 12}$$

Which leads to the Bias Number, B:

$$B = \frac{\tau_{er} - F_{er} \cdot d_{sc}}{F \cdot d_{cd}} \quad \text{Eq. 13}$$

Equation 13 provides a simple and effective way to evaluate the significance of bias on a system. Values of B greater than or equal to 1 indicate that a system is not assemblable given the torque error, force error, distance from center and distance from sensor. Values of B less than one can be assembled with increasing accuracy as B approaches zero. To illustrate the utility of the bias number an example is provided from each of the formulations.

Example 1 – Determining the Need for Bias Compensation

During uncompensated assembly, the bias wrench effectively acts as noise in the system. Thus the need for bias compensation can be determined by calculating the value of equation 13 given τ_{er} and F_{er} are the anticipated change in torque and force over the workspace. A hypothetical bias source experiences a $\Delta\tau_{er}$ of 3 Nm and ΔF_{er} of -1 N over its workspace. The connector used for the experiments described later has a center distance d_{cd} of 0.015m and should not

be subjected to forces in excess of 100 N. (Alternatively the capabilities of the robot may limit the maximum applicable force.) The distance from the center point to the force/torque sensor is 0.05m.

Thus:

$$\tau_{er} = 3N \cdot m \qquad F_{er} = -1N$$

$$d_{cd} = 0.015m \qquad d_{sc} = 0.05m$$

$$F_{\max} = 100N$$

$$B = \frac{3N \cdot m + 1N \cdot 0.05m}{100N \cdot 0.015m} = 2.333$$

The bias number is greater than unity and therefore the system requires some type of bias compensation in order to be assembled under the given constraints.

Example 2 – Determining the Compensated Minimum Necessary Force

During assembly under bias compensation, noise is the sum of sensor error and estimation error. By solving equation 13 for F, allowing τ_{er} and F_{er} to represent the maximum expected noise, setting d_{cd} and d_{sc} equal to the physical constraints of the system and setting the bias number to one, the minimum force that must be applied to ensure that an unambiguous signal is obtained from the contact can be computed.

$$\tau_{er} = 0.20N \cdot m \qquad F_{er} = -0.50N$$

$$d_{cd} = 0.015m \qquad d_{sc} = 0.05m$$

$$B = 1.0$$

$$F = \frac{\tau_{er} - F_{er} \cdot d_{sc}}{B \cdot d_{cd}} \qquad \text{Eq. 14}$$

$$F = \frac{0.20N \cdot m + 0.50N \cdot 0.05m}{0.015} = 15N$$

Example 3 – Determining Uncompensated Minimum Necessary Force

During assembly of biased elements without bias compensation the whole bias acts as noise as described in example 1. A small modification of the above examples yields an estimate of the minimum force needed to perform unambiguous assembly under uncompensated bias. Using equation 14 the minimum necessary force for uncompensated assembly can be determined.

$$F = \frac{3N \cdot m + 1N \cdot 0.05m}{0.015m} = 203.33N$$

Thus a minimum force of 203.33 N is needed to unambiguously assemble the hypothetical system when the bias is uncompensated. This value is particularly useful when defining the concept of 'gentle' assembly, discussed in Chapter 6 – Experimental Introduction.

5.2 Interpretation of the Bias Number

In the interpretation of the bias number the significance of unity has been discussed, the meaning of values less than one will now be explored. Equation 13 shows that given constant force and torque error the bias number asymptotically approaches zero as the applied force increases. Alternatively, as the value of the bias number approaches zero the distance error decreases.

As the error bars decrease it is possible to insert additional resolvable contact points into the range, as shown in figure 5.5. Thus, lower values of B equate to increasing accuracy and the opportunity to add resolvable contact points. In the general case the presence of the term $F_{er} \cdot d_{sc}$ in the denominator of equation 13 prevents the formulation of a direct relationship between values of B and the number of resolvable contact points, P_{rc}. This is in contrast to the degenerate case where d_{sc} approaches zero and the correlation between B and the number of resolvable contact points is well defined.

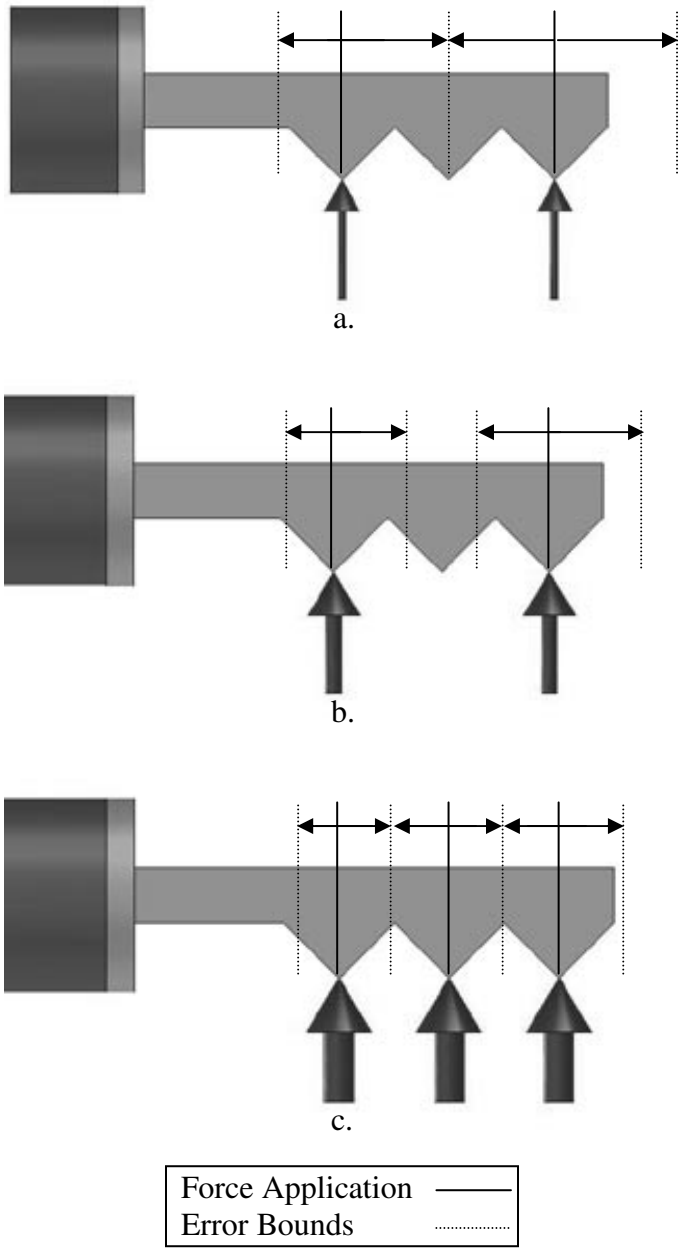

Figure 5.5 – Increasing the forces applied to a connector reduces the error bounds until an additional resolvable contact point can be added.

In the degenerate case ($d_2 \rightarrow 0$) when resolvable contact points are distributed symmetrically (or nearly so) about the center of a force/torque sensor the distance d_{sc} equals zero. However, any additional intersection points still have non-zero sensor to center

distance values as shown in figure 5.6. In a small range around the zero point the values of intersections can be approximated as zero, allowing for a simplification of the bias equation and subsequent interpretation.

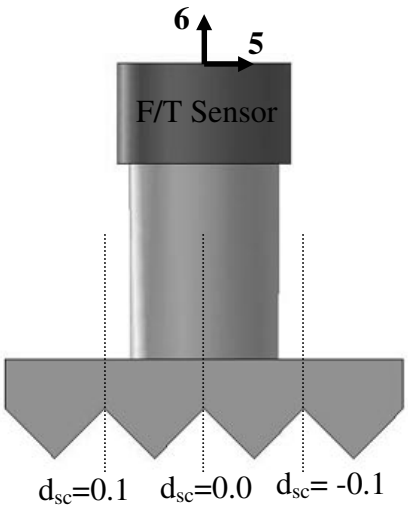

Figure 5.6 – The sensor to center distance equals zero when the connector and sensor are aligned.

In such configurations the bias number can be approximated as:

$$B = \frac{\tau_{er}}{F \cdot d_{cd}} \qquad \text{Eq. 15}$$

Unlike the general case, where the width of resolvable contact points changes with distance from the sensor centerline, the resolvable contact points in the degenerate case are assumed to be of equal width. Thus, the number of resolvable contact points is a function of the bias number as shown in equation 16.

$$P_{rc} = \left\lfloor \left(\frac{1}{B} \right) + 1 \right\rfloor \qquad \text{Eq. 16}$$

where $\lfloor\ \rfloor$ indicates rounding down. Resolvable contact points are evenly distributed over the contact range, thus the distance between resolvable points can be determined using equation 17.

$$d_{rp} = \frac{2 \cdot d_{cd}}{P_{rc} - 1} \qquad \text{Eq. 17}$$

Non-integer values of P_{rc} prior to rounding indicate the presence of gaps between the resolvable points. A distance measurement falling within a gap can only be

localized to the gap plus or minus the error magnitude. This value is always less than or equal to the distance between the resolvable points.

Equation 18 enables the calculation of gap width, d_g.

$$d_g = \frac{\left[2 \cdot d_{cd} - \frac{2 \cdot d_{cd} \cdot P_{rc}}{\left(\frac{1}{B}\right)+1} \right]}{P_{rc} - 1} \qquad \text{Eq. 18}$$

Where the left half of the numerator corresponds to the full width between outer resolvable points and the right half of the numerator is the distance occupied by the resolvable points and their error envelopes. The denominator is the number of gaps over which the total gap width is divided.

5.3 Determining Minimum Force

The examples thus far have considered a simple binary controller in which the connector will turn either clockwise or counter-clockwise. With the addition of resolvable points more complicated control schemes can be implemented but the minimum force applied to resolve individual contact points must increase. Figure 5.6 shows a connector with four, evenly spaced contact points, determining F_{min} for this connector is not as simple as finding a bias number less than unity. The approaches for finding the minimum force in the degenerate and general cases are different and will be treated separately.

5.3.1 Degenerate Case

Determining minimum contact force for the degenerate case is relatively simple. Rearranging equation 16 yeilds:

$$B = \left(\frac{1}{P_{rc} - 1} \right)$$ Eq. 19

If the number of contact points desired is four, then the bias number must equal 0.33. Solving equation 15 for F yields equation 20 and the minimum force needed to resolve four contact points.

$$F_{\min} = \frac{\tau_{er}}{B \cdot d_{cd}}$$ Eq. 20

Increasing the force beyond this minimum will generate the gaps referred to previously. In the case where there are discrete contact points a reading equal to a gap indicates contact at both neighboring points. Thus gaps can be used to identify stable contact states and issue commands accordingly. In the continuous contact case these gaps essentially provide twice the number of resolvable contact points. The utility of such points is limited however, given that the sum of their widths is always less than the width of one resolvable point.

5.3.2 General Case

Determining the minimum force for a four point connector in the general case is significantly more complicated than the degenerate case. Resolvable contact points are not evenly spaced due to the term $F_{er} \cdot d_{sc}$. As the value of this term increases the dissimilarity of resolvable contact point widths also increases. Thus, it is possible that in some circumstances the distribution would be so irregular as to make implementation on a connector with evenly spaced contact points impossible. An example of this is shown in figure 5.7.

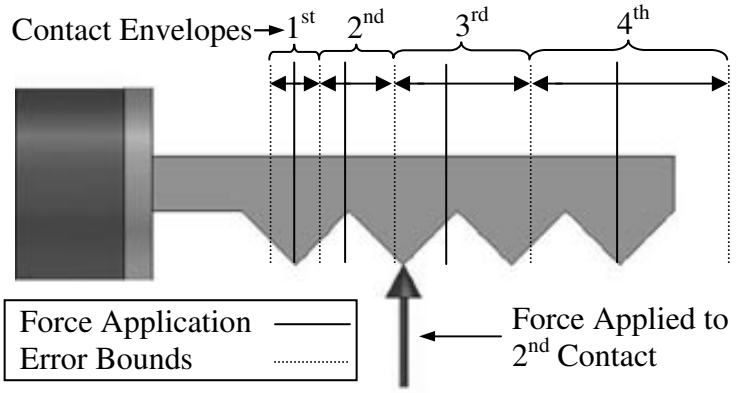

Figure 5.7 $-F_{er} \cdot d_{sc}$ makes the contact envelopes irregular such that the force applied at the 2nd contact registers in the 3rd contact envelope.

Identification of the minimum contact force for the multiple contact, general case is based on equation 8 solved for d_{cd}:

$$d_{cd} = \frac{\tau_{er} - F_{er} \cdot d_{sc}}{F} \qquad \text{Eq. 21}$$

It can be seen that given a distance from the sensor (d_{sc}) and the errors in force and torque, modifying F widens or narrows the center distance. Consider the

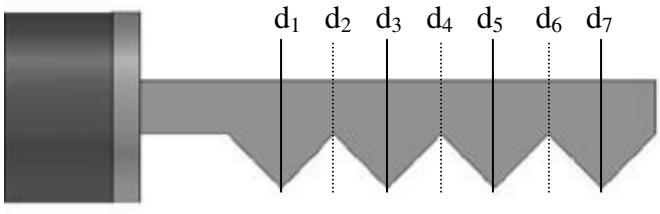

Figure 5.8 – Determining the minimum contact force for a multiple contact general case connector.

illustration in figure 5.8; d_1 is the proximal contact point and d_7 is the distal contact point. The distance between these points is shown in equation 22.

$$d_7 - d_1 = 2 \cdot \left(\frac{\tau_{er} - F_{er} \cdot d_2}{F} \right) + 2 \cdot \left(\frac{\tau_{er} - F_{er} \cdot d_4}{F} \right) + 2 \cdot \left(\frac{\tau_{er} - F_{er} \cdot d_6}{F} \right) \qquad \text{Eq. 22}$$

The minimum contact force, F, is the force at which the sum of all the center distances equals the distance between the proximal and distal contact points. Eliminating the unknown variables yields a 3rd order polynomial in F. One of the roots of this polynomial is the minimum force needed to resolve four contact points.

Unlike other formulations already presented, this approach considers the whole contact range from proximal contact to distal contact. In the previous approach the resulting force is calculated based on half the workspace and assumes symmetry. If this approach had been implemented here the resulting force would have been incorrect because the midpoint of the connector is not the same as the point d_4.

5.4 Non-Orthogonal Contact

This approach has been presented under the assumption that all forces applied to the connector are perpendicular to the connector axis as shown in figure 5.9a. This assumption restricts contact to surfaces parallel with the connector axis and mandates frictionless interaction between connectors. The assumption can be relaxed to allow general contact as long as any given contact force vector only intersects the contact surface once. As

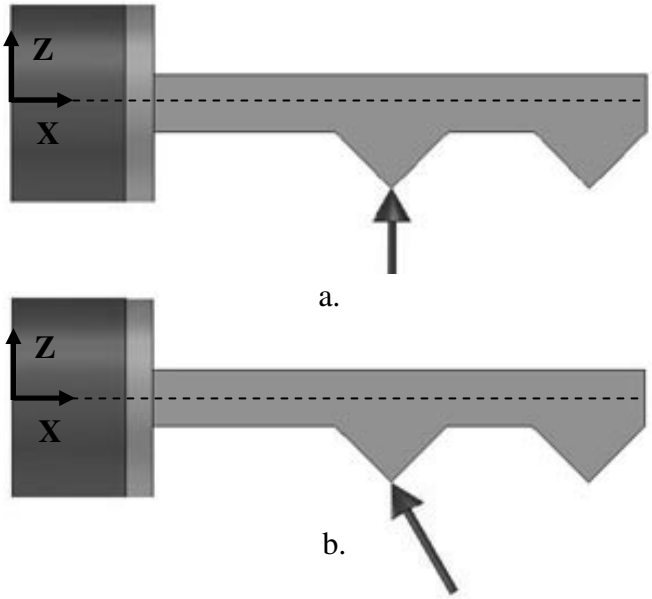

Figure 5.9 – a.) Force vector is perpendicular to connector axis. b.) Force vector is not perpendicular.

shown in figure 5.10, the angle of the vector can be determined by the individual force components. When this information is combined with the distance from the vector to the sensor a force vector can be projected that intersects the surface at the contact point. In such cases the geometry of the connector must be known and the effects of noise on angled vectors must be considered. For example, small changes in the distance, d, shown in the figure 5.10 may result in significant changes in actual contact position. If noise resulted in a slightly larger estimate of d, the contact may be estimated as occurring not on the contact prong but to the right of it on the flat. Thus, noise may result in large changes in contact distance.

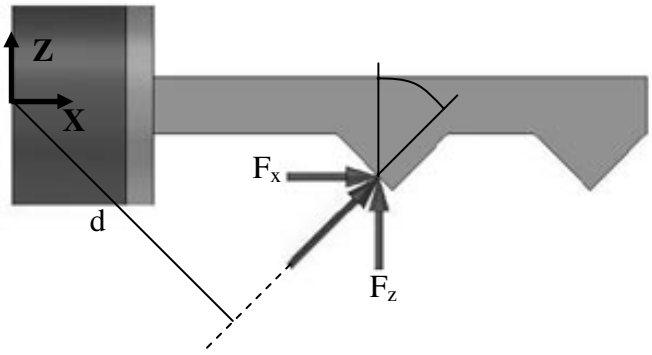

Figure 5.10 – Given the shape of the contact surface, and the angle and distance of the force vector the contact point can be determined.

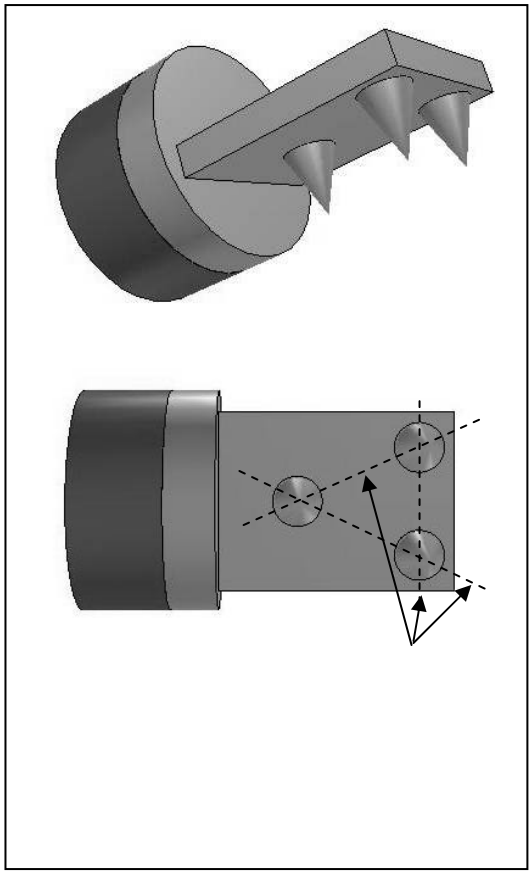

The connector used in this research experiences non-orthogonal contact. The problems associated with such contact are mostly avoided through the implementation of a compliant controller. This controller acquiesces to non-orthogonal forces such that the forces imparted to the connector are approximately orthogonal.

5.5 Application to Three Dimensions

The planar formulation of the bias number may be applied to three dimensional connectors. By applying the number between sets of contact points the bias number and minimum necessary force can be calculated. Consider the connector shown in figure 5.11. Treating each pair of contacts as a separate planar case allows the simple application of the tools developed to the three dimensional case. The values of the bias number and minimum necessary force for the connector are the largest values obtained from the individual planar cases. In many cases these values will correspond to the plane connecting the two closest contact points. In some situations, for example when sensor noise is much larger on one axis than another, the largest values of bias and minimum necessary force will not correspond to the two closest contacts.

Chapter 6

Experimental Introduction

Five experiments are performed to demonstrate the principles and utility of the methodology of this research. These experiments are chosen to illustrate issues in bias compensation pertaining to cables, bending beams and swinging pendulums. In each experiment, force guided assembly is performed under bias while preventing contact wrenches from exceeding maximum force and torque thresholds.

The bias in each experiment is sufficient to prevent assembly by traditional force guided assembly methods. The uncompensated minimum necessary force is greater than the manipulator capabilities and the wrench limits of the connector. Thus, without bias compensation, assembly failure is assured.

6.1 Process

All of the experiments conducted for this research have the same operational process. This process is illustrated in figure 6.1 and explained below.

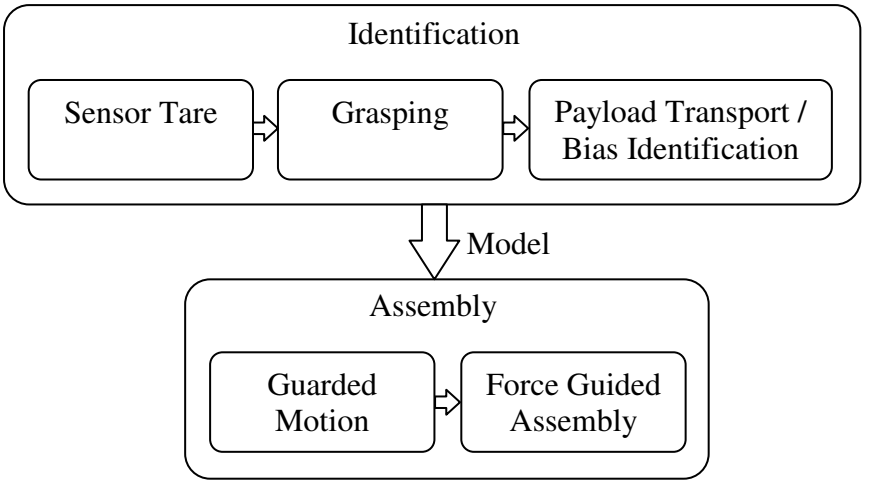

Figure 6.1 – Experimental operational process.

6.1.1 Identification

- *Sensor Tare* - Prior to 'grasping' the payload the force/torque sensor is zeroed to remove the wrenches due to internal stresses in the sensor. This is performed prior to grasping so that the bias wrenches don't influence the zero point.

- *Grasping* - Autonomous grasping of the connector is beyond the scope of this research. For the purposes of this work, 'grasping' refers to the insertion of the biased connector into the end effector of the manipulator.

- *Payload Transport* – It is assumed that the tare point is separated from the receptacle staging point by some non-zero distance. The receptacle staging point is defined as the location where the assembly trajectory begins. This point is aligned with the anticipated location of the receptacle but offset by a distance greater than the sum of the connector and receptacle position errors in the z axis as shown in figure 6.2. This offset prevents accidental collision of connector and receptacle before force guided assembly is enabled.

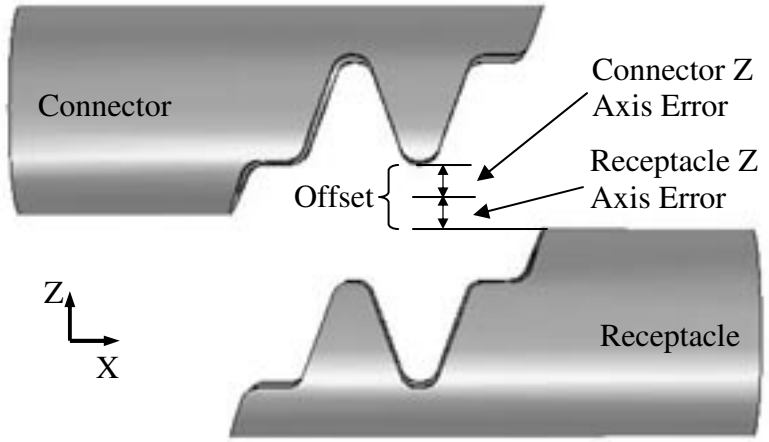

Figure 6.2 – Connector and receptacle are offset by the sum of the respective Z axis errors.

- *Bias Identification* – The path followed during transport is a function of the identification process which determines the relationship between the system state and bias wrenches. If the identification process is not complete when the connector arrives at the receptacle staging point additional motions are added until identification is completed.

6.1.2 Assembly

- *Guarded Motion* – Transition to assembly initiates the bias estimator and prompts the guarded motion of the connector to establish contact with the receptacle. Bias free force/torque signals are directed to the controller, enabling the detection of contact and the transition to force guided assembly.

- *Force Guided Assembly* – The assembly controller operates until the connector achieves stable contact. Stable contact is characterized by the application of a preset contact wrench with no resultant motion. The contact wrench required in this research consists of a constant z axis force applied at

the connector control point and the corresponding torque but zero on all other axes.

6.2 Model Accuracy

The determination of model accuracy for off-line bias model evaluation is specific to the domain in which the bias resides. In the spatial domain distance degrades the quality of bias estimates, in the temporal and temporal-spatial domains, estimate accuracy decreases as a function of time. It is assumed that the identification approach is stable and produces approximately the same results when given the same set of starting conditions. Thus, knowing the accuracy of bias estimates enables designers to limit the use of a bias estimator to high accuracy regimes and allows conclusions to be drawn regarding when or where an estimator must be updated or re-identified.

6.2.1 Spatial Domain

Evaluating the accuracy of bias models in the spatial domain is accomplished by moving the identified bias source through a work envelope in a raster-like pattern. By comparing the actual bias and the estimated bias at each point, the bias estimation error can be determined for a space. The results can then be represented as a graphical representation of the error called an error map.

Generating an error map requires visiting a series of points in a space. Due to the assumption that these bias elements are quasi-static, motion from point to point must be slow enough that it does not excite oscillation in the element. Depending on the dynamics of the system this may result in significant mapping times. Equation 1 provides an estimate of the time needed to perform a mapping operation.

$$t_{map} \geq (t_{s1} \cdot s_1) \cdot (t_{s2} \cdot s_2) \cdot \ldots \cdot (t_{sn} \cdot s_n) \qquad \text{Eq. 1}$$

Where t_{map} is the total mapping time, t_{sn} is the time to complete one sample and move to the next sample point in the n^{th} degree of freedom and s_n is the number of samples in the n^{th} degree of freedom. The value of t_{map} is greater than or equal to the right side of the equation because there are often motions in raster patterns that take additional time and are not accounted for in this equation.

When the values of t_{s1} through t_{sn} are equal and the number of samples per degree of freedom s_1 through s_n are equal, equation 1 can be simplified to equation 2.

$$t_{map} \geq (t_s \cdot s)^N \qquad \text{Eq. 2}$$

Where N is the total number of degrees of freedom. This equation shows that the mapping time increases exponentially with the number of degrees of freedom. Thus limiting the size of the search space is often necessary.

The envelope is bound by several different criteria. As the connector moves farther from the starting point (the point at which the bias model is completed and in theory the point of lowest error) the estimation error increases. One approach to bounding the mapping envelope is to include the space where the bias number is less than or equal to one. Given the equation for bias number shown in Chapter 5 – Bias Number, it is possible to generate a surface that represents the bias number as a function of position. (Figure 6.3) The curve, B=1, bounds a space beyond which the fidelity of sensor readings is not assured. The space bound by this curve can be referred to as the *wrench error envelope*.

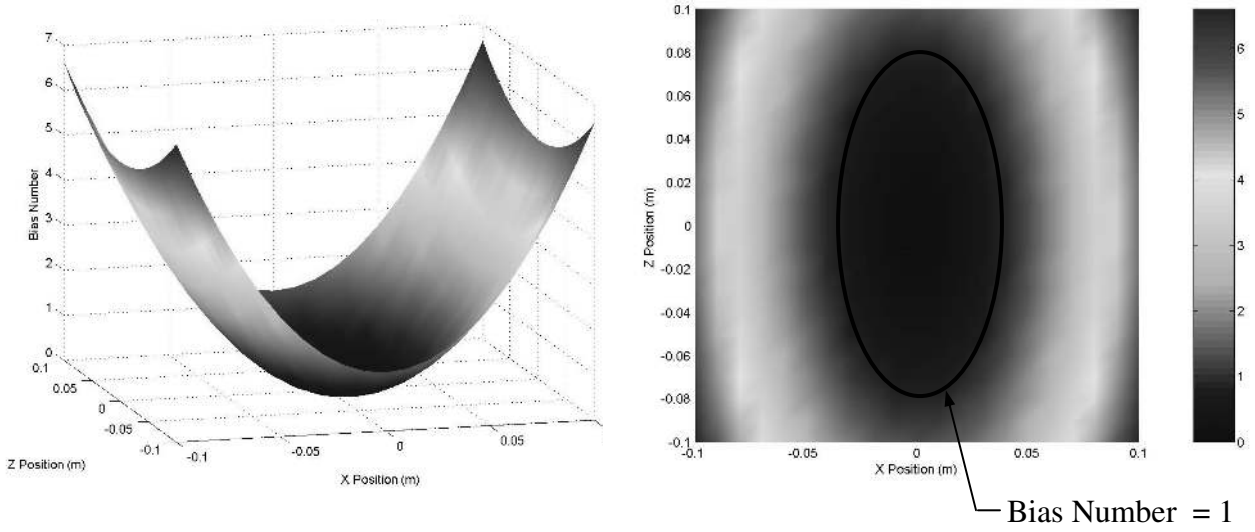

Figure 6.3 – The wrench error envelope is bounded by the curve B=1.

Another space, referred to as the *spatial error envelope*, is bound by the maximum position and orientation errors between connector and receptacle. These errors are the sum of the maximum position uncertainty of the connector and receptacle.

Whenever possible, the spatial error envelope should be a subset of the wrench error envelope. This is presented in equation 3 and figure 6.4. When this is true, contact state readings are guaranteed to be accurate over the workspace.

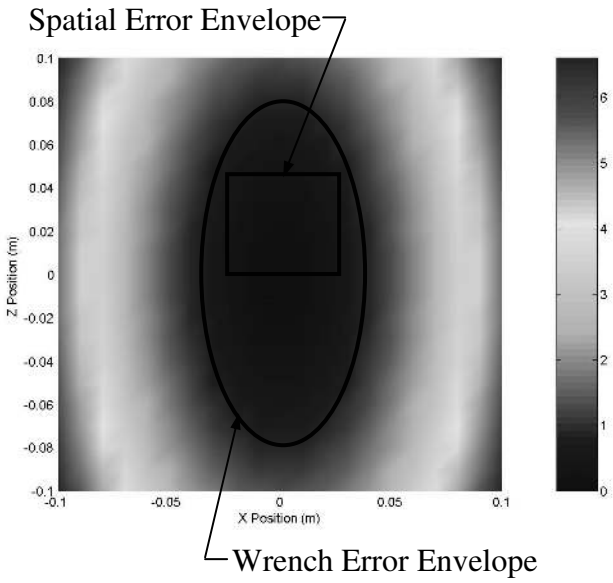

Figure 6.4 – The spatial error envelope should be a subset of the wrench error envelope.

$$E_{SE} \subset E_{WE} \qquad \text{Eq. 3}$$

In this case, the spatial error envelope is used to describe the bounds of the raster motion**.** If, however, the spatial error envelope is not a subset of the wrench error envelope, then there exist portions of the workspace where incorrect contact state readings may occur. In this case, the bounds of the raster motion are described by the smallest closed space described by the surfaces of both the wrench and spatial error envelopes.

For example, figure 6.5 shows an example in which the wrench error envelope and the spatial error envelope are overlaid. It can be seen that bounding the envelope by the smallest combination of the two spaces significantly reduces the work envelope and subsequently the mapping time. It may also be concluded from this graph where incorrect contact state readings may occur.

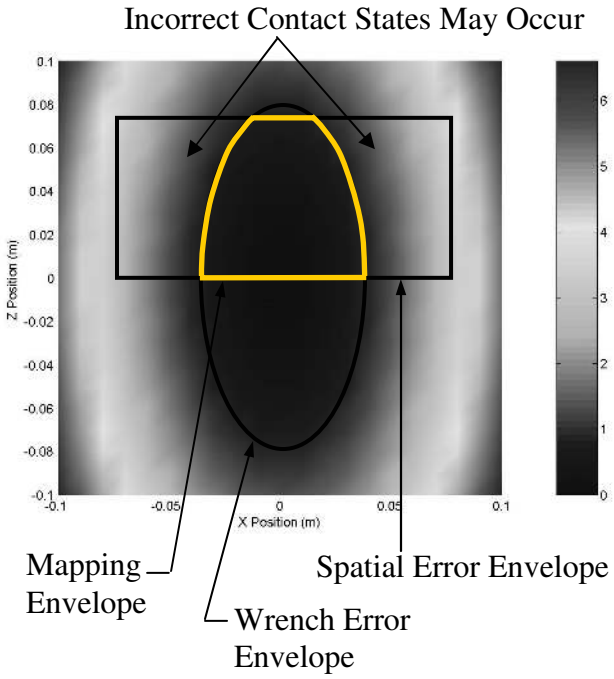

Figure 6.5 – Mapping envelope is bounded by the smallest combination of wrench and spatial envelopes.

If the connector is commanded to move into an area where incorrect contact readings are anticipated, the bias parameters should be re-identified with the new starting point as close as possible to the current position.

The bounds adopted during the mapping process only provide a guideline for bounding the workspace during assembly. The parameter fluctuations that

motivate the identification process also govern the shape and size of the smallest workspace. For example, in stiffer beams model accuracy as a function of position degrades more quickly than that for a flexible beam. Thus, the workspace bounds obtained for a "soft" set of parameters may differ from those obtained for a "stiff" set.

The experiments that follow are performed in a planar space with two translational and one rotational degree of freedom. Representing the resultant error maps in an intuitive manner is not straight forward. A representation is adopted in which the maps are depicted as multiple, two degree of freedom plots like that shown in figure 6.6, where each plot represents the error in a particular degree of freedom for a fixed value of θ.

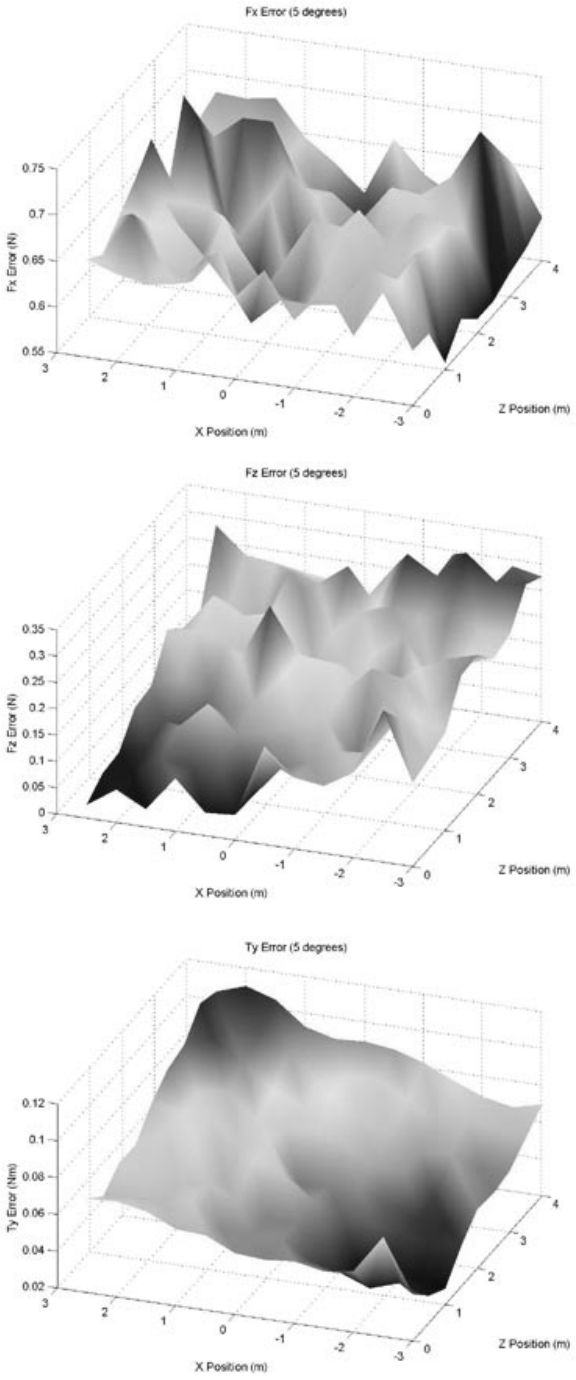

Figure 6.6 – Sample error maps for F_x, F_z, and T_y at one fixed value of θ (5 degrees).

6.2.2 Temporal Domain

Evaluating the accuracy of bias models in the temporal domain is accomplished by observing estimation error over time. In this way the bias estimation error can be determined as a function of time and limits on assembly duration can be established. The results can be represented graphically. This work considers temporal domain bias sources that generate sinusoidal bias wrenches.

Temporal domain estimation error stems from errors in four parameters: force offset, amplitude, phase shift and period. Errors in each of the four parameters manifest different types of force error. Errors in force offset shift the sinusoid in the positive or negative direction yielding a constant force error as illustrated in figure 6.7. Identifying this parameter by taking the average value over multiple cycles minimizes parameter and force error.

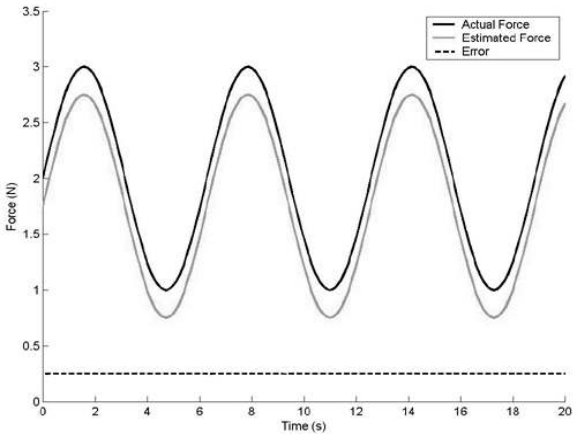

Figure 6.7 – Errors in force offset shift the sinusoid along the force axis yielding a constant estimation error.

Errors in amplitude yield a sinusoidal error (figure 6.8) that is phase shifted from the signal by either zero or 180 degrees depending on the sign of the amplitude error. The models used to estimate temporal domain biases do not account for damping but all real systems experience damping.

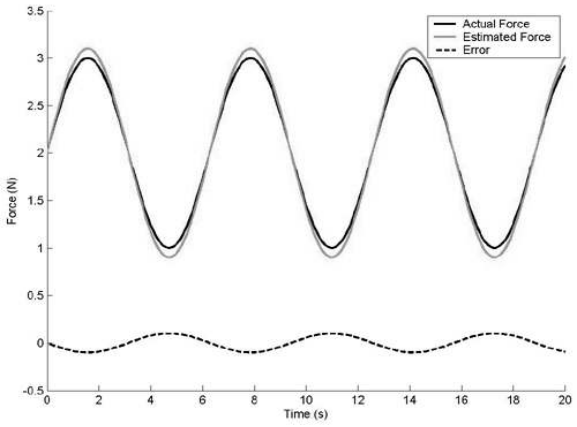

Figure 6.8 - Errors in amplitude yield a sinusoidal estimation error.

Consequently all force estimates experience a steady increase in the amplitude of the force error. (figure 6.9) The magnitude of the damping is directly proportional to the growth rate of the force error due to amplitude errors.

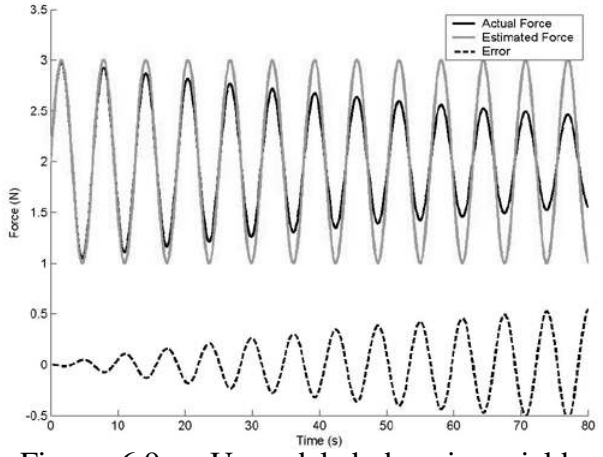

Figure 6.9 – Unmodeled damping yields steadily increasing sinusoidal estimation error.

Errors in phase shift manifest as a constant amplitude sinusoid proportional to the magnitude of the phase shift. (figure 6.10) The maximum error occurs when the phase is off by 180 degrees, at which time the amplitude of the force error is twice the amplitude of the force signal. Phase shift error on the order of several degrees is typical and yields minimal force error.

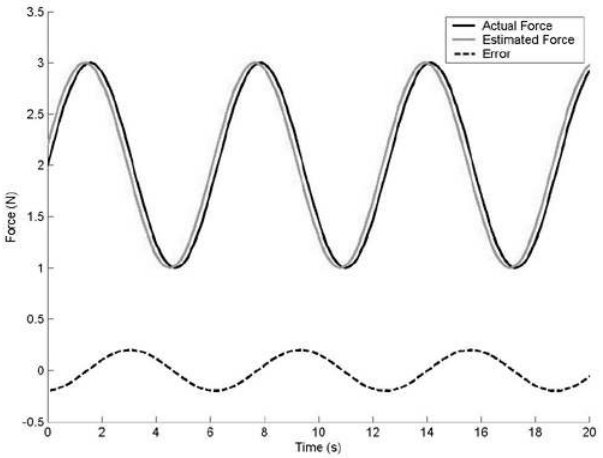

Figure 6.10 – Errors in phase shift yield a sinusoidal estimation error.

Errors in period manifest as the product of two sinusoids, one high and one low frequency. (figure 6.11) The high frequency sinusoid has a period approximately equal to the force signal and a magnitude that is a function of signal amplitude and the errors in the other parameters. The extent to which the high frequency sinusoid's period differs from the signal's period is the parameter error in question.

The low frequency sinusoid has a period proportional to the magnitude of the error. A period estimate error of n% yields a low frequency period equal to 100/n

high frequency cycles. In figure 6.11, the period estimate error is 10%, thus the low frequency sinusoid has a period equal to 10 cycles of the high frequency sinusoid. The maximum error between the actual and estimated forces occurs when they are 180 degrees out of phase. Thus a period estimate error of n% yields the greatest error at 100/2n cycles.

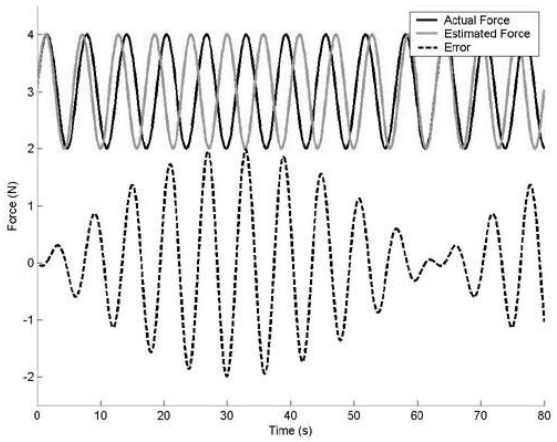

Figure 6.11 – Errors in period yield an estimation error that is the product of two sinusoids.

Estimating the maximum anticipated error for each of the parameters and calculating the resultant force error as a function of time enables the estimation of the time allowed to complete assembly. For example, given the parameters and estimated errors shown in table 6.1, equation 13 is used to determine the resultant force error.

$$F_{er} = \left[A\sin(\omega_n t) + FO\right] - \left[(A + A_{er})\sin((\omega_n + \omega_{er})t + \phi_{er}) + (FO + FO_{er})\right] \qquad \text{Eq. 13}$$

Parameter	Value	Error Value	% Error
Amplitude	1.00	1.01	1.0
Period	1.26	1.24	1.6
Force Offset	0.50	0.51	2.0
Phase Shift	2 π	0.025	0.4

Table 6.1 – Parameter values and estimated error example.

Figure 6.12 illustrates that a maximum error of 0.65 N is exceeded 13.1 seconds after identification. Thus, if a stable assembly is not achieved by that time, the connector is withdrawn and the identification process is repeated. Thus, this approach is useful for determining the amount of time a temporal domain bias compensator is able to operate before the data it produces contains too much error and it must be re-identified.

6.3 Gentle Assembly

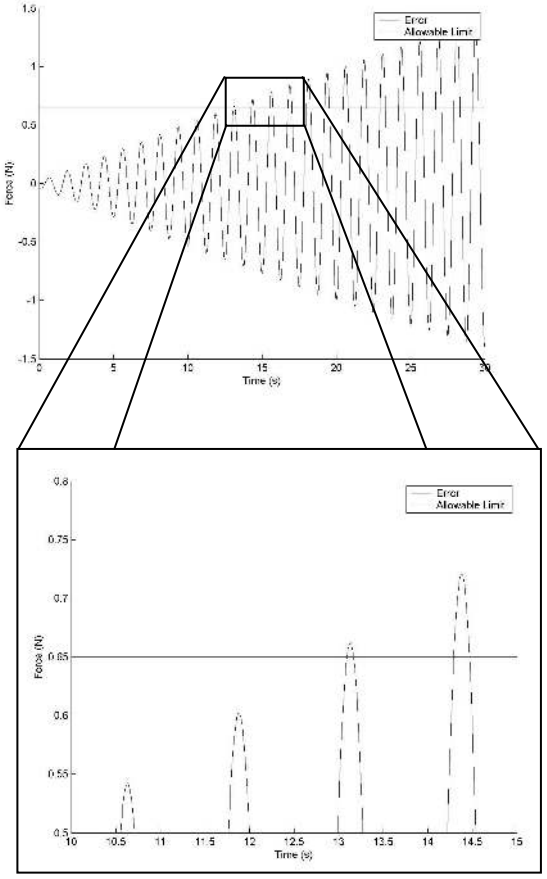

Figure 6.12 – This sample independent oscillator exceeds the maximum allowable error of 0.65 N in 13.1 seconds.

In this research, 'gentle assembly' refers to the connection of components while maintaining contact forces below specified thresholds. There is no absolute measure of gentleness, thus the magnitudes of such thresholds are determined based on connector failure limits, manipulator capabilities and uncompensated minimum necessary forces. The connector failure limits are the forces and torques that can be applied to a connector without causing failure. The uncompensated minimum necessary force, as discussed in Chapter 5 – Bias Number, is the minimum z axis force needed to ensure unambiguous contact readings when performing uncompensated assembly of biased elements. An assembly operation is termed 'gentle' if the compensated minimum necessary force is less than the connector failure limits, within the manipulator capabilities and less than the uncompensated minimum necessary force. In other words, an assembly is 'gentle' if the connector does not break, the manipulator can complete the task and the operation exerts less force with the bias compensator than without. Based on this definition, two metrics are use to evaluate the gentleness of assembly operations for each experiment.

One approach establishes a hypothetical set of connector failure limits. In this approach, limits are established on each of the active axes. Completion of assembly while maintaining contact wrenches below the established thresholds indicates successful gentle assembly. The magnitudes of the force and torque limits are presented in table 6.2. These limits are assumed to be less than the manipulator capabilities. As such, the wrenches are not compared to the manipulator capabilities.

Axis	Threshold
Fx	30 N
Fz	30 N
Ty	3 Nm

Table 6.2 – Connector force and torque failure limits.

Another approach calls for the determination of the compensated minimum necessary force as defined in Chapter 5 – Bias Number. The compensated minimum necessary force provides a theoretical limit to how little force a manipulator can exert while still ensuring successful assembly. Actual contact forces always exceed the compensated minimum necessary force. The degree to which contact forces exceed the minimum force is a function of manipulator control bandwidth and the control algorithm. The force control accuracy of a manipulator increases as the control bandwidth increases. Consequently, given a minimum force, manipulators with greater control bandwidth exhibit smaller maximum forces and are gentler during assembly.

6.4 Connector

The experiments presented in this research use the Force Assemblable Connector-1 (FAC1). The FAC1, shown in figure 6.13, is based loosely on NASA's Joint 4 (figure 6.14), a space qualified structural connector. The FAC1 is force assemblable, meaning that contact forces always result in error reducing motions if the connector is within the receptacle's workspace. The FAC1 is not designed for structural purposes and is suitable only for experimentation.

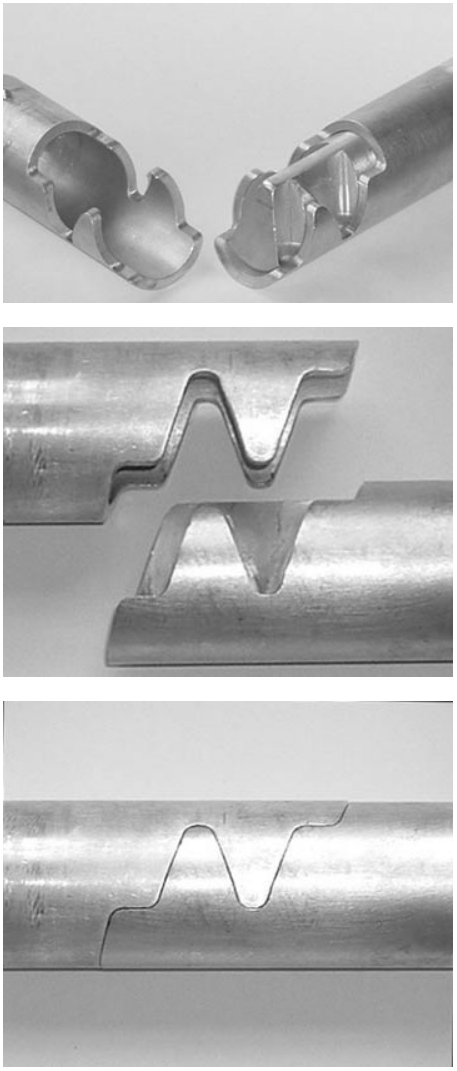

Figure 6.13 – Force Assemblable Connector -1

The FAC1 is composed of two halves, a connector and a receptacle which mate by interlocking grooves and prongs. Both halves are hollow cylinders, approximately 40 mm in diameter with a 5 mm wall thickness. The contact surfaces are cut directly from the cylinders and each half features a pair of grooves and prongs. Mating of the connector and receptacle requires the flush alignment of the grooves from one with the prongs of the other.

The receptacle features a wedge shaped core that aids connector alignment and enables the locking of connector halves. This core locking component has two

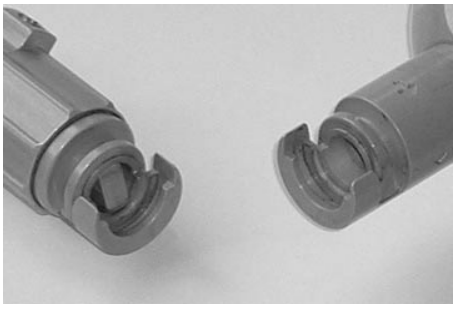

Figure 6.14 – Joint 4

alignment channels that force the connector in the correct direction during approach to ensure proper mating. Once flush contact has been made the core locking component can translate along the axis of the receptacle. This motion engages the connector and locks the connector and receptacle together.

Axis	Max Error
X Disp.	± .010 m
Y Disp.	± .015 m
X Rot.	± 65 deg.
Y Rot.	± 20 deg.
Z Rot.	± 20 deg.

Table 6.3 – FAC-1 maximum acceptable errors.

Table 6.3 details the maximum acceptable error for each axis of the FAC1. These error bounds are based on a fixed admittance in which the force vector is perpendicular to the connector

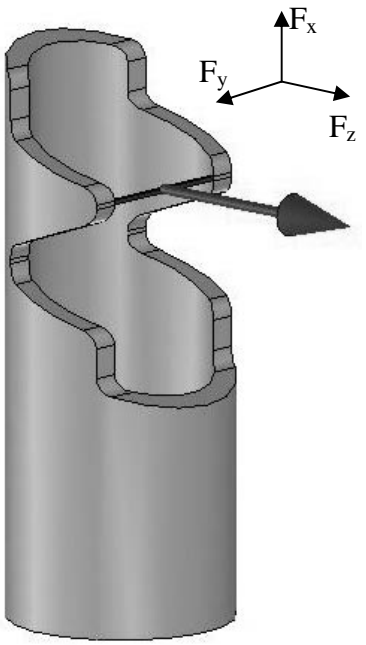

Figure 6.15 – Fixed admittance force vector

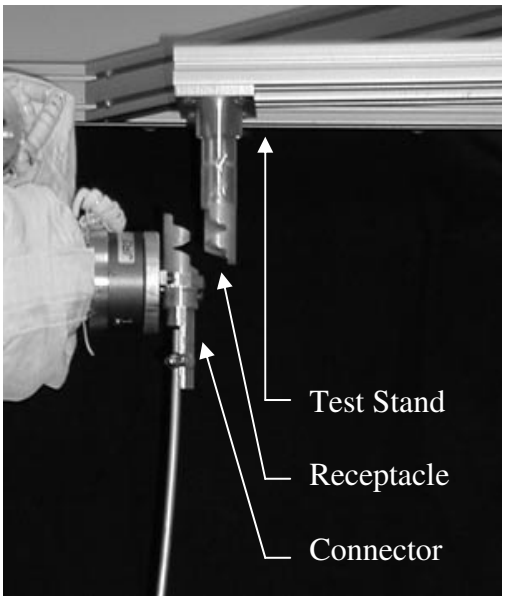

Figure 6.16 – In single manipulator experiments the receptacle is mounted to a test stand.

axis and radiates through the midpoint of the line connecting the contact prongs as shown in figure 6.15. Error in multiple degrees of freedom at once reduces the acceptable errors on individual axes. The connector advances along the z direction, thus no error is provided for that axis.

During experiments, the connector is rigidly mounted on the end effector of the manipulator distal to the force/torque sensor. The receptacle mounting changes depending on the experiment performed. In all single manipulator experiments the receptacle is mounted to a test stand that allows modification of receptacle position. (Figure 6.16) In the dual manipulator experiment the receptacle is mounted on the end effector of the second manipulator distal to the force/torque sensor. (Figure 6.17)

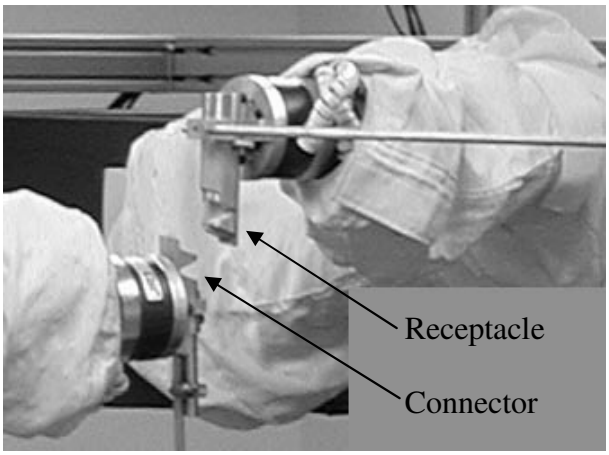

Figure 6.17 – In the dual manipulator experiment the receptacle is mounted on the second manipulator.

In the experiments that follow the connector's control point (described in Chapter 5 - Bias Number) is offset from the force/torque sensor's coordinate frame along the x axis. (Figure 6.18) Thus, the distance from center to sensor is 0.065 m and the general case must be used to calculate the bias number, contact states and minimum necessary force. The x axis center distance, d_{cd}, is 0.015 m (0.30 m contact to contact).

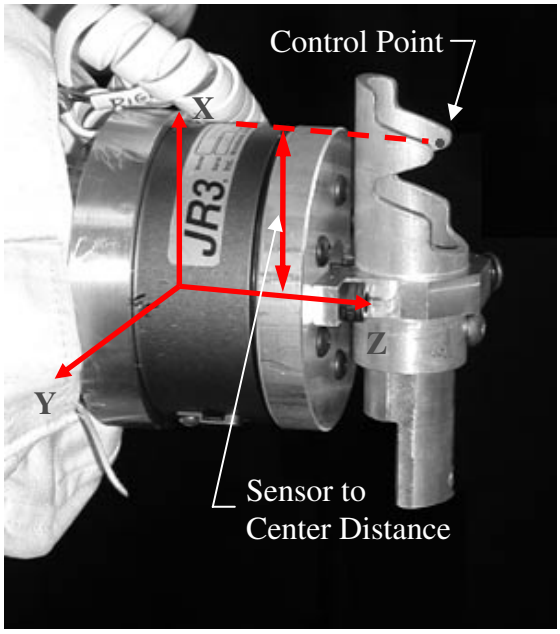

Figure 6.18 – The connector's control point is offset along the X axis.

6.5 Bias Sources

Three general types of bias are examined in this work, quasi-static bias from cables and beams and dynamic bias from pendulums. In all experiments the bias source is attached directly to the connector. As such, the frame in which bias is applied to the system is neither aligned with the tool frame nor with the force/torque sensor frame. Specific details regarding bias sources and experimental setup are addressed in the chapters that follow.

6.6 Success Criteria

In each experiment the success of the assembly is based on four measures:

- Flush Contact – The physical alignment of the connector halves must be sufficient for the core locking component to engage. A gap between any part of the contact surfaces in excess of 0.5 mm is considered a failed assembly.

- Stable Contact – Stable contact is defined as the application of a preset contact force with no resultant motion.

- Efficient Contact – The alignment of components must be efficient and intentional. Under dynamic bias, vibratory motion of components can occasionally result in assembly regardless of the presence of biases. These assemblies are characterized by periodic conflicting motion commands and excessively long assembly durations.

- Gentle Contact – The contact forces and torques exerted during assembly must not exceed the wrench limits set for that task. If the contact wrench exceeds the wrench limit, the controller attempts to retract the connector in an effort to reduce the contact load.

6.7 Traditional Approach

Demonstrating the validity of the experiments presented in the following chapters requires both successful assembly under bias compensation and failure under traditional force guided assembly. In showing the failure of traditional approaches the insufficiency of the previous state of the art is exposed and the value of the bias compensation approach is highlighted.

The traditional experiments for each bias source utilize the same control code developed for the respective bias compensation experiments. The specific treatment of the bias source and the results of such tests are discussed in the individual experiments.

Chapter 7

Experiment 1 – Assembly Under Spatial Domain Cable Bias

7.1 Motivation

Cables, tethers and hoses are present on space structures in a variety of roles. These elements constitute a class of bias source that require a reliable method for assembly. Hoses are used for the transport of fluids, like ammonia coolant, oxygen and hydrogen fuel. Power and data cables enable remote operation of sensors and equipment. Stay cables and structural tethers provide rigidity to flexible elements and assemblies.

Stay cables are characterized by a non-zero bending radius in flexure and high longitudinal stiffness in tension. In some cases they attach to beams that flex and bend when a cable is manipulated. These elements are designed to operate under tension thus the assembly of stay cables occurs under significant biasing force.

Cables with these characteristics can not be assembled using traditional force guided assembly and motivate the use of force guided assembly under bias. The bias source in this experiment is fashioned to emulate a structural cable attached to a flexible beam.

7.2 Assumptions

It is assumed that:

- The location of the manipulator and the cable attachment point are known with respect to the world frame. This allows the calculation of the unknown spring parameters with respect to the actual displacement and orientation. It is possible to relax this assumption and calculate the approximate cable attachment point during identification. However, this yields less accurate bias estimates.

- The cable being attached is under constant tension from the axial spring and remains taut for the duration of the experiment. Cables that are not under tension in a gravity free environment display complicated dynamics and assume complex configurations that are not addressed in this work.

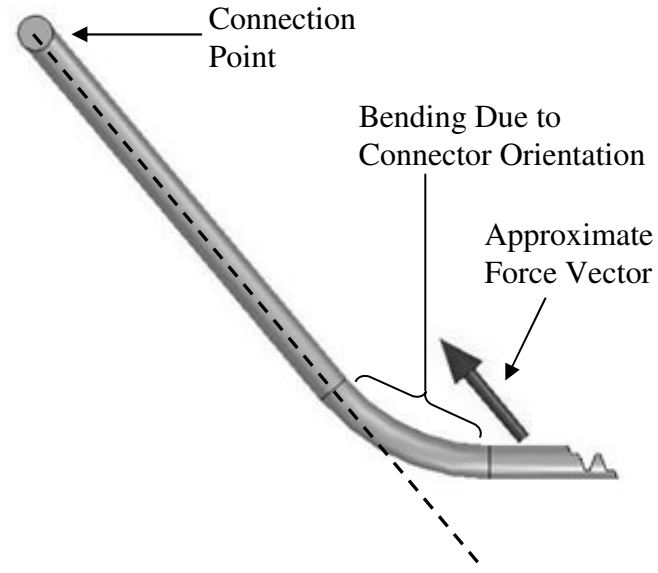

Figure 7.1 – The cable is well approximated by a straight line except where bending due to connector orientation.

- The cable is well approximated by a straight line except where bending due to connector orientation. (Figure 7.1) As the connector is displaced from the starting point the force vector changes orientation. The assumption of straightness allows the cable attachment point to be used as the center of rotation of the force vector.

- Gravity does not affect the shape of the cable or the direction of the force vector. This assumption is necessary because gravity bends the cable into a catenary. As the degree of bending increases, the assumption of straightness fails and the equation describing the orientation of the force vector becomes more complicated. (Figure 7.2) This assumption is fulfilled when in a gravity environment by orienting the cable as close to vertical as possible.

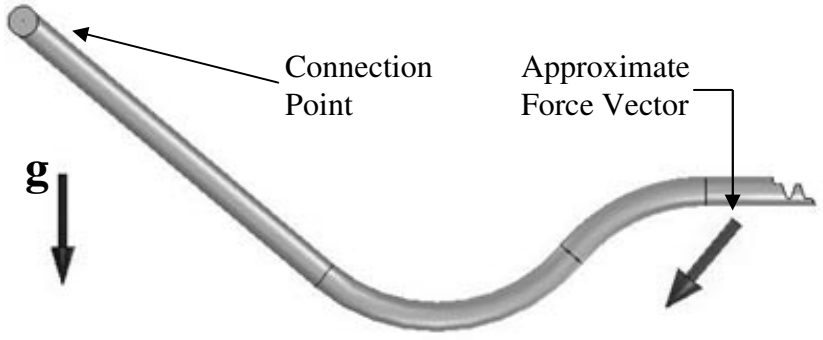

Figure 7.2 - Gravity bends the cable into a centenary invalidating the assumption of straightness.

- The springs being emulated do not necessarily exhibit zero force and torque when the connector is at the zero position. Alternatively, the springs under consideration exhibit a *slack length* or a *slack angle* defined as the distance or angle at or below which the spring does not generate force or torque respectively.

- The cable does not experience any axial torsion. The planar model does not accommodate the forces and torques generated by torsion about the connector axis.

- The system does not experience hysteresis. The presence of hysteresis is not accounted for in the bias models thus the magnitude of any hysteresis must be small enough such that it can be neglected.

7.3 Model

The cable model for wrench emulation consists of a longitudinal spring in series with a flexural spring. The model also incorporates a passive joint to prevent the generation of torsional stresses. The connection between the cable and the world (ground) is modeled as a pin joint and the attachment to the connector is fixed such that the bias element can exert both forces and torques on the connector.

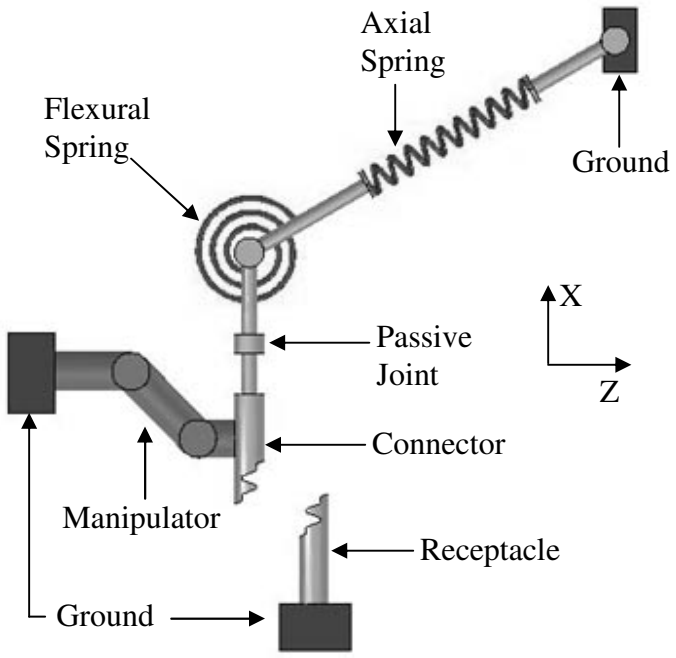

Figure 7.3 – Cable model and experimental configuration.

The model states include the position and orientation of the connector which is located at the end of the cable. Figure 7.3 illustrates the cable model. The actual experimental configuration may be seen in figure 7.7. Equations 1 and 2 present the models for the total force, F_T, and flexural torque, τ. The biasing element used in this experiment is well approximated by linear models, in the case of elements with more complex characteristics, non-linear models are used in place of equations 1 and 2.

$$F_T = k \cdot d + F_c \qquad \text{Eq. 1}$$

Where k is the spring constant, d is the elongation of the spring and F_c is the force at the starting distance.

$$\tau = \kappa \cdot \theta + \tau_c \qquad \text{Eq. 2}$$

Where κ is the torsional spring constant, θ is the angular displacement of the connector and τ_c is the torque at the starting orientation.

The simplified cable model shown in figure 7.3 does not account for several aspects of the real system and is only sufficient for rough estimates of the generated wrenches. More subtle aspects of the wrenches are emulated using linear models applied locally. For example, inaccuracies in the z force component stemming from incorrect angle estimates are corrected using a local linear model. Figure 7.4 shows an example of actual force in the z direction and the estimated z force derived from the total force (equation 1). The resulting error is approximately linear and can be characterized as a linear function over a local area. Thus, identifying the slope and intercept of the error and estimating it as a function of the connector orientation enables the revised z force estimate illustrated.

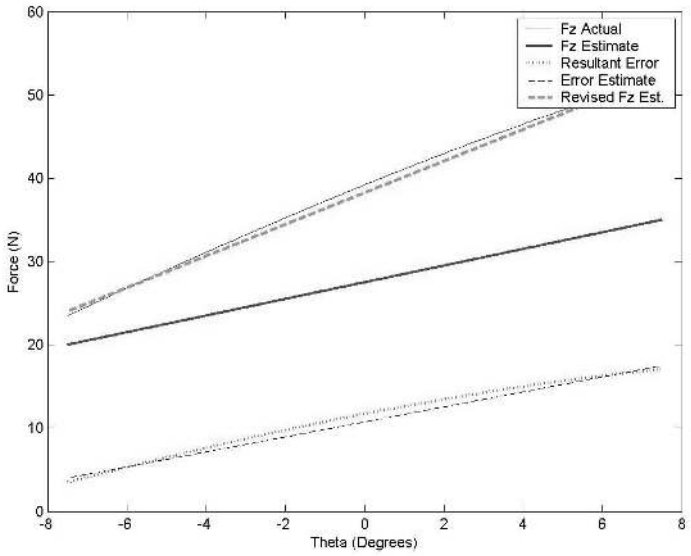

Figure 7.4 – Example of F_z estimation error and locally applied linear model.

Another model adjusts the length of the cable as a function of the angle of the connector. As the connector rotates, the distance from the connector attachment point to the ground attachment point changes. (Figure 7.5) Solving for the actual change in distance requires a complete representation of the experimental geometry. Some of the parameters necessary to calculate this distance are assumed to be unknown and so an alternative method, creating a linear model for local estimation, is adopted. Combining these simple linear models enables the emulation of a complex non-linear system.

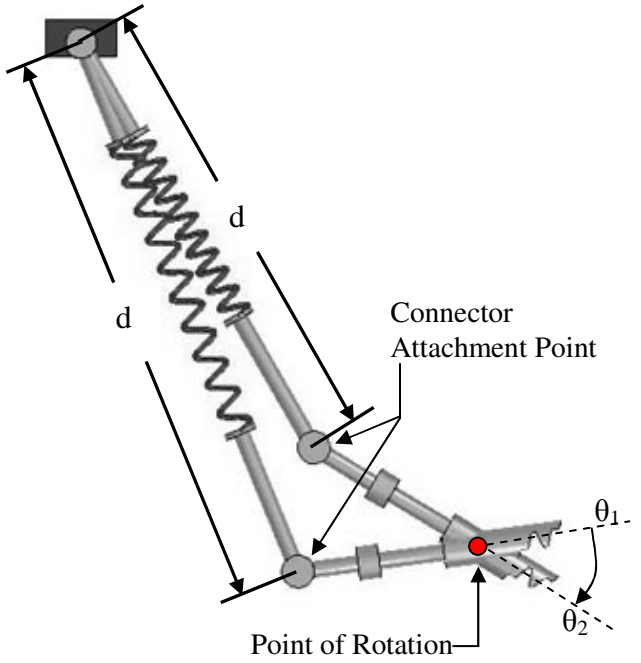

Figure 7.5 – As the connector rotates, the distance from the connector attachment to ground changes.

The estimate of the force in the z direction is based on the total force model. (Equation 1) The total force is rotated to the correct frame based on manipulator orientation and combined with the linear model to arrive at the final z component force as shown in equation 3.

$$F_z = (k \cdot d + F_c) \cdot \sin(\theta) + (m_z \theta + b_z) \qquad \text{Eq. 3}$$

Where m_z and b_z are the slope and intercept of the linear z estimate error model.

The estimate of the force in the x direction is arrived at by exploiting the available geometric constraints. An estimate of total force is available from equation 1 and

an estimate for the z component is available from equation 3. Thus the force in the x direction can be represented as in equation 4.

$$F_x = \left(k \cdot d + F_c\right) \cdot \cos\left(\sin^{-1}\left(F_z / F_T\right)\right) \qquad \text{Eq. 4}$$

This approach avoids the creation of a third physically based model but creates a direct relationship between the x component error and the errors of the constituent models.

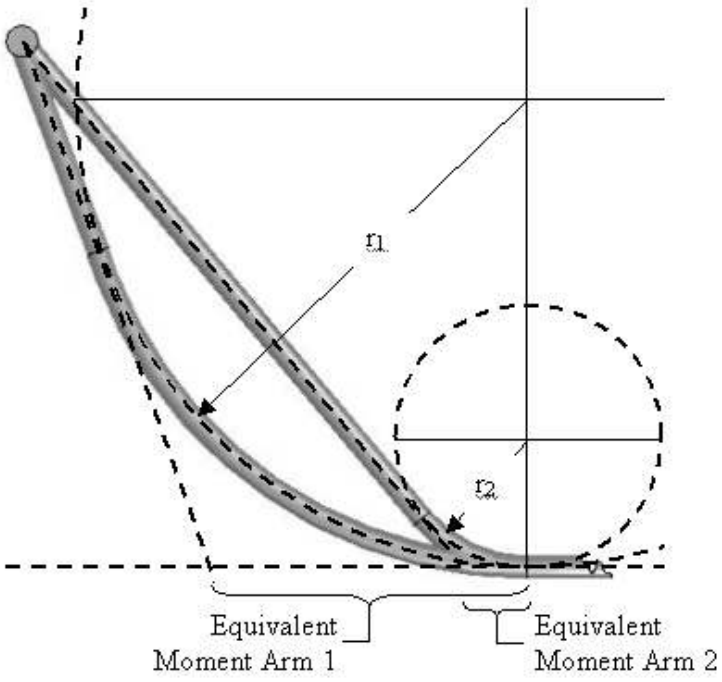

Figure 7.6 – The equivalent moment arm is a function of the bending radius of the cable.

Torque is modeled assuming a known moment arm in the z direction and an unknown moment arm in the x direction. This assumption is consistent with the model already presented. It is assumed that the moment arm in the z direction is known because the offset is coaxial with the connector. However, the moment arm in the x direction is a function of the bending radius of the cable and must be

learned. (Figure 7.6) The torque generated by the z component force is learned as a linear function shown in equation 5.

$$\tau_z = \left(F_z \cdot d_x + c_\tau\right) \qquad \text{Eq. 5}$$

Where d_x is the moment arm in the x direction and c_τ is a torque offset. This calculation is combined with the x component torque to arrive at the final torque estimate, τ, as shown in equation 6.

$$\tau = \left(F_z \cdot d_x + c_\tau\right) + F_x \cdot d_z \qquad \text{Eq. 6}$$

Where d_z is the moment arm in the z direction.

The model presented in this section is not limited to the planar case. Given the assumption that the cable does not resist axial torsion, this model is extensible to the three dimensional space. When axial torsion is not present, a cable in flexure can always be described as belonging to a plane. By implementing the model in the coordinate frame described by this plane and transforming the results to the connector frame the model presented can be used for the three dimensional case.

7.4 Experimental Setup

7.4.1 Configuration

The experimental setup of the cable bias experiments is shown in figure 7.7. Tests are performed with a five degree of freedom manipulator operating in a plane. The receptacle is attached to an adjustable receptacle stand and placed within the workspace of the manipulator. The bias element is attached to the world frame directly above the manipulator and receptacle stand.

7.4.2 Bias Source

The bias source for this experiment is composed of two parts, the axial spring and the 'cable'. The axial spring is an elastic polymer with an approximately linear relationship between elongation and force. The magnitude of the force is varied between experiments by adjusting the preload on the spring. The spring is attached to the world frame at one end by a flexible cable that approximates a pin joint. The other end is attached to the 'cable' element.

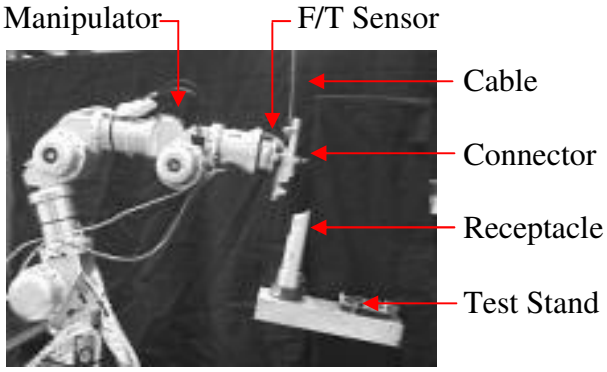

Figure 7.7 – Experimental setup of cable bias experiment.

Three separate 'cable' elements are used for the experiments presented. The elements vary in flexural stiffness to demonstrate the general applicability of the model and approach. Under the loads applied by the manipulator, the most

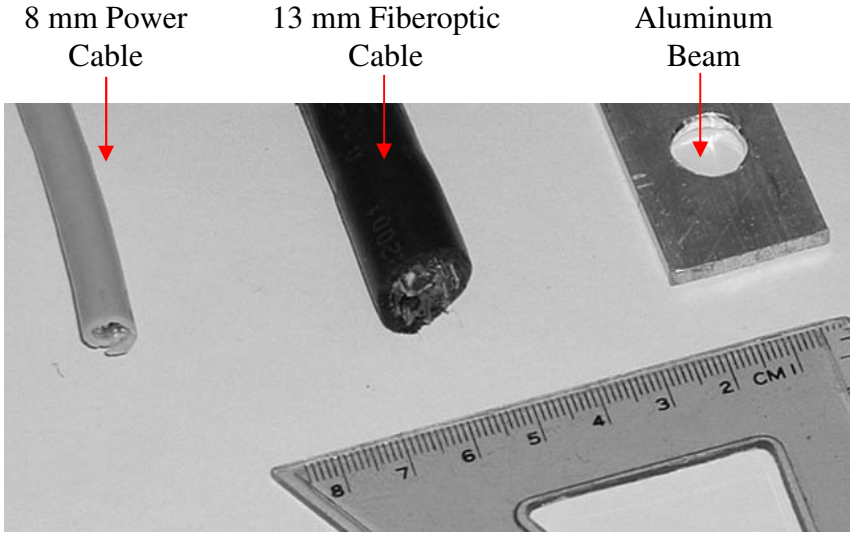

Figure 7.8 – Three separate 'cable' elements are used for the experiment presented.

flexible of these elements, an 8 mm power cable, has an effective bending radius on the order of 0.01-0.02 meters. (Figure 7.8) The medium stiffness element, a 13 mm fiberoptic communications cable, has a bending radius on the order of 0.1-0.2 meters. The stiffest of the three elements is a rectangular aluminum beam with a 3 mm by 25 mm cross section and a bending radius on the order of 1.0-2.0 meters.

The wrenches generated by each of these elements are very different but the basic model applies. Thus a variety of cables are emulated by changing the axial spring preload and the 'cable' element.

7.4.3 Identification

Identification of the spring parameters is performed using a least squares algorithm. The axial spring parameters are identified by moving the connector along a line radiating from the attachment point. The flexural spring parameters are determined by rotating the connector to the maximum angles anticipated during assembly. The parameters of the linear models used to adjust for basic model error are identified during the motions described for the axial and flexural springs.

7.4.4 Issues

The tests described in the Results section of this chapter document the assembly of a connector under quasi-static cable bias. The average assembly time for these tests is approximately 35 seconds from first contact to completion. The speed of assembly is limited by the control bandwidth of the manipulator (50 Hz) and not the bias compensation approach. Increasing the speed of the manipulator while maintaining the control frequency yields oscillatory contact behavior.

The force/torque sensor used for this experiment exhibits significant noise. This may be attributed to the relatively low magnitude of the applied wrenches and the sensor configuration. The forces and torques applied to the sensor are a fraction of the permissible ranges, thus the signal to noise ratio is not as high as is possible. The sensor is configured such that it outputs a set of amplified analog signals from internal strain gauges. The signals are conducted to an external analog to digital converter and then sent to the CPU. This configuration makes the signals particularly susceptible to external sources of noise.

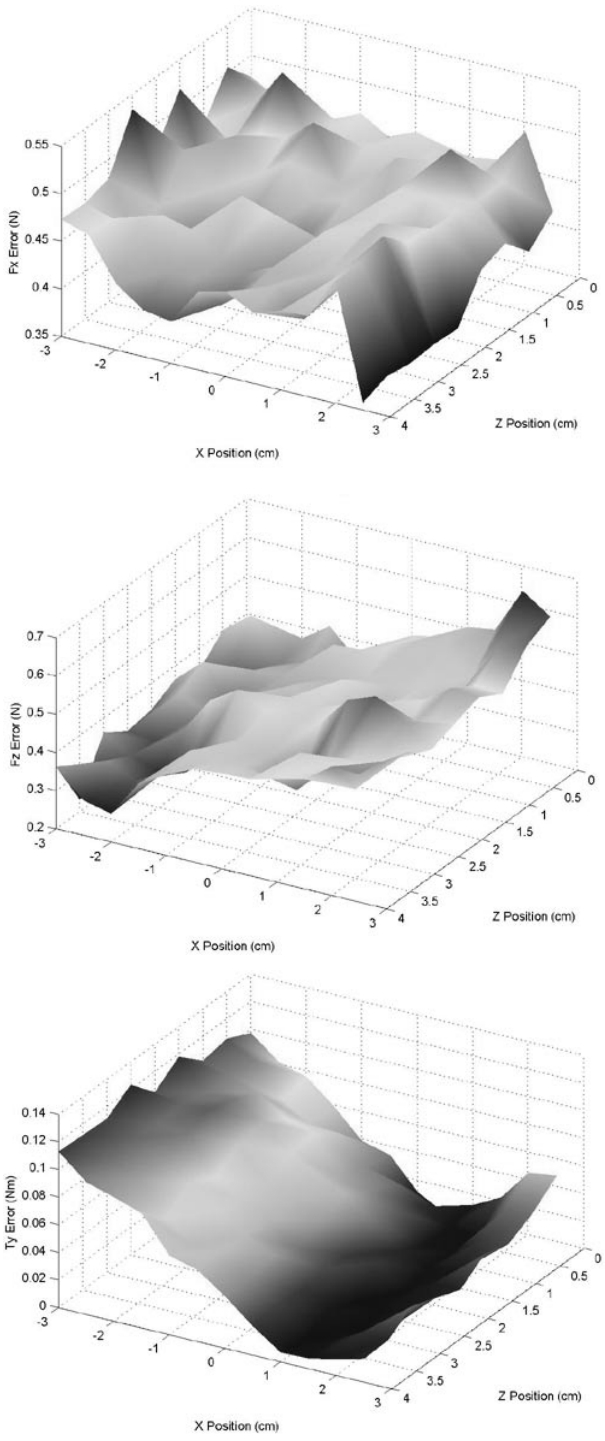

Figure 7.9 – Error map for 13 mm fiberoptic cable at 5 degrees.

The manipulator configuration constrains all motion to the plane and prevents even small changes out of plane to accommodate misalignment of the manipulator and receptacle stand. This limitation complicates the experimental setup, mandating the precise alignment of the two halves. This alignment is difficult given the unwieldiness of the halves and the precision necessary to ensure flush mating.

7.5 Results

7.5.1 Model Accuracy

Wrench model accuracy influences the minimum force needed for accurate assembly as discussed in Chapter 5 - Bias Number. The accuracy of the model proposed for cable emulation is examined and conclusions regarding its utility are drawn.

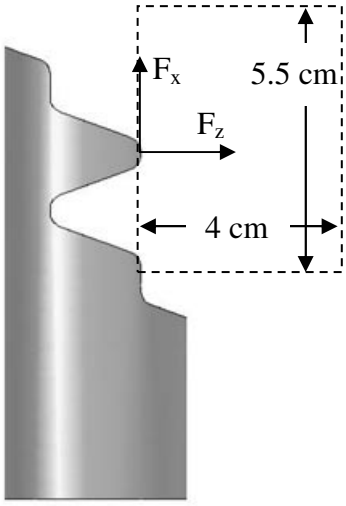

Figure 7.10 – Coordinate frame and mapping envelope.

A portion of the error map for the medium stiffness flexural element is shown in figure 7.9. The figure shows force estimation errors in the x and z axes and torque estimation error about the y axis at an orientation of 5 degrees from the starting orientation. Figure 7.10 shows the coordinate frame and mapping envelope used for the error maps presented.

The general trends exhibited by the error maps reveal the divergence of the models from the real systems. The pitted texture of the surfaces is attributed to sensor noise in combination with small oscillations in the cable during the mapping process. A single sample is taken for each sample position; noise reduction is possible by sampling multiple times at a single position. The model error for both the x and z axes is, in many cases, comparable to sensor noise. This indicates that further refinement of the model in those regions would have no discernable effect. It also complicates interpretation, making identification of trends in the error more difficult. The sensor noise for the torque about y is significantly lower than the force errors, yielding more room for model improvement and more easily interpreted trends.

All F_x error maps exhibit a step increase from the first to the second position in the x direction. This step increase, illustrated in figure 7.11, averages approximately 0.1 N and is a result of hysteresis. The step corresponds to the point at which the raster pattern changes direction and can be attributed to a change in manipulator position without a corresponding change in the length of the axial spring. The exact source of hysteresis is unclear but may be due to any of the parts of the bias element.

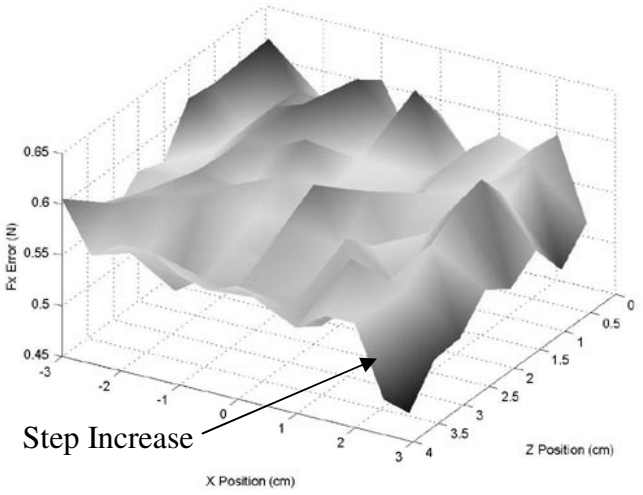

Figure 7.11 – All F_x error maps exhibit a step increase due to hysteresis.

In all cases, regardless of flexural element and connector orientation, there is a significant increase in torque error as the connector moves along the x axis. Motion of the connector along the x axis primarily maps to a change in length of the axial spring. Although in many cases there is also an increase in F_z error, this is not the situation in all cases. Thus it must be concluded that the torque error is primarily a product of inaccuracies in the torque model. In those cases where the F_z error is also increasing, the poor performance of the force model contributes to the torque error.

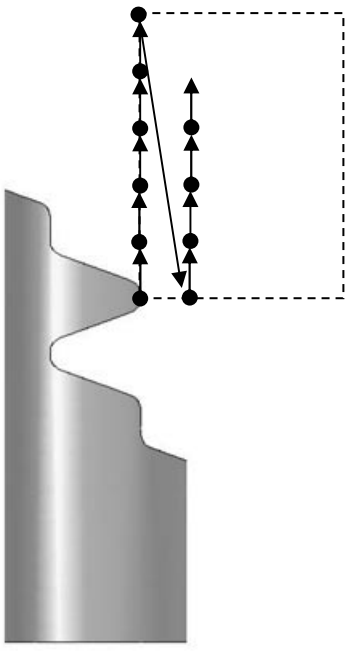

Figure 7.12 – Raster pattern used to create error maps.

As the stiffness of the flexural elements increase the insufficiency of the torque model becomes clearer. Figure 7.13 illustrates the difference in

torque error between the three flexural elements when the connector is rotated five degrees from its learning orientation. These graphs show that as the flexural stiffness of the bias element increases, the estimation error also increases.

The cable bias emulation model estimates the forces and torques generated by the medium stiffness source to within 0.60 N on the x axis, 0.65 N on the z axis and 0.2 Nm about the y axis. (Figure 7.14a) Figure 7.14b shows an alternative representation of the error map with error as a function of the sample number. This graph shows that the changes in F_x, F_z, and τ_y are approximately 6 N, 8N, and 2 Nm respectively. Figure 7.14c shows the percent error for the estimates in figure 7.14a. The comparatively high percent error associated with the first

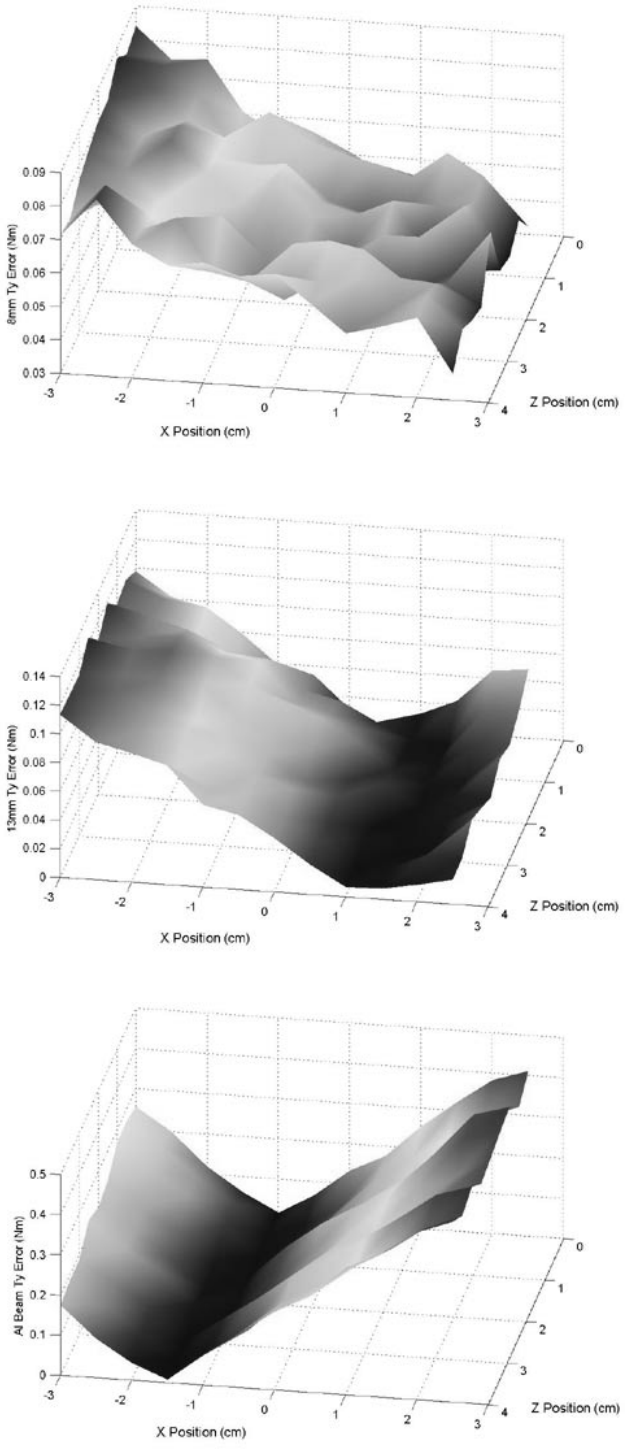

Figure 7.13 – T_y Error at 5 degrees for the 8mm, 13mm and Aluminum sources respectively.

portion of the z axis corresponds to the low z axis biases shown in figure 7.14b. For the most part, the emulation error for the z axis remains below 6% while the errors for x axis and torque about y remain below 5% and 2% respectively.

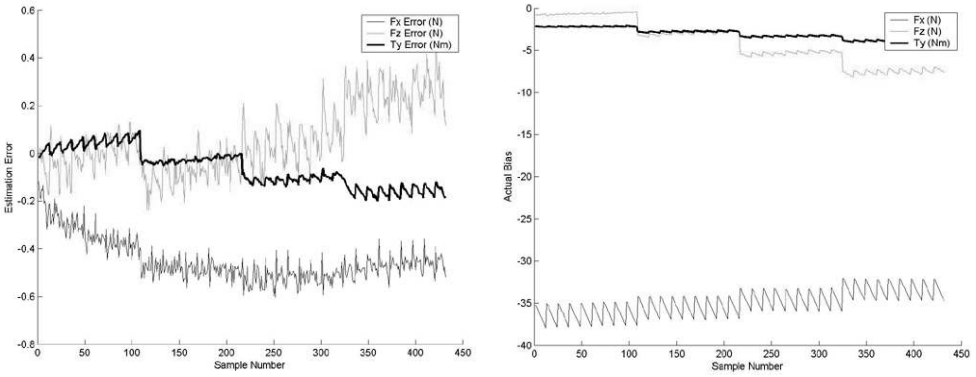

Figure 7.14 – a) Estimation error, b) Actual bias values, and c) Percent error as a function of sample number in a raster scan.

Given the connector-sensor geometry described in Chapter 6 – Experimental Introduction, the change in actual bias from figure 7.14b, and the 30 N limit on F_z (from Table 6.1) the bias number is calculated using equation 13 from Chapter 5:

$$B = \frac{\tau_{er} - F_{er} \cdot d_{sc}}{F \cdot d_{cd}} = \frac{1.98Nm + 7.73N \cdot 0.065m}{30N \cdot 0.015m} = 5.52$$

The value of B is significantly larger than unity, indicating that bias compensation is necessary to achieve gentle assembly. The value of the bias number is calculated using the maximum torque and force errors over the space

considered, providing a single measure for the whole space. Alternatively, the bias number can be calculated for each sample point in a space.

7.5.2 Gentle Assembly

The actual and estimated F_x, F_z, and T_y during a sample force guided assembly under cable bias are shown in figure 7.15. The graphs show the assembly process starting from before contact is established to when stable contact and flush assembly are achieved. The process is divided into three sections and separated by events Alpha and Beta. Prior to Alpha the connector performs guarded motion. Event Alpha corresponds to first contact between the connector and receptacle. When contact is made the connector advances without changing orientation until the minimum z axis force is established. Event Beta corresponds to the contact state which generates a stable

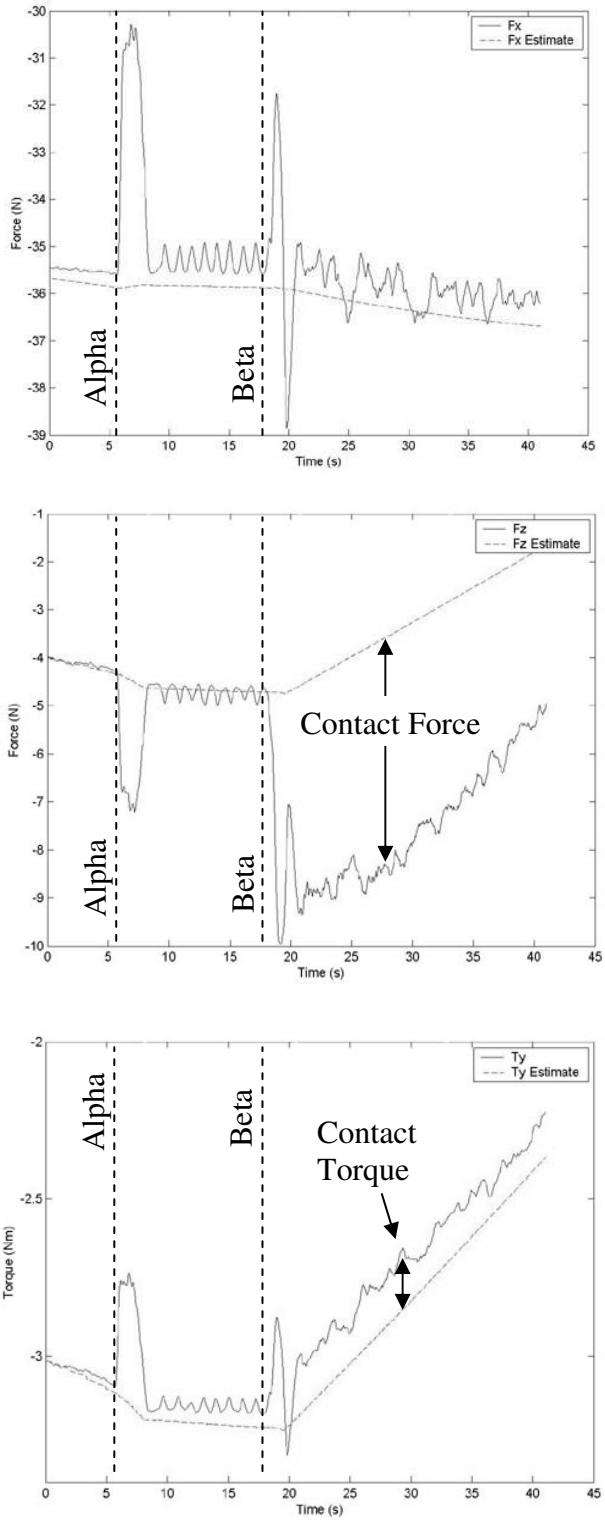

Figure 7.15 – Actual and estimated F_x, F_z, and T_y during a force guided assembly.

resultant force in the z direction. Subsequent to event Beta the minimum force for an unambiguous contact signal is maintained (seen as the constant force offset between the F_z estimate and the actual F_z) and both orientation and position of the connector are modified until flush assembly is established.

A set of 20 tests are performed to quantify the efficacy of the proposed approach. The tests vary the orientation and position of the connector's starting point relative to the receptacle. The starting position is offset by ± 0.01 m in the x direction, - 0.02 m in the z direction and ± 15 degrees relative to the nominal starting position. Despite significant alignment errors, the approach had a 100% success rate over the test set.

The minimum necessary force is calculated using equation 8 from Chapter 5 - Bias Number:

$$F = \frac{\tau_{er} - F_{er} \cdot d_{sc}}{d_{cd}} = \frac{0.2Nm + 0.65N \cdot .065m}{0.015m} = 16.15N$$

The minimum force is set to 17.0 N for the tests described to reduce the bias number and provide additional margin.

The maximum change in torque encountered over the workspace is 1.98 Nm and the change in force is 7.73 N. Given the physical dimensions of the connector, the uncompensated minimum necessary force is 157.56 N. Thus, based on a compensated minimum necessary force of 16.15 N, the bias compensator yields a 90% reduction in necessary z axis force.

The reader may note that the minimum force (the offset between actual and estimated force in the z direction after event Beta) shown in figure 7.15 is not 17 N. The data used to generate figure 7.15 stems from an earlier test set in which the minimum force necessary for unambiguous contact is calculated as 6 N. The

data presented in figure 7.15 is chosen because it presents a particularly clear delineation between the different stages of assembly.

7.6 Traditional Approach

Implementation of the traditional approach is performed by removing the bias identification and compensation functions from the assembly controller. The manipulator is allowed to move the connector directly to the receptacle staging point, bypassing the identification operation. The bias is assumed to be constant and the bias wrench at the staging point is identified and subtracted from the sensor data, taring the sensor.

Using this approach the manipulator is unable to complete the assembly of the biased element. A series of ten tests are performed to verify the failure of this approach. The initial position and orientation of the connector are modified for each test within the same bounds described for the bias compensated tests. The starting position is offset by ± 0.01 m in the x direction, - 0.02 m in the z direction and ± 15 degrees relative to the nominal starting position.

The traditional approach fails 80% of the time when under cable bias. The tests that did not fail had initial conditions with orientations approaching 0 degrees relative to the receptacle. In these cases the bias wrenches generated do not exceed the control thresholds and subsequently do not issue incorrect commands during assembly.

Two failure modes are encountered in the failed tests. Failure to achieve flush contact during assembly is the primary failure mode. The presence of uncompensated bias prevents the identification of flush contact from wrench data. When bias is not present or is compensated, flush contact is established by rotating the connector until the sum of the applied torques equals zero. This indicates that contact is established on both sides of the control point and that

approximately equal forces are being applied. When uncompensated bias is present the point at which the sum of the applied torques equals zero does not correspond to flush contact. Thus, servoing to the zero point does not ensure flush assembly.

The generation of excessive contact wrenches is the second failure mode encountered when implementing traditional force guided assembly. Corrupted wrench data and control commands result in more frequent jamming of connector components and subsequently the generation of excessive contact wrenches.

Chapter 8

Experiment 2 – Assembly Under Spatial Domain Beam Bias

8.1 Motivation

One assembly task in space construction is the connection of structural beams to form trusses. These long, light beams are called longerons and are relatively fragile with wall thicknesses measured in fractions of a millimeter but lengths of tens of meters.

Longerons can carry heavy loads along their length but are usually compliant in flexure. This yields a bias source with little or no axial compliance but both torsional and bending flexure. Connecting such elements when one end is already rigidly attached to the structure requires twisting and bending.

Longerons that are constrained at one end cannot be assembled using traditional force guided assembly techniques and motivate the use of force guided

assembly under bias. The bias sources in the experiments of this research are fashioned to emulate a longeron in flexure. The axial stiffness associated with these elements is not emulated and the beam is allowed to comply along its axis. The motivation behind this simplified model is discussed in the Experimental Setup – Issues section of this chapter.

8.2 Assumptions

It is assumed that:

- Beams contact the world frame through frictionless roller supports and that the forces exerted on connectors in the x axis are negligible. Real systems experience forces along the x axis from both friction and a component of the normal force at roller supports when beams are in flexure.

- The slope of a beam at a roller support is small enough during flexure that cantilever beam models remain accurate. Real systems experience slopes in excess of 20 degrees during experimentation and the models used remain accurate.

- Manipulator location is known with respect to the world frame but that the location of the roller support is unknown. Models used to emulate beam bending do not rely on the world frame location of the roller support.

- Bias forces and torques of un-modeled degrees of freedom remain below specified thresholds. Exceeding these thresholds indicates contact with a receptacle and initiates compliance in the connector.

- Hysteresis is not present. The presence of hysteresis is not accounted for in the bias models thus the magnitude of any hysteresis must be small enough such that it can be neglected.

- Beam cross sections and bending moduli remain constant over the lengths of the beams. Changes in these parameters generate complex force profiles as a function of displacement.

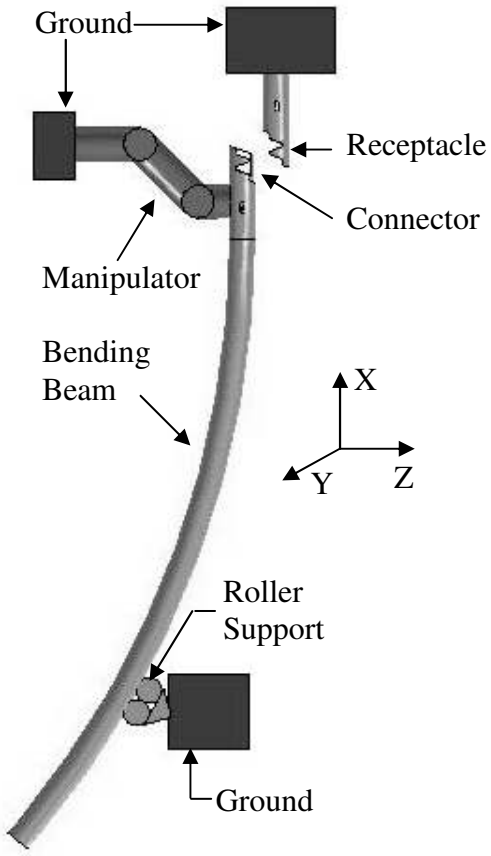

Figure 8.1 – Test configuration for Experiment 2 – Bending Beam Bias.

8.3 Model

The test configuration for this experiment is shown in figure 8.1. The beams are statically determinate, meaning that the bending moment can be determined solely from the applied forces. The governing equation relating the second derivative of beam deflection and moment independent of boundary conditions is presented in equation 1.

$$\frac{d^2y}{dx^2} = \frac{M(x)}{EI} \qquad \text{Eq. 1}$$

Where M(x) is the bending moment at a position x along the beam, E is the modulus of elasticity, and I is the moment of inertia of the beam cross section.

The beams are rigidly attached to connectors, thus the position and orientation of the end of the beams are constrained and both forces and torques are applied.

The assumption that the force application point can be modeled as a roller support means that the transverse displacement is controllable but the slope is not. This combination of boundary conditions allows the treatment of the beam as a cantilever.

The moment, M(x), at a point along the length of a cantilever beam is described by equation 2.

$$M(x) = F_z \cdot (L - x)$$

Eq. 2

Where F_z is the applied force, x is the position along the beam as shown in figure 8.2 and L is the total length of the beam. Combining equations 1 and 2 and integrating twice yields equation 3.

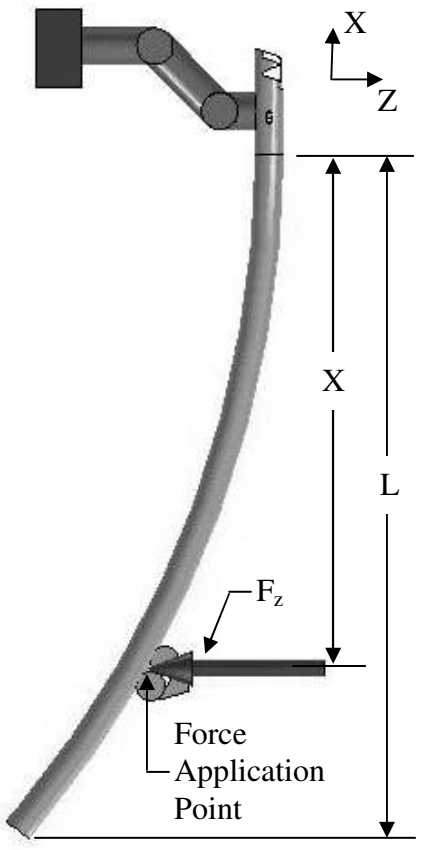

Figure 8.2 – Dimensions and force application point for bending beam bias.

$$z = \frac{F_z}{E \cdot I} \cdot \left(\frac{Lx^2}{2} - \frac{x^3}{6} \right) + c_1 \cdot x + c_2$$

Eq. 3

Where z is the deflection at the point x. The constants of integration, c_1 and c_2, are equal to zero due to the boundary conditions. Solving this equation for the point at which x = L yields equation 4, the displacement at the end of the beam.

$$z = \frac{F_y \cdot L^3}{3 \cdot E \cdot I}$$

Eq. 4

And solving for F yields equation 5.

$$F_z = \frac{3 \cdot E \cdot I \cdot z}{L^3} \qquad \text{Eq. 5}$$

Thus, given a beam of uniform cross section and composition, the relationship between the perpendicular displacement and the resultant force in the z direction is a linear function.

When the force application point does not correspond to the end of the cantilever beam as shown in figure 8.2, the derivation for the force in the z direction still holds. In this case, equation 6 describes the force F_z.

$$F_z = \frac{3 \cdot E \cdot I \cdot z}{x^3} \qquad \text{Eq. 6}$$

Where the length of the beam, L, has been replaced by the position of the force application point, x. Linearizing equation 6 yields equation 7.

$$F_z = \frac{3 \cdot E \cdot I}{x^3} \cdot \Delta z - \frac{9 \cdot E \cdot I \cdot z}{x^4} \cdot \Delta x \qquad \text{Eq. 7}$$

The torque about y is related to the force in the z direction by equation 8, also a linear function.

$$\tau_y = F_z \cdot L \qquad \text{Eq. 8}$$

Thus the emulation of the bending beam can be performed with the two simple linear models shown in equations 9 and 10.

$$F_z = \Omega_1 \cdot x_\theta + \Omega_2 \cdot z_\theta + \Omega_3 \qquad \text{Eq. 9}$$

$$\tau_y = \Gamma_1 \cdot x_\theta + \Gamma_3 \qquad \text{Eq. 10}$$

Where Ω_n and Γ_n are the learned parameters and x_θ and z_θ are the values of x and z transformed into the connector coordinate frame which is dependant on θ. The values x_θ and z_θ are described by equations 11 and 12.

$$x_\theta = d \cdot \cos(\theta) \qquad \text{Eq. 11}$$

$$z_\theta = d \cdot \sin(\theta) \qquad \text{Eq. 12}$$

Where d is the distance between the fixed end of the cantilever and the force application point and θ is the angle between the line d and the connector axis. Figure 8.3 illustrates the geometric basis for x_θ and z_θ.

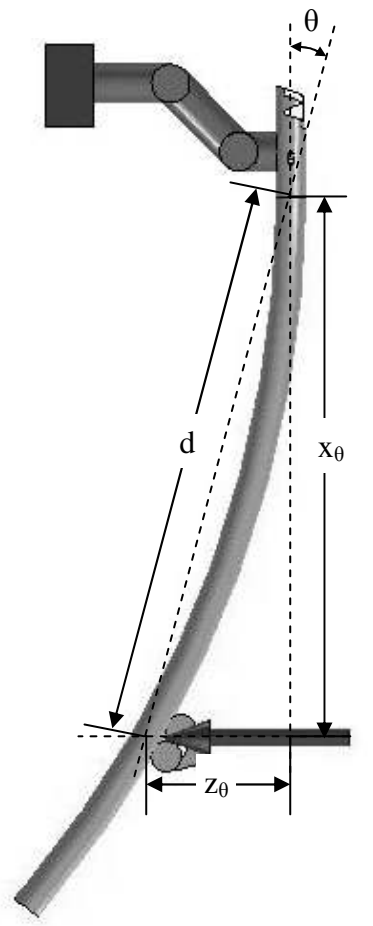

Figure 8.3 – Illustration of the geometric basis for x_θ and z_θ.

An alternative model is also developed based on observations of the experimental system. In the experimental system the force in z and the torque about y are both well approximated by linear functions of the world frame coordinates x, z and θ as shown in equations 13 and 14.

$$F_z = \Omega_1 \cdot x + \Omega_2 \cdot z + \Omega_3 \cdot \theta + \Omega_4 \qquad \text{Eq. 13}$$

$$\tau_y = \Gamma_1 \cdot x + \Gamma_2 \cdot z + \Gamma_3 \cdot \theta + \Gamma_4 \qquad \text{Eq. 14}$$

The accuracies of each of these models are examined in the Results section of this chapter. Over a local area, the alternative model exhibits lower error and is used for the experiments presented.

8.4 Experimental Setup

8.4.1 Configuration

The beam bias experimental configuration is shown in figure 8.4. Experiments are performed using a seven degree of freedom manipulator operating in a six dimensional space. The receptacle is attached to an adjustable receptacle mount which is attached to the world frame. The bias element contacts the world frame through a roller support, the position of which is adjustable in both the x and z axes.

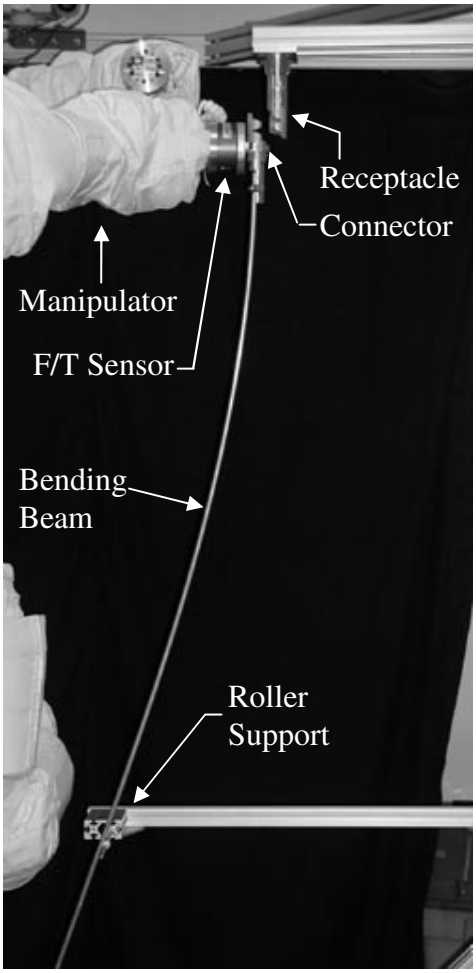

Figure 8.4 – Beam bias experimental configuration.

8.4.2 Bias Source

The bias source for these experiments is a 0.01 m diameter aluminum beam. The beam is clamped at one end directly to the connector such that the orientation of the connector mandates the orientation of the beam at the connection point. The beam exhibits an approximately linear relationship between displacement and force over small displacements.

The stiffness of the beam is adjusted by changing the distance from the connector to the point of force application. It can be seen from equation 5 that changing the distance between these points changes the stiffness of the spring by a factor of $1/L^3$. Experiments are conducted at three separate length settings

1.22 m, 1.37 m, and 1.52 m. Calculating the spring constant using equation 15 yields constants of 56.77 N/m, 40.09 N/m and 29.35 N/m respectively.

$$k_z = \frac{3 \cdot E \cdot I}{L^3} \qquad \text{Eq. 15}$$

Thus diverse spring characteristics are achieved using a single bias element with different force application points.

8.4.3 Identification

Identification of the spring parameters is performed using a batch least squares algorithm. Separate motions are performed in each axis, allowing the isolation and identification of the dependent parameters. This approach is used to emulate both the force in z and the torque about y.

8.4.4 Issues

As is the case with Experiment 1, the control bandwidth of the manipulator in this experiment is 50 Hz. This relatively low bandwidth limits the speed at which the manipulator can be moved while in contact with the environment. Increasing the speed of the manipulator again yields oscillatory contact behavior.

The limitations of the control bandwidth motivate the simplified bias configuration described in the Model section of this chapter. Instability and damage to the manipulator are risked when axes are rigidly constrained by connection to ground. Without sufficient compliance, small jitters due to low bandwidth control create large forces. These forces can excite a divergent feedback loop, potentially commanding the manipulator in such a way as to damage equipment and people.

The force/torque sensor used in these experiments is different than that used in Experiment 1. The Experiment 2 sensor utilizes an onboard analog to digital converter with a 9 kHz sample frequency and built in noise filters. The combination of onboard analog to digital conversion and filters reduces signal noise. This allows for the more accurate emulation of bias and contact wrenches and ultimately, more gentle assembly of components.

The manipulator configuration in this experiment calls for the connection of the force/torque sensor to a mounting plate located distal to the final rotational joint. The joint incorporates a harmonic drive and is configured such that the flexspline is distal to the rest of the joint. Thus, the mounting plate is directly attached to a portion of the joint that periodically deforms. This deformation generates internal stresses in the mounting plate and subsequently phantom wrenches in the force torque sensor. A 0.025 m thick mounting plate is installed to reduce the effects of the deformation and bring the phantom wrenches to within the range of noise.

8.5 Results

8.5.1 Model Accuracy

Two separate bias models are presented in the Model section of this chapter. One is based on the physical structure of the bias element and the theory of statically determinate cantilever beams. The other assumes a simple linear relationship between system states and the resultant forces and torques.

The absolute values of the force and torque errors for each model as a function of sample number are shown in figure 8.5. This representation simplifies the comparison of model error over the entire workspace. In this illustration the top row shows the force and torque of the physical model and the bottom row shows the linear model.

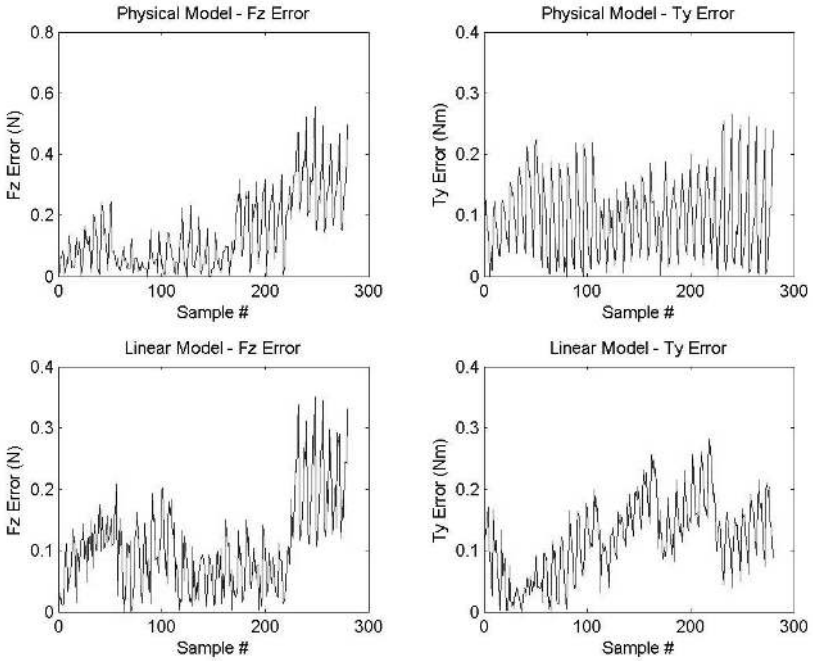

Figure 8.5 – Absolute values of force and torque errors for both the linear and the physical model.

Determination of the maximum errors for each axis provides the data needed for calculating the minimum contact force for unambiguous signals. Comparison of the respective force errors in the left column shows that the physical model has a larger maximum error of 0.56 N compared to 0.35 N in the linear model. The maximum torque error of the physical model is 0.26 Nm compared to 0.28 Nm for the linear model. The difference between these maxima is less than the sensor noise and is negligible. Although the smaller force error in the linear model may seem to indicate that the linear model is superior, the relative unimportance of force due to the small distance from the sensor to the center of contact makes the model performance nearly identical.

Based on the presented error data and the physical constraints of the system, the minimum force needed for an unambiguous signal can be calculated for each sample point. Determining the minimum force over a workspace allows the direct comparison of two models by weighting the force and torque errors based on the

physical constraints of the system. Figure 8.6 shows that the linear model requires a marginally smaller minimum force than the physically based model.

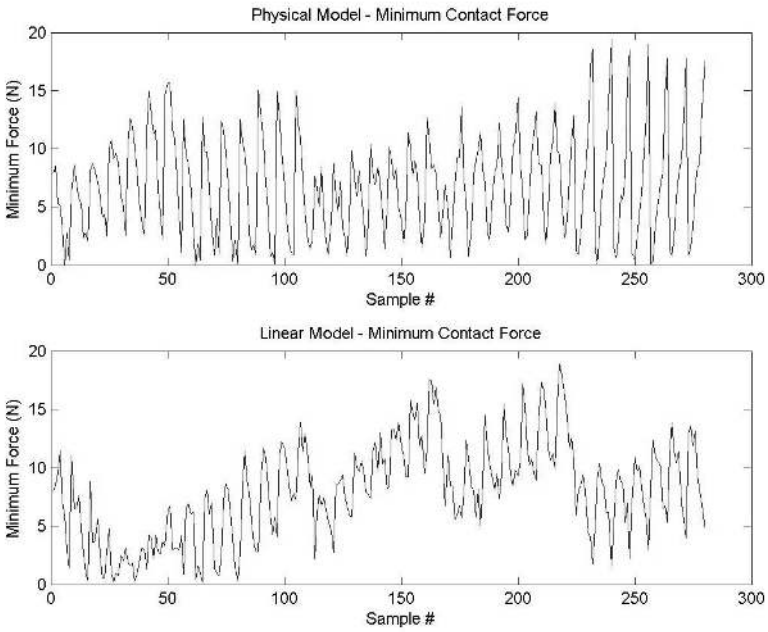

Figure 8.6 – Comparison of minimum required force for the physical and the linear model.

Given that the performance of both models is effectively the same the linear model is used for all subsequent experiments. This model is not only easier to realize but is also applicable to a larger set of bias sources. The realization and validation of general bias models enables the relaxation of assumptions associated with the physical model. For example, because the linear model is used for the experiments in this chapter there is no need to know the location of the roller support, a variable that is necessary if the physically based model is used.

Portions of the error maps from both of the models discussed are shown in figure 8.7. (A complete map can be found in Appendix 3) The pitted appearance of the maps is a result of sensor noise. The sensor noise experienced in this experiment is smaller than that of experiment 1. Table 1 illustrates that the

typical sensor noise from experiment 2 is approximately half that from experiment 1. This decrease in sensor noise is attributed in part to the superior force/torque sensing available for experiment 2 as discussed in the Experimental Setup – Issues section of this chapter.

Experiment	F_z	T_y
1	0.2 N	.05 Nm
2	0.1 N	.03 Nm

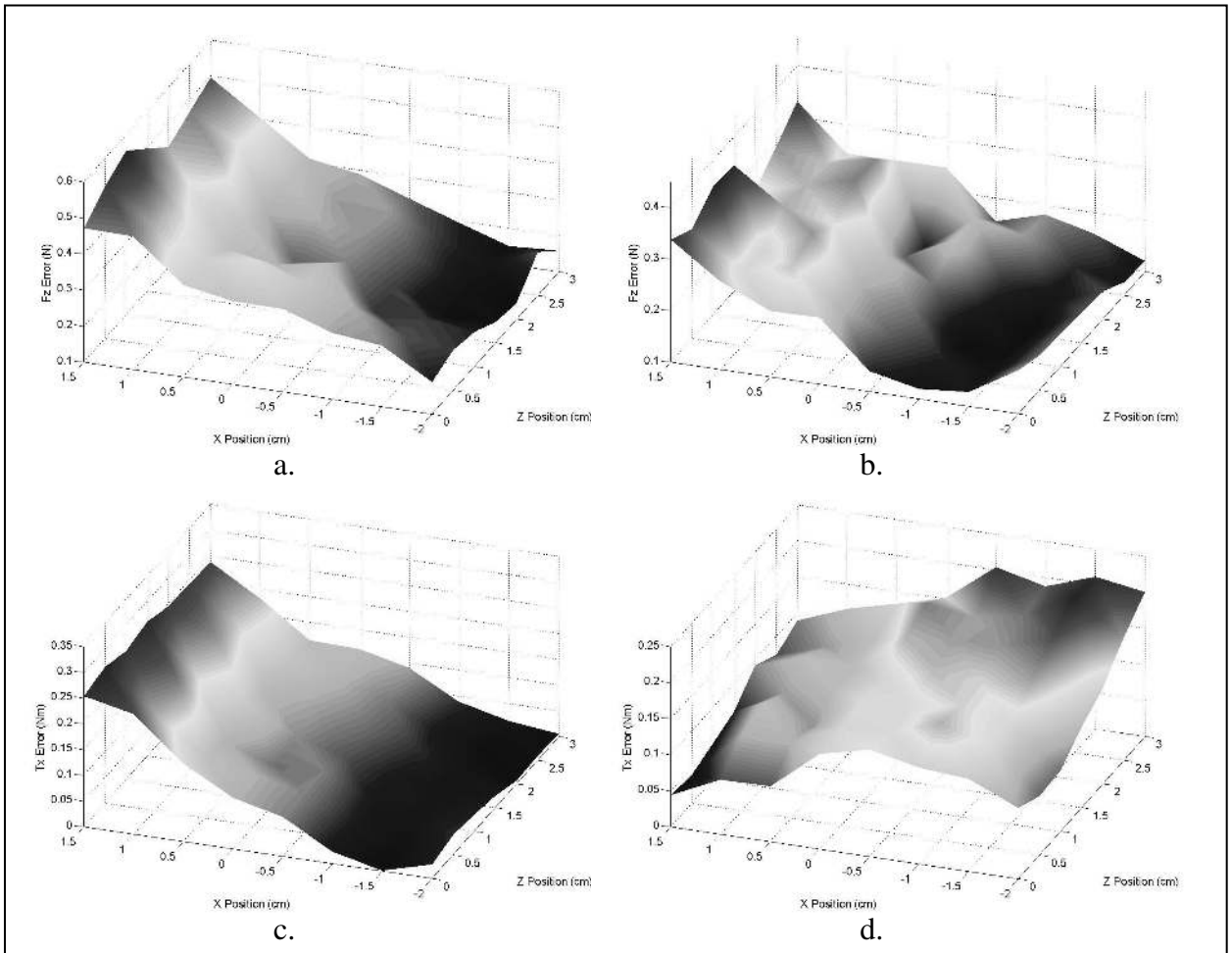

Figure 8.7 – Error maps for the physical and linear models at 5.5 degrees. a) Force map for physical model, b) Force map for linear model, c) Torque map for physical model, and d) Torque map for linear model.

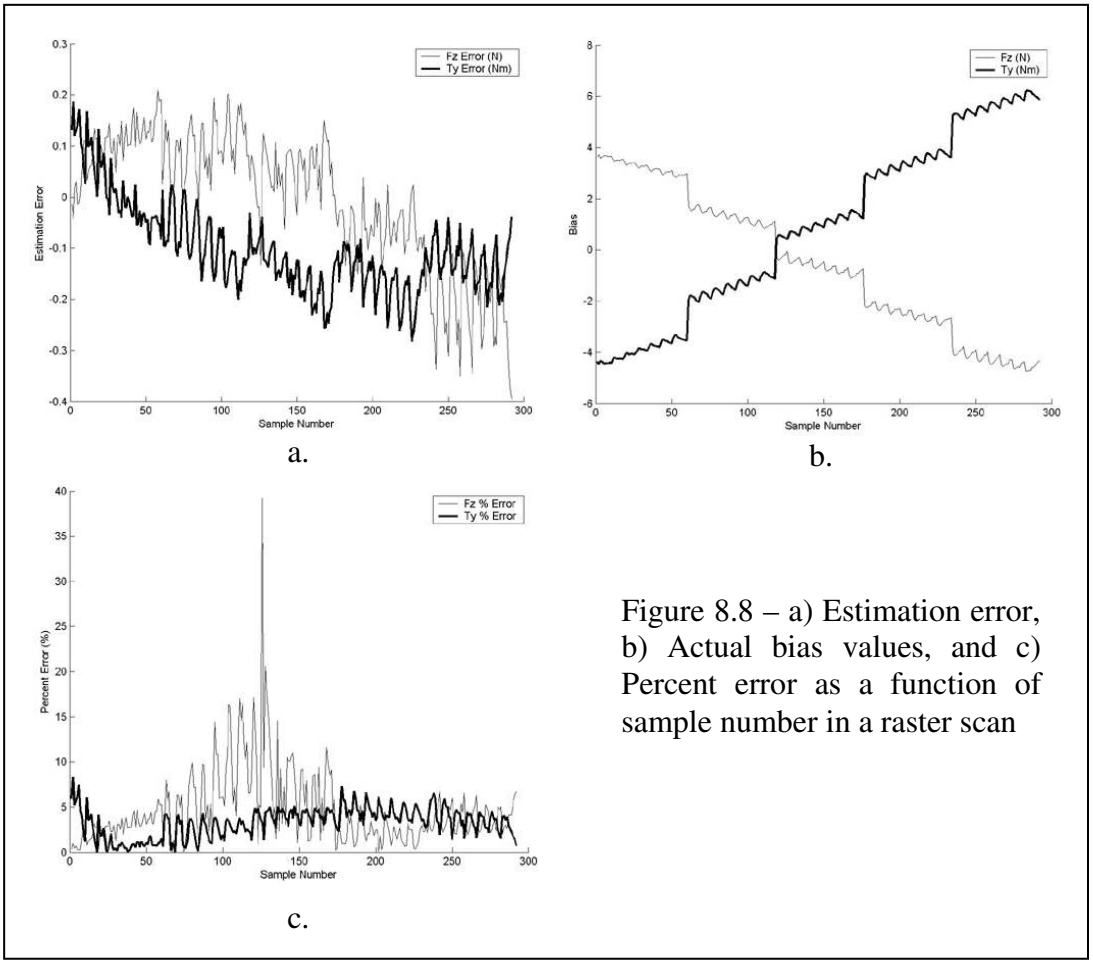

Figure 8.8 – a) Estimation error, b) Actual bias values, and c) Percent error as a function of sample number in a raster scan

The linear model estimates the forces and torques generated by the beam to within 0.35 N on the z axis and 0.28 Nm about the y axis. Figure 8.8a shows a two dimensional representation of the emulation error for each of the degrees of freedom over the workspace. Figures 8.8b and 8.8c show the corresponding bias and percent error respectively.

Given the connector-sensor geometry, the change in actual bias from figure 8.8b, and the 30 N limit on F_z the bias number is calculated:

$$B = \frac{\tau_{er} - F_{er} \cdot d_{sc}}{F \cdot d_{cd}} = \frac{10.98Nm + 8.42N \cdot 0.065m}{30N \cdot 0.015m} = 25.62$$

The value of B is significantly larger than unity, indicating that bias compensation is necessary to achieve gentle assembly.

8.5.2 Gentle Assembly

The actual and estimated F_z, and T_y during force guided assembly under cable bias are shown in figure 8.9. The assembly is again divided into three parts where events Alpha and Beta delineate transitions. As was described in the Results section of Chapter 7 – Experiment 1, the graphs show the assembly process starting from prior to contact to when flush assembly is achieved. Prior to event Alpha the connector performs guarded motion. Event Alpha corresponds to first contact between the connector and receptacle. When contact is made the connector advances without changing orientation until the minimum z axis force is established. Event Beta corresponds to the contact state which generates a stable resultant force in the z direction. Subsequent to event Beta the minimum force for an unambiguous contact signal is maintained (seen as the constant force offset between the F_z estimate and the actual F_z) and both orientation and position of the connector are modified until flush assembly is established.

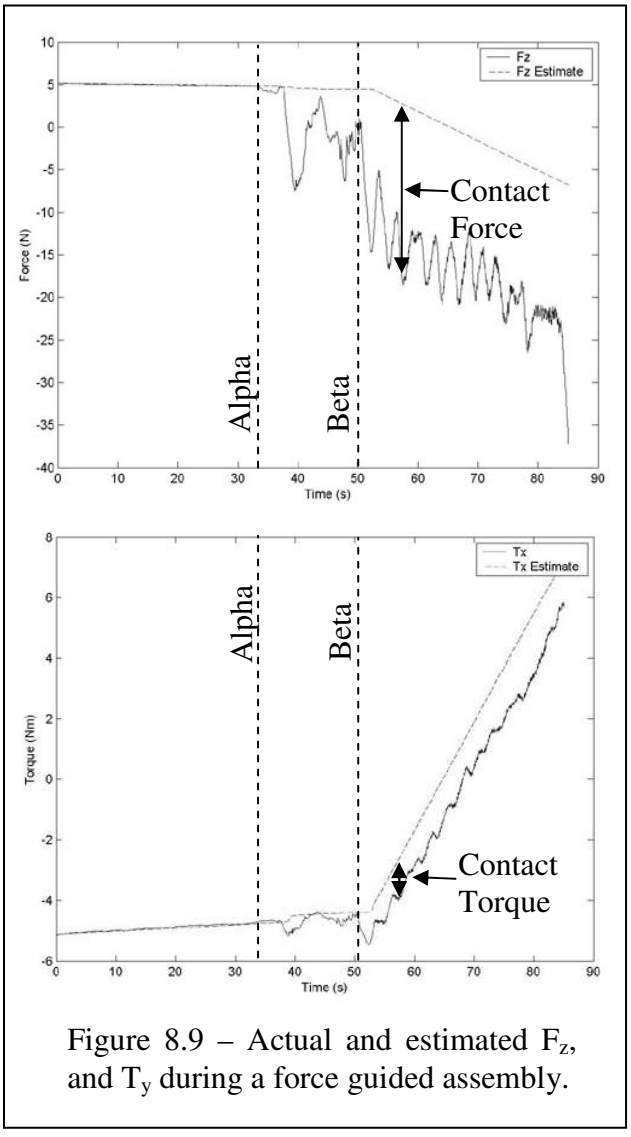

Figure 8.9 – Actual and estimated F_z, and T_y during a force guided assembly.

Thirty tests are performed to quantify the efficacy of the proposed model and approach. In each test the starting orientation and position relative to the receptacle are changed. The starting position is offset by ± 0.01 m in the x direction, - 0.01 m in the z direction and ± 5 degrees relative to the nominal starting position.

The angular errors introduced for this test were limited to ± 5 degrees. This was done to limit both the bias model error and the curvature of the beam. The curvature of the beam is a function of the orientation of the connector, the bending modulus (E·I), and the distance from the connector to the force application point. Thus a relatively small change in orientation can generate significant deformation in a beam depending on the other parameters. Given the configuration and parameters of the bias source in this experiment, limiting the change in orientation is necessary to maintain assumptions regarding small slopes at the force application point.

The maximum change in torque encountered over the workspace is 10.68 Nm and the change in force is 8.42 N. Given the physical dimensions of the connector, the uncompensated minimum necessary force is 739.91 N.

The compensated minimum necessary force is calculated using equation 14 in chapter 5 – Bias Number. The workspace used to determine the force and torque errors is equal to 0.03 m by 0.035 m. Based on a maximum torque error of 0.28 Nm and force error of 0.35 N, the minimum necessary force is 19.97 N. Thus, implementing the bias compensator yields a 97% reduction in necessary z axis force. The 19.97 N force is labeled as the contact force in figure 8.9. The actual value fluctuates around and below 19.97 due to connector motion.

The approach has a 97% success rate over the test set, failing once out of the 30 tests performed. This failure is due to the incomplete mating of the connector and receptacle. When the connector and receptacle contact in a configuration

similar to that shown in figure 8.10 it is possible for the parts to jam. This either prevents flush mating or causes the contact wrench to exceed the wrench limits.

The failed attempt was the 26th test in the series, the starting position was offset by approximately 0.0 m in x, -0.01 m in z and 1.0 degrees about y. Subsequent tests at the same starting position completed successfully.

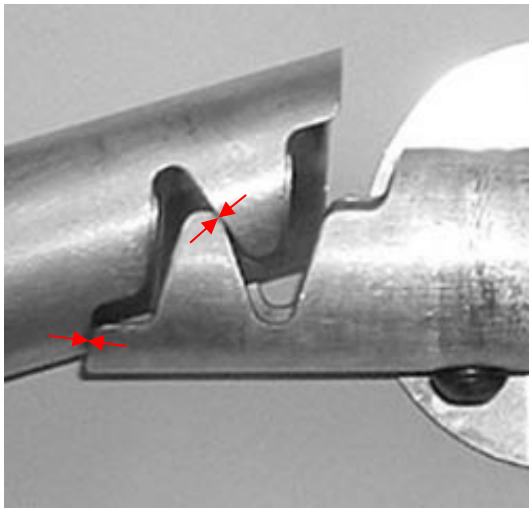

Figure 8.10 – Occasionally when the FAC1 contacts as shown, jamming may occur.

8.6 Traditional Approach

Traditional force guided assembly is implemented by removing the bias identification and compensation functions from the control code. The beam bias is assumed to be constant and the force/torque sensor is tared at the receptacle staging point to remove the bias wrench.

A set of ten tests are performed to confirm the failure of the traditional approach. The starting position and orientation of the connector are modified for each test. The starting position is offset by ± 0.01 m in the x direction, - 0.01 m in the z direction and ± 5 degrees relative to the nominal starting position. These values are identical to those used for the bias compensated approach. The traditional approach fails 100% of the time when under beam bias.

The failure modes encountered using the traditional force guided assembly approach include failure to achieve flush contact and the generation of excessive contact wrenches. As is discussed in the Traditional Approach section of

experiment 1, these failure modes result from the presence of uncompensated bias.

The failure rate in this experiment is greater than that of experiment 1 because of the comparatively high stiffness of the bias source. As the stiffness of the bias source increases so does the rate of change in the bias wrench as a function of displacement and orientation. Thus, even small changes in orientation and displacement yield large changes in bias wrenches and result in failed assembly.

Chapter 9

Experiment 2b – Dual Manipulator Assembly Under Spatial Domain Beam Bias

9.1 Motivation

The connection of multiple elements, that experience individual biases that can not be represented as a single bias, calls for dual manipulator assembly. Consider, for example, the configuration shown in figure 9.1. A robot, attached to ground, attempts to connect a pair of perpendicular longerons. Both of these elements are attached to a rigid structure, preventing motion

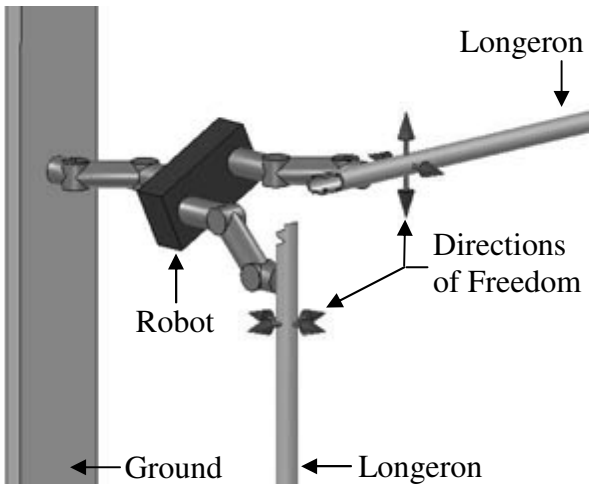

Figure 9.1 – Two constrained perpendicular longerons being assembled by a grounded robot.

along their respective axes. Without the freedom to move along the axis of the longeron, manipulating a single element does not ensure access to the receptacle position. (Figure 9.2) Thus, both longerons must be manipulated in order to achieve assembly. In this scenario, the robot is attached to ground and the forces applied to one element are not equal and opposite to the forces applied to the other. Consequently, multiple manipulators are required to individually identify the bias for each element and perform assembly.

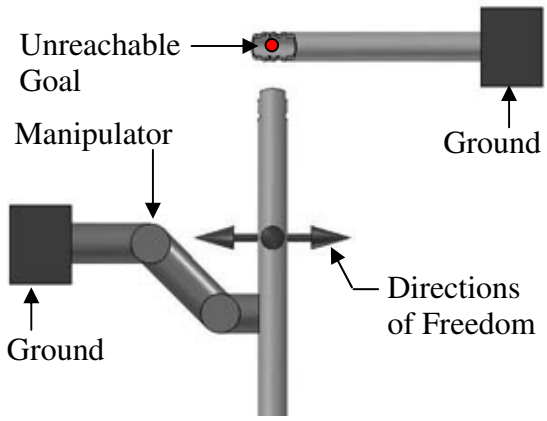

Figure 9.2 – In some assembly scenarios manipulating a single element does not ensure access to the receptacle position.

The accessible space for an axially constrained connector can be approximated as a plane for small deflections. When connector and receptacle are each attached to an axially constrained longeron the resultant assembly space is the intersection of the respective planes, a line, as shown in figure 9.3. The need to move both elements requires the identification of biases for each beam. This motivates the use of two force/torque sensors, referred to here as dual manipulator assembly.

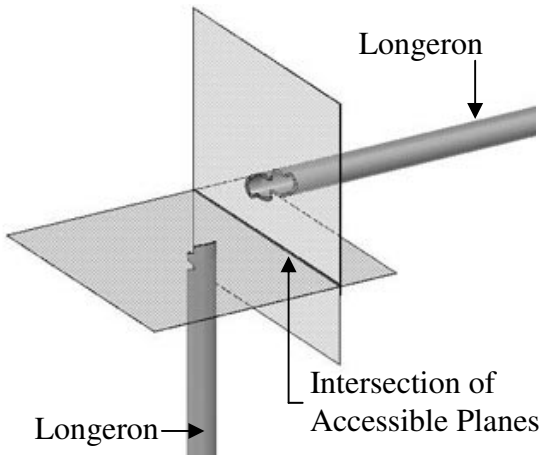

Figure 9.3 – The space where connector and receptacle may be joined is the line describing the intersection of the accessible planes.

As in the previous experiment, the axial stiffness associated with these elements is not emulated and the beam is allowed to comply along its

axis. This constrains the beam to a plane as with the true bias configuration, but does not rigidly attach the manipulator to the world frame. Although this approach yields a wholly different set of biases the concept and many of the lessons are directly applicable to the actual scenario.

9.2 Assumptions

All of the assumptions presented in the previous chapter regarding bending beams apply to both of the beams in this experiment.

In addition it is assumed that:

- The planes that describe the accessible space for each of the beams are orthogonal. The configurations of the experimental bias sources prevent changing the angle between the planes about the line of intersection. (Figure 9.4) Thus, misalignment of the connector and receptacle about this axis can not be compensated for.

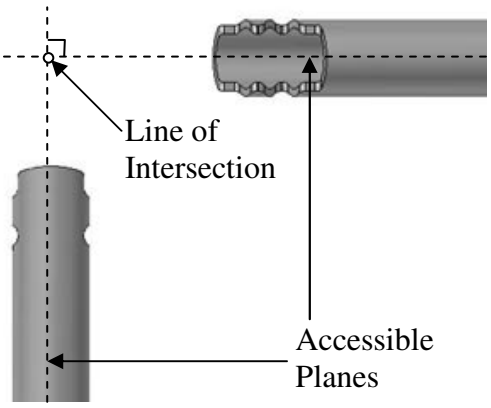

Figure 9.4 – The experimental setup mandates that the accessible planes remain perpendicular.

9.3 Model

The linear model used in the previous chapter is applied to both beams in the following experiment. This approach allows the individual identification of the parameters for each of the beams. Thus no assumptions need be made regarding similarity of beams.

9.4 Experimental Setup

9.4.1 Configuration

The configuration for the dual manipulator beam bias experiment is shown in figure 9.5. Experiments are performed using two seven degree of freedom manipulators each operating in a three dimensional space. The receptacle is attached to the second manipulator, allowing active motion to accommodate for misalignment.

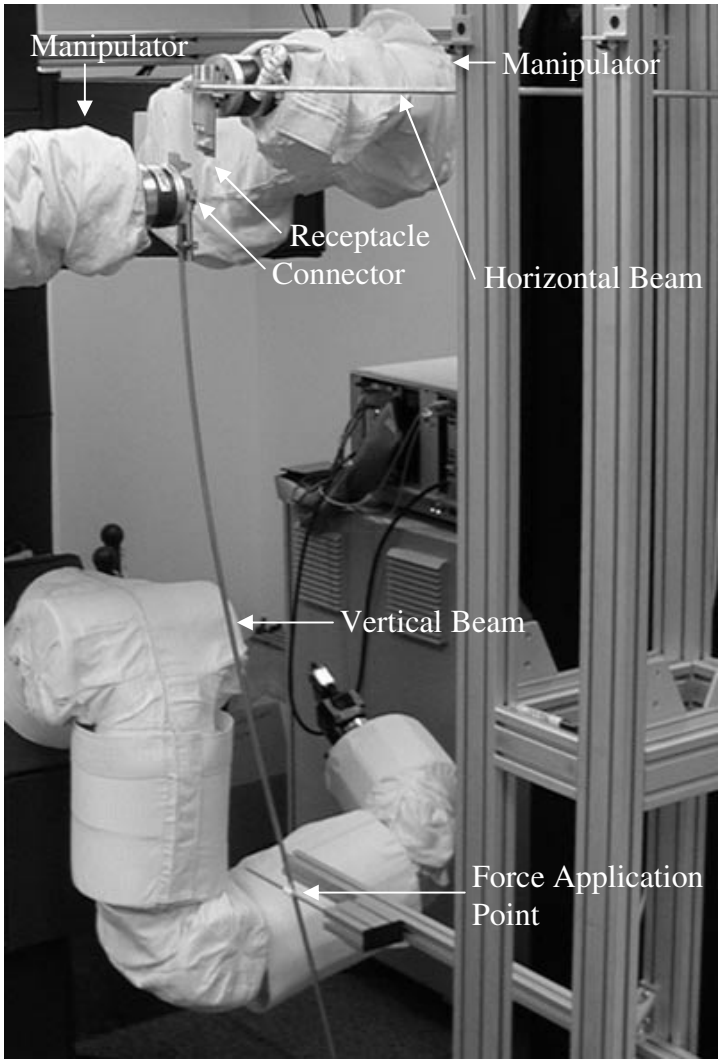

Figure 9.5 – Dual manipulator experimental configuration. (Force application point for horizontal beam is beyond the field of view.)

The bias elements contact the world frame through roller supports, the position of which are adjustable in both the x and y axes of the beams.

9.4.2 Bias Source

The bias sources for these experiments are two 10 mm diameter aluminum beams. The beams are clamped directly to the connector (and receptacle) at one end and contact the world frame through roller supports at the other end. Over small changes in displacement and orientation the forces and torques generated by the beams are approximately linear.

Beam stiffness is adjusted by changing the distance from the connector to the point of force application. The stiffness of the beam attached to the connector is modified during experiments. The bias configurations used during tests are the same as those used in Experiment 2. The stiffness of the receptacle beam is held constant through all experiments.

9.4.3 Identification

The same identification approach used for the previous experiment is implemented on each of the beams of this experiment.

9.4.4 Issues

The motivation behind the modified bias configuration extends from the limitations of the control bandwidth. In order to avoid potential damage to the manipulator the bias configuration does not include a rigid attachment from the manipulator to ground.

This modification changes the bias characteristics and subsequently the models used for emulation. One aspect of this change is the different orientation of the planar workspace. Figure 9.6 illustrates that the modified bias source operates in

a plane perpendicular to the clamped beam bias source that motivates this experiment. More importantly, the clamped beam is statically indeterminate and is described by governing equations wholly different than those used to describe the determinate cantilever case.

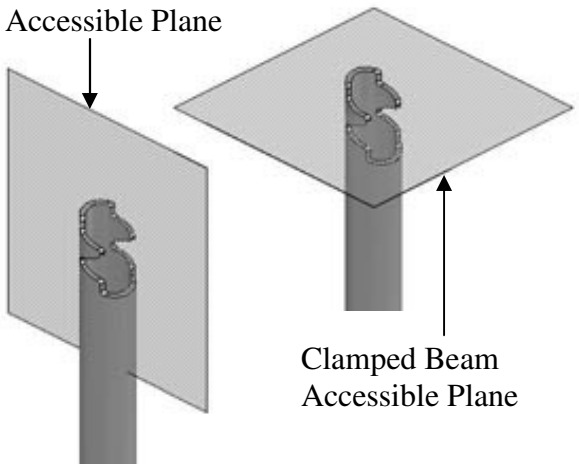

Figure 9.6 – The modified bias source used for this experiment has an accessible plane perpendicular to that of the clamped beam that motivates the experiment.

The bending beam bias sources are configured in such a way as to limit motion to a plane. As a result the completed assembly must fall on a line defined by the intersection of these two planes. Moreover, in order to complete an assembly the orientation between the connector and receptacle must be correct. Because there is no ability to change the angle between the planes, the relative starting orientation of the connector and receptacle must equal the final orientation.

The force/torque sensors used in this experiment are identical to those used in Experiment 2 and exhibit similar noise characteristics.

9.5 Results

9.5.1 Model Accuracy

The bias models used in this experiment are identical to those used for the single manipulator experiment. As such the models were not re-evaluated.

9.5.2 Gentle Assembly

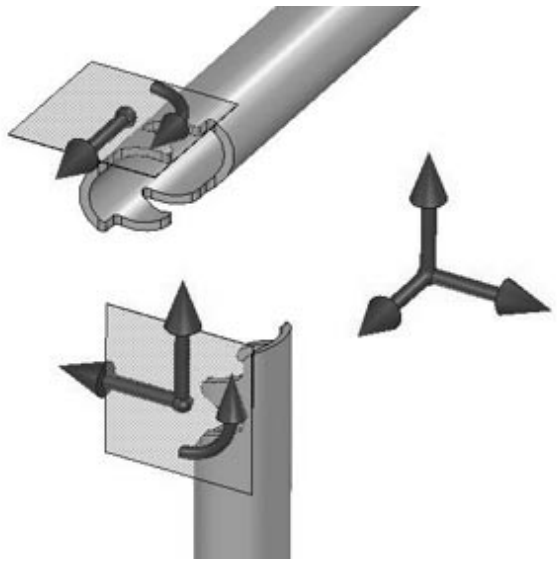

Figure 9.7 – Available degrees of freedom are divided between the two

Manipulator control for this experiment is conducted in a slightly different manner from the previous two experiments. Prior to contact, guarded motion is performed by both manipulators. Both are allowed to advance so that the bias estimators share the error accumulated by moving. Subsequent to contact the available degrees of freedom are divided between the two manipulators. (Figure 9.7) Thus, commands for translation in x and z and rotation about y are sent to one manipulator while translation in y and rotation about x are sent to the other. This approach simplifies the control code and prevents accidental motion of constrained axes.

The error maps used for the previous experiment are assumed to be directly applicable in this case. For this reason the maps were not reevaluated for the Model Accuracy section and the estimates of compensated and uncompensated minimum necessary force are the same as those discussed in the Gentle Assembly section of Chapter 8 – Experiment 2.

Twenty five tests are performed to quantify the efficacy of the proposed approach. The starting orientation and position of the connector and receptacle are modified between tests. The starting position of the connector is offset by ± 0.01 m in the x direction, - 0.01 m in the z direction and ± 5 degrees relative to the nominal starting position. The starting position of the receptacle is offset by ± 0.01 m in the y direction and +0.01 m in the z direction.

The approach has a 96% success rate over the test set, failing once out of the 25 tests performed. This failure is due to the incomplete mating of the connector and receptacle as a result of connector jamming. The failed attempt was the 3rd test in the series, the starting position was offset by approximately +0.005 m in x, -0.005 m in y and +5 degrees about y. Subsequent tests at the same starting position completed successfully.

9.6 Traditional Approach

The traditional approach tests performed for experiment 2 are considered directly applicable to this experiment and are not repeated.

Chapter 10

Experiment 3 – Assembly Under Independent Pendulum Bias

10.1 Motivation

The transport of a flexible beam results in beam oscillation. Thin walled longerons are stiff in the axial direction but flex readily under perpendicular loads. Manipulation and transport of such elements prior to connection can excite dynamics and yield harmonic oscillation with appreciable amplitude.

Longerons for space applications are characterized by lightweight, thin walled structure with relatively massive connectors at either end. These characteristics are best emulated by a complete dynamic model which is discussed in chapter 11.

A simpler approach is to assume that the longeron is well emulated by a single degree of freedom, torsional mass-spring-damper system. (Figure 10.1) This

system is emulated in the laboratory by a pendulum. This approach allows the application of well understood equations of harmonic motion while exploiting the effects of gravity to provide a simple and uniform torsional spring.

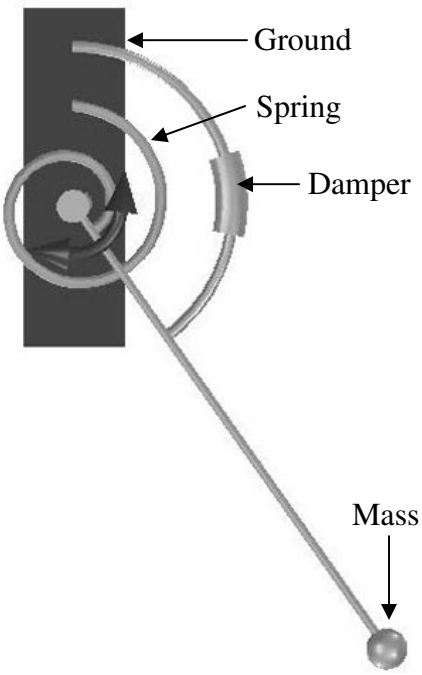

Figure 10.1 – A single degree of freedom, torsional mass-spring-damper system.

10.2 Assumptions

It is assumed that:

- Pendulum motion is independent of manipulator motion and pendulum state is entirely a function of the temporal domain. This assumption allows the simplified treatment of pendulums and avoids full dynamic modeling. It is only applicable if the direction of motion of the manipulator is orthogonal to the plane of oscillation or if the magnitudes of the accelerations from manipulator motion are small enough as to be considered negligible.

- Connector and receptacle are properly oriented and all error stems from position uncertainty. This assumption further simplifies the treatment of the dynamic system, eliminating the need to transform wrenches into alternate coordinate frames.

- The pendulum oscillates in a plane. The model is not sufficient to emulate wrenches generated by oscillation in three-space.

- The coefficient of viscous damping is sufficiently small as to be negligible. This allows the asymptotic decrease in amplitude of the forces to be ignored

over the time span under consideration. Addition of a damping term is possible but not considered for this experiment.

- The duration of pendulum oscillation is long enough to both learn the wrench emulation parameters and perform assembly. This assumption ensures that the bias wrenches will remain interesting over the entire assembly process.

- The angle through which the pendulum swings is sufficiently small that small angle approximations remain applicable. This assumption enables the linearization of sinusoid terms for small angles.

10.3 Model

The configuration of the pendulum for this experiment is shown in figure 10.2. Due to the assumption of independence, the beam oscillation can be modeled as a function of time only. This means that bias wrenches are harmonic functions and allows the use of equations that describe harmonic oscillation to emulate the bias wrenches.

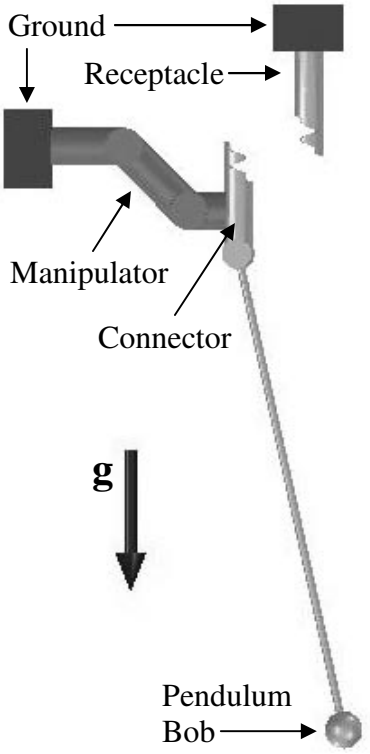

Figure 10.2 – Pendulum model and experimental configuration.

The assumptions constraining the oscillation to a plane and precluding changes in connector orientation allow the bias to be modeled as only two forces. The equation of motion for the pendulum is shown in equation 1.

$$ml^2\ddot{\theta} + mgl \cdot \sin\theta = 0 \qquad \text{Eq. 1}$$

Where m is the mass of the pendulum, l is the length of the pendulum arm and g is the acceleration due to gravity. If the pendulum angle remains small the sine of theta is approximately equal to theta. By substituting and rearranging, equation 1 can be approximated as:

$$\ddot{\theta} + \omega_n^2 \theta \approx 0 \qquad \text{Eq. 2}$$

Where ω_n is equal to $\sqrt{g/l}$. The solution of equation 2 is presented in equation 3.

$$\theta(t) = A \cdot \sin(\omega_n t + \phi) \qquad \text{Eq. 3}$$

Where A is the amplitude of the oscillation and ϕ is the phase shift. The point at which the time equals zero can be set arbitrarily and is chosen such that ϕ equals zero.

The force diagram for the pendulum is shown in figure 10.3. Equation 4 describes the force applied to the pendulum bob in the radial direction. This force is reacted on the connector and yields the bias forces for the system.

$$F_r = mg\cos\theta + ml\dot{\theta}^2 \qquad \text{Eq. 4}$$

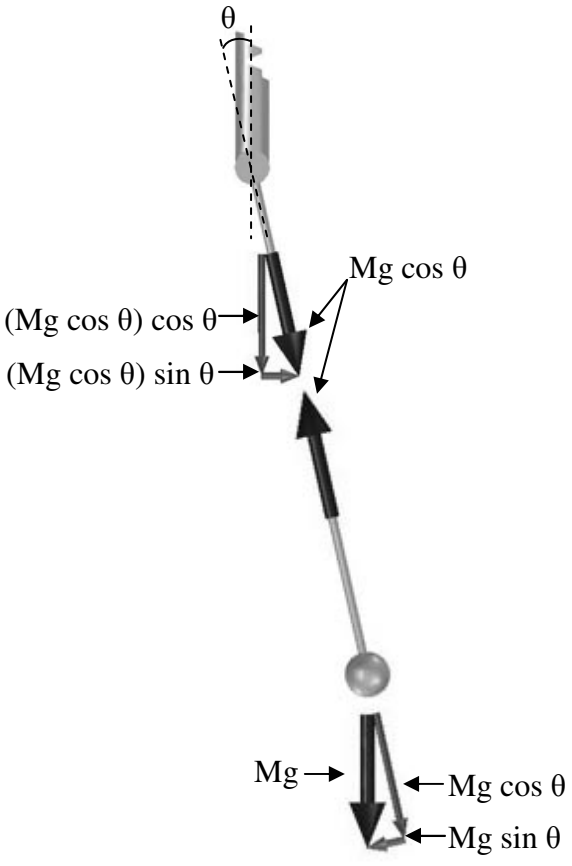

Figure 10.3 – Pendulum force diagram.

Where the first term is due to gravity and the second stems from radial acceleration. Thus the forces in the x and z directions are:

$$F_x = F_r \sin\theta \qquad \text{Eq. 5}$$

$$F_z = F_r \cos\theta \qquad \text{Eq. 6}$$

Taking the derivative of equation 3 and expanding equations 5 and 6 the full expressions for the forces in x and z can be determined.

$$F_x = mg\left(\cos\left(A\cdot\sin(\omega_n t)\right) + A^2\cos^2(\omega_n t)\right)\sin\left(A\cdot\sin(\omega_n t)\right) \qquad \text{Eq. 7}$$

$$F_z = mg\left(\cos\left(A\cdot\sin(\omega_n t)\right) + A^2\cos^2(\omega_n t)\right)\cos\left(A\cdot\sin(\omega_n t)\right) \qquad \text{Eq. 8}$$

Again drawing on the small angle approximation the sine of theta is replace by theta and the cosine of theta is replace by unity.

$$F_x \approx mg\left(A\cdot\sin(\omega_n t) + A^3\cos^2(\omega_n t)\sin(\omega_n t)\right) \qquad \text{Eq. 9}$$

$$F_z \approx mg\left(A^2\cos^2(\omega_n t) + 1\right) \qquad \text{Eq. 10}$$

The term $A^3\cos^2(\omega_n t)\sin(\omega_n t)$ in equation 9 is much less than $A\cdot\sin(\omega_n t)$, thus the force in the x direction can be approximated as shown in equation 11. Also, $\cos^2(\omega_n t)$ can be represented as $\frac{1}{2}+\frac{1}{2}\cos(2\omega_n t)$ and the force in the z direction can be estimated as shown in equation 12.

$$F_x \approx mgA\cdot\sin(\omega_n t) \qquad \text{Eq. 11}$$

$$F_z \approx \frac{mgA^2}{2}\cos(2\omega_n t) + \left(\frac{mgA^2}{2} + mg\right) \qquad \text{Eq. 12}$$

Thus, the forces in the x and z directions can be estimated as simple time dependent sinusoids with an unknown amplitude, period and offset.

10.4 Experimental Setup

10.4.1 Configuration

The pendulum experimental configuration is shown in figure 10.4. Experiments are performed using a seven degree of freedom manipulator operating in a two dimensional space. The receptacle is attached to an adjustable receptacle mount which is attached to the world frame. Unlike previous experiments the bias element does not contact the world frame.

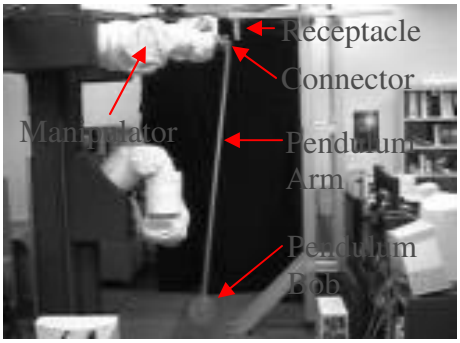

Figure 10.4 – Pendulum experimental configuration.

10.4.2 Bias Source

The bias source for these experiments is a 3 kilogram aluminum disk attached to a rigid 1.8 m pendulum arm. The pendulum is attached to the connector at one end and allowed to swing freely. The amplitude of the oscillation is modified with every test.

10.4.3 Identification

It is assumed that the amplitude of oscillation, period, phase shift, and force offset are all unknown. The period of the sinusoid is determined by identifying four local maxima and determining the average time between them. The same maxima are used to determine the amplitude of the sinusoid. Setting the value of time to equal zero at the first maxima implies that the sinusoid is cosine and the phase shift is zero. The force offset is determined by calculating the average

value of over the three periods. This approach is applied to each of the force axes individually and no relationship between periods or amplitudes is assumed.

10.4.4 Issues

As in the other experiments, the control bandwidth of the manipulator mandates relatively slow assembly speeds. In addition, the 50 Hz control bandwidth limits control accuracy.

The oscillation of the pendulum exerts a sinusoidal force on the manipulator. The PD joint controller is unable to compensate for this force and the control bandwidth is too slow to implement a better performing controller. Thus the pendulum incites an oscillation in the manipulator with amplitude of approximately 3 mm.

The force/torque sensor used in these experiments is the same as those used for experiments 2 and 2b.

10.5 Results

10.5.1 Model Accuracy

Model accuracy of the independent pendulum can be determined from assembly data. Figure 10.5 shows the signal, estimate and error during a sample assembly. Prior to contact at 27 seconds, the divergence of the model from the real system is evident from the steady increase in the error amplitude. This trend continues throughout the contact portion of the assembly.

The error signal is a result of errors in multiple parameters. Part of the error is a product of the unmodeled effects of damping. The real system has a small damping constant that has an appreciable effect on the amplitude of the real

signal over the time span. Figure 10.6 shows the reduction in the error signal when damping is added to the model. The figure illustrates damping has a significant effect over the timeframe examined.

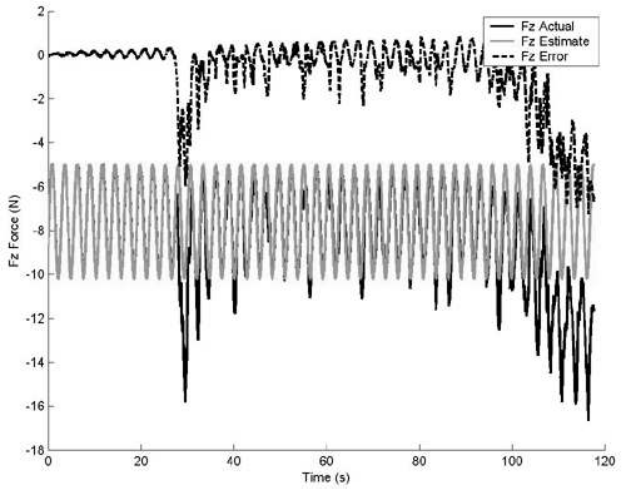

Figure 10.5 – F_z Actual, F_z Estimated and F_z Error.

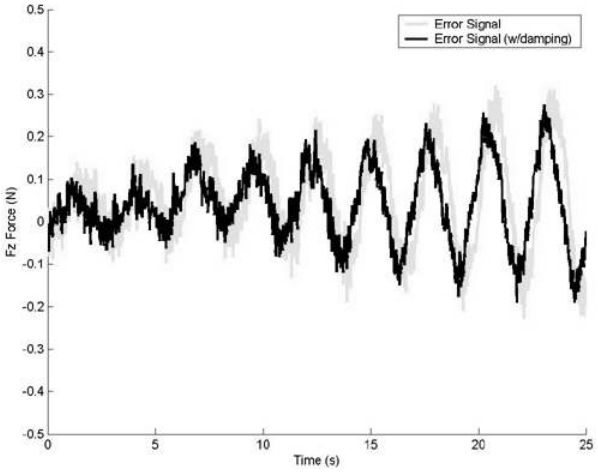

Figure 10.6 – Change in error signal when damping parameter is more accurate.

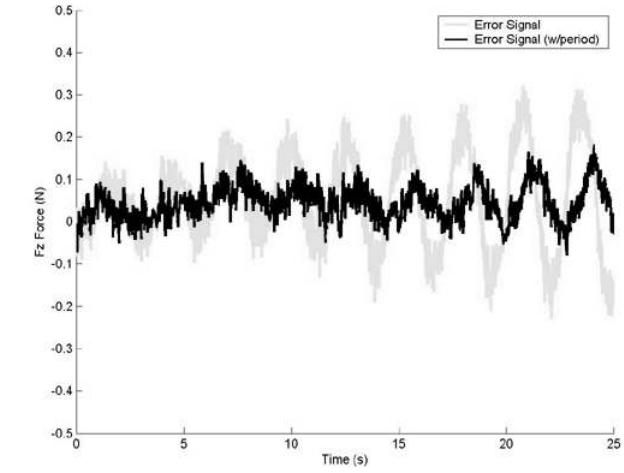

Figure 10.7 – Change in error signal when period parameter is more accurate.

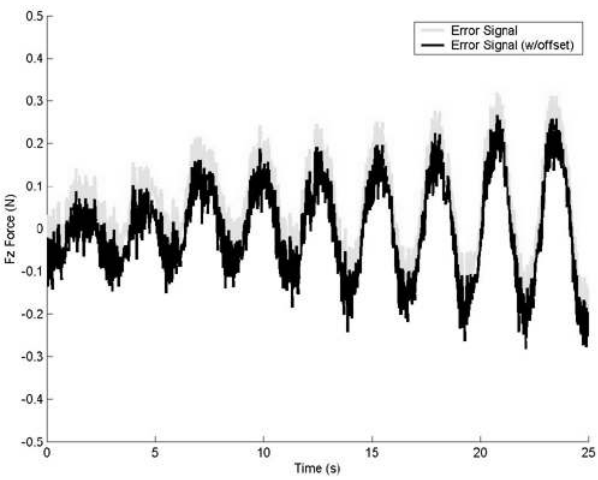

Figure 10.8 – Change in error signal when offset parameter is more accurate.

Careful inspection of the data from figure 10.5 shows that the period error is approximately 0.13%. Although this value is very small, it also has an

appreciable effect on the error. Accounting for the contribution of period error reduces the error signal as shown in figure 10.7.

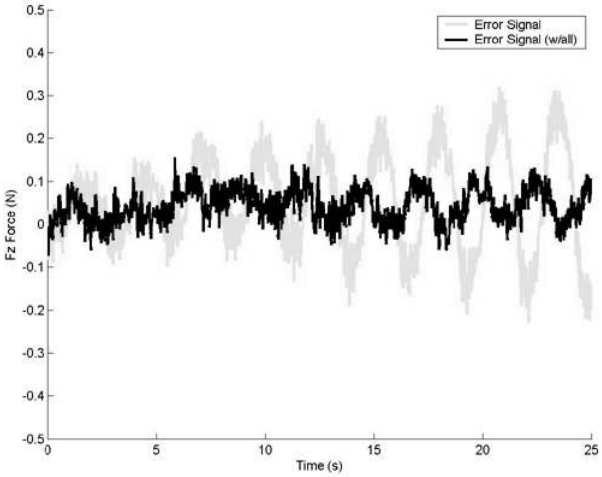

Figure 10.9 – Change in error signal when all parameters are more accurate.

The average value of the error over the first eight periods of the error signal is 0.0534 N. This value indicates that the estimate of force offset also displays error as shown in figure 10.8. The phase shift of the signal is small enough that it is obscured by the sensor noise and is not estimated for this experiment.

Removing the effects of all of the parameter errors from the error signal enables the visualization of the effects of those errors. (Figure 10.9) The parameter error estimates presented in this section are not perfect due to the effects of sensor noise, thus the error signal presented in the figure is not zero.

10.5.2 Gentle Assembly

The actual and estimated F_z during force guided assembly under pendulum bias are shown in figure 10.10. The assembly is again divided into three parts where events Alpha and Beta delineate transitions. The graph shows assembly from prior to contact to flush connection. Prior to first contact (Event Alpha)

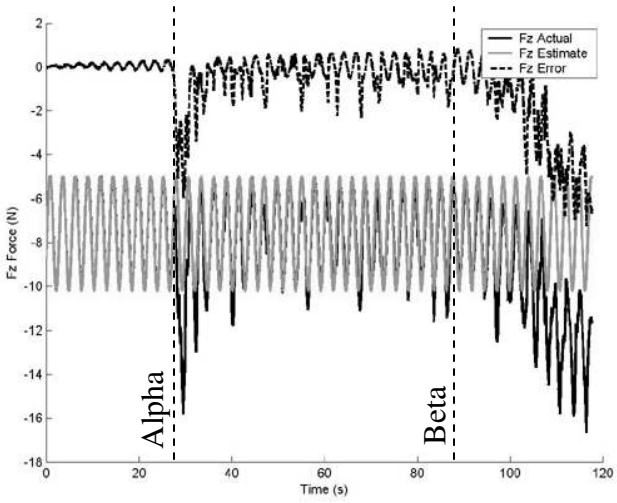

Figure 10.10 – Actual and estimated F_z during force guided assembly under pendulum bias.

guarded motion is performed. Between events Alpha and Beta the connector advances, adjusting for misalignment in the y axis. At event Beta the connector and receptacle are correctly mated. Subsequent data shows that the connector advances until a minimum z axis force is established.

Event Alpha, the transition from guarded motion to sliding contact, is show in figure 10.11. Left of the event, the forces exerted on the connector are due solely to bias, consequently the difference between actual and estimated bias yields the estimator error. At the point of contact the estimator error is approximately 0.3 N and increasing. After contact the data shows that the connector periodically contacts the receptacle until event Beta.

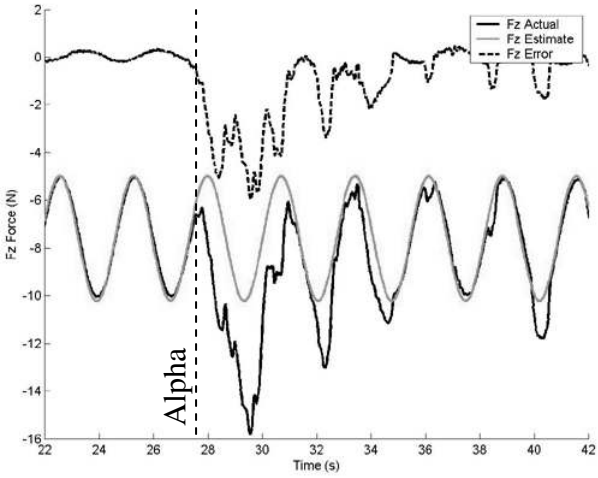

Figure 10.11 – Zoomed in view of event Alpha.

Event Beta, the transition from sliding contact to flush contact, is shown in figure 10.12. Due to the manipulator oscillations discussed in the Experimental Setup - Issues section of this chapter, there is no exact point of transition. Rather, as the manipulator oscillates, the connector repeatedly makes and breaks contact. The points labeled A show that as the pendulum swings forward contact is

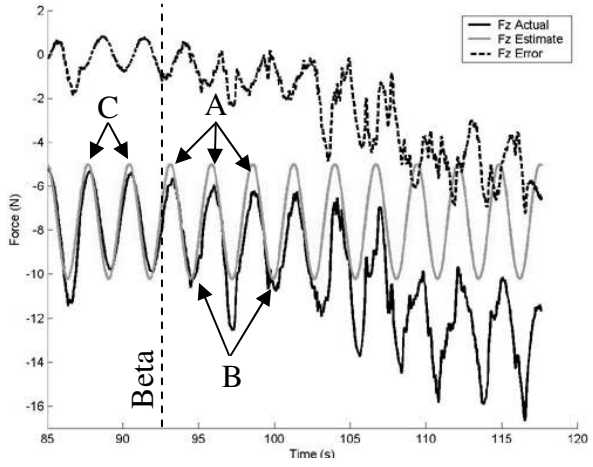

Figure 10.12 – Zoomed in view of event Beta.

established and the actual force is less than that expected. At the same time the points labeled B show that as the pendulum swings backward contact is broken and the actual force is consistent with the estimate. Also evident in this figure is the amplitude error that stems from damping and is discussed in the Model Accuracy portion of this chapter. The estimation error due to amplitude error is seen at the points labeled C. The divergence of the actual value from the estimated value is a result of contact wrenches.

A portion of the actual and estimated forces in the x direction are shown in figure 10.13. The signal to noise ratio of this data is approaching unity; consequently the estimator incorrectly identifies the system parameters and the estimation error is greater than the signal amplitude. This failure illustrates the brittle nature of the approach implemented and advocates a more robust identification approach. In this case, using only the force offset to estimate the bias force would have yielded better results than achieved.

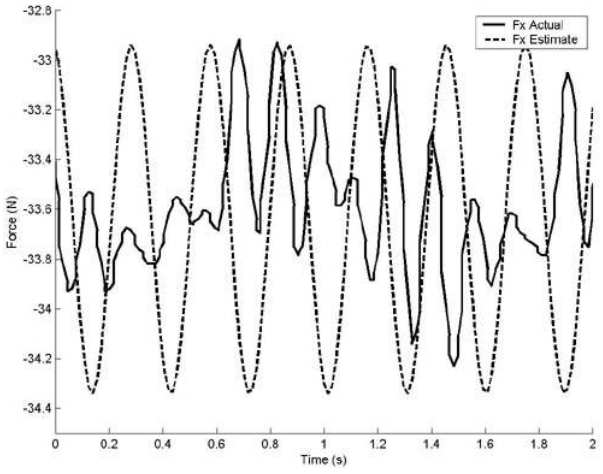

10.13 – Sample of actual and estimated forces in the x direction.

Unlike previous tests, a minimum z axis force is not needed to disambiguate contact points. This is due to the assumption that the orientation of the connector is known. For this reason the comparison of compensated and uncompensated minimum necessary force is not conducted for this experiment. However, a minimum force is still needed to establish when flush and stable contact has been established.

A set of 15 tests are performed to quantify the efficacy of the proposed model and approach. In each test the starting position relative to the receptacle is changed. The starting position is offset by ± 0.015 m in the x direction and - 0.02 m in the z direction relative to the nominal starting position.

The approach has a 100% success rate over the test set, not failing during the 15 tests performed.

10.6 Traditional Approach

In the traditional approach the manipulator moves the connector directly to the receptacle staging point. Wrench data is gathered prior to engaging the receptacle so that the force offset can be determined for each axis. This data is used to tare the sensor. Using the force offset is, in itself, a form of bias compensation and the argument could be made that taring the sensor with the bias wrenches at a particular instant in time is a better representation of the traditional approach. Regardless, the chosen approach is more robust and has a better chance of completing assembly.

A series of ten tests are performed to verify the failure of this approach. The starting position is offset by ± 0.015 m in the y direction and - 0.02 m in the z direction relative to the nominal starting position.

The traditional approach fails 100% of the time when under pendulum bias. As the bias oscillates about the force offset the controller transitions between several different states. Figure 10.14 illustrates an example scenario in which a pendulum swings from region 1 to region 4. During the swing the control

Region	Control Command
1	Retract – Speed 2
2	Retract – Speed 1
3	Hold Position
4	Advance – Speed 1

Table 10.1 – Different control commands are issued in each region.

commands transition as shown in table 10.1. This pattern reverses as the pendulum returns to the initial region. As long as the pendulum oscillates, the control commands will also transition. In the presence of damping, the amplitude of oscillation decreases over time, incrementally eliminating control commands until the advance command is the only command issued.

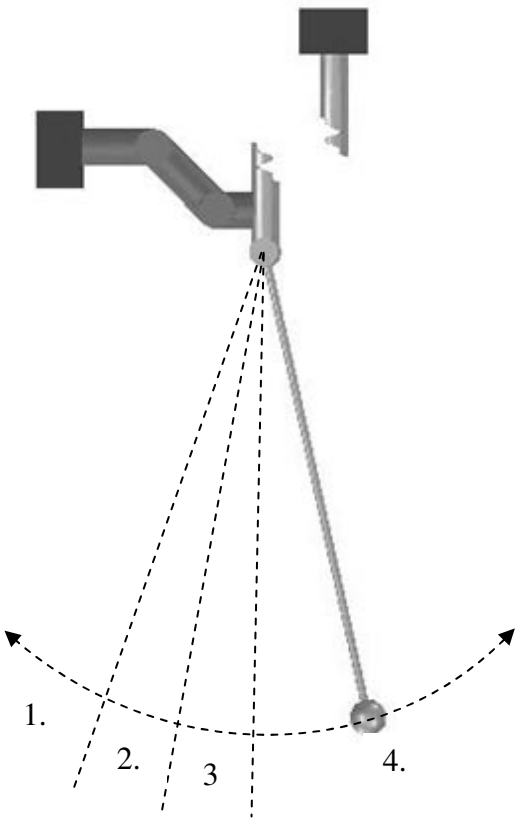

Figure 10.14 – If bias is not compensated the motion of the pendulum creates fictitious contact commands.

The command transitions described in the example occur in the actual experiments using the traditional approach. Conflicting commands are issued in a periodic manner, preventing the efficient and deliberate contact outlined in the Success Criteria section of chapter 6 – Experimental Introduction. Although the traditional approach does on occasion result in flush contact, assembly times are nearly twice as long because control commands oscillate between the hold and advance commands. This command oscillation and extended duration assembly disqualify even flush connections from being counted as successful.

Chapter 11

Experiment 4 – Assembly Under Spatial-Temporal Pendulum Bias

11.1 Motivation

Gossamer and low mass construction components, prevalent in the space environment, often exhibit flexibility in one or more axes. The application of loads during transport or manipulation can excite harmonic oscillation, a form of bias. The simplified model presented in chapter 10 – Experiment 3 does not account for the changes in oscillation due to acceleration of the component.

Accounting for these accelerations relaxes a significant assumption, that accelerations are small enough or perpendicular to the plane of oscillation such that the oscillating body may be considered independent. Introducing a model that accounts for the state of the bias source enables the application of this approach to a more general class of components.

11.2 Assumptions

It is assumed that:

- The angles through which pendulums swing is sufficiently small that small angle approximations remain applicable. This assumption enables the linearization of sinusoid terms for small angles.

- Pendulums swinging at small angles may be approximated as two masses connected by springs and dampers vibrating along a line. This assumption allows the application of a single-input single-output adaptive observer. Where the system input is the applied force and the output is position of the connector. (Figure 11.1)

- The duration of pendulum oscillation is long enough to both identify parameters and perform assembly. This assumption ensures that the bias wrenches will remain interesting over the work time span. When damping

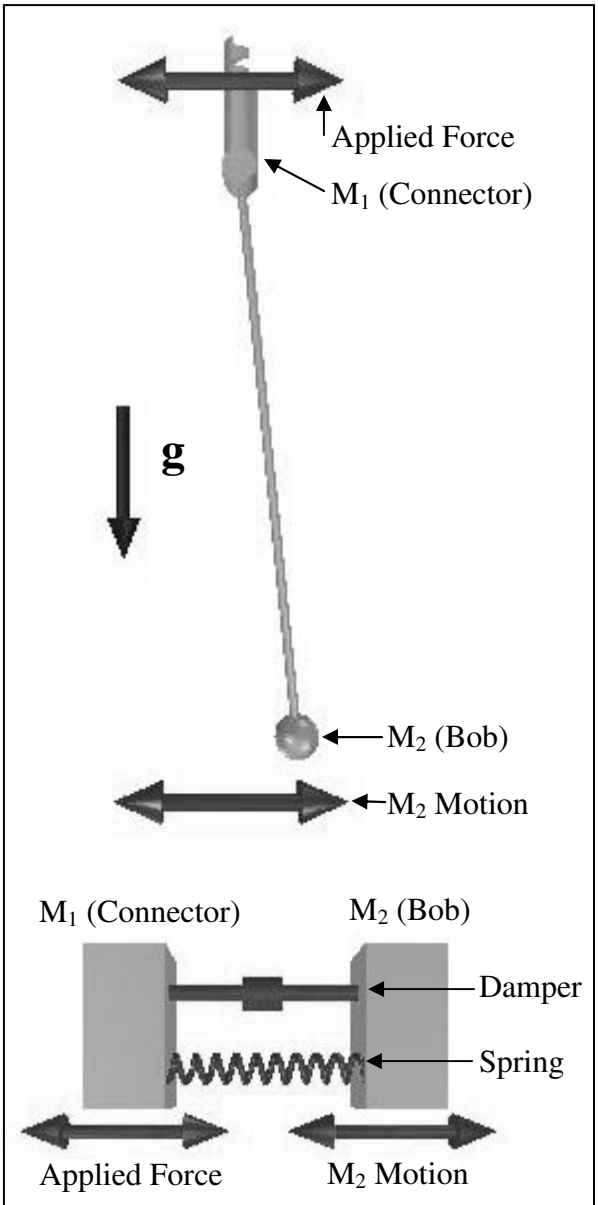

Figure 11.1 – Pendulums swinging at small angles can be modeled as two masses connected by a spring and damper.

is present the bias becomes less and less significant as the assembly progresses.

11.3 Model

The configuration of the pendulum for this experiment is identical to the configuration from the previous chapter and is shown in figure 11.2. The oscillation of the pendulum is constrained to a single plane, this causes the pendulum bob to travel along a nearly straight curve and allows the assumption regarding motion along a straight line.

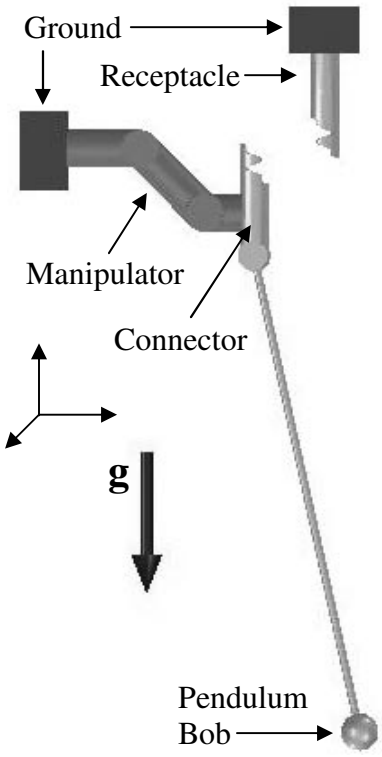

Figure 11.2 – Pendulum model and experimental configuration.

The dynamic equations of motion for a pendulum with an attachment point that may move in the z direction and a viscous damper are: (equation 1)

$$m_2 l^2 \ddot{\theta} - b\dot{\theta} - m_2 g l \cdot \sin\theta = -m_2 \ddot{z}_1 l \cos\theta \qquad \text{Eq. 1}$$

Where m_2 is the mass of the pendulum bob, l is the length of the pendulum arm, b is the coefficient of viscous damping, g is the acceleration due to gravity, θ is the angle between the gravity vector and the pendulum arm, and z_1 is the horizontal displacement of the connector. Rearranging yields:

$$\ddot{\theta} = \frac{b\dot{\theta}}{m_2 l^2} + \frac{g}{l} \cdot \sin\theta - \frac{\ddot{z}_1}{l}\cos\theta \qquad \text{Eq. 2}$$

Given the geometry illustrated in figure 11.3 and equations 3 through 6, equation 2 may be simplified. (equation 7)

$$\sin\theta = \frac{z_2 - z_1}{l} = \frac{z}{l} \qquad \text{Eq. 3}$$

$$\cos\theta = \frac{x}{l} = \frac{\sqrt{l^2 + (z_2 - z_1)^2}}{l} = \frac{\sqrt{l^2 + z^2}}{l} \qquad \text{Eq. 4}$$

$$\dot{\theta} = \frac{\dot{z}}{l\cos\theta} = \frac{\dot{z}}{x} \qquad \text{Eq. 5}$$

$$\ddot{\theta} = \frac{\ddot{z}}{x} + \frac{\dot{z}z}{x^2} \qquad \text{Eq. 6}$$

$$\ddot{z}_2 - \ddot{z}_1 = -\frac{b\dot{z}}{m_2 l^2} - \frac{gzx}{l^2} - \frac{\ddot{z}_1 x^2}{l^2} - \frac{\dot{z}z}{x} \qquad \text{Eq. 7}$$

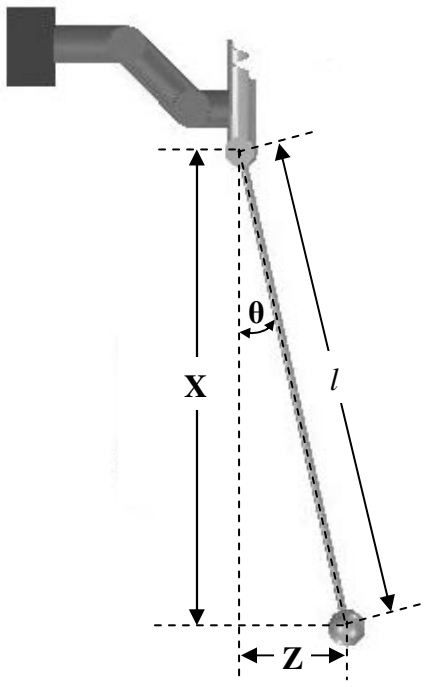

Figure 11.3 – Pendulum geometry.

Given that at small angles of θ the value of x may be approximated as L, equation 7 is solved for the acceleration of the pendulum bob in z coordinates. (equation 8)

$$\ddot{z}_2 = -\frac{b\dot{z}}{m_2 l^2} - \frac{gz}{l} - \frac{\dot{z}z}{l} \qquad \text{Eq. 8}$$

Determining the equations of motion for the connector, m_1, requires the derivation of the forces applied by the bob to the connector. (equation 9)

$$F_R = m_2 g\cos\theta + m_2 \ddot{z}_1 \sin\theta + m_2 \dot{\theta}^2 l \qquad \text{Eq. 9}$$

Given the radial force, F_R, the equation of motion for the connector in mixed coordinates is: (equation 10)

$$m_1 \ddot{z}_1 = F_A + F_R \sin\theta \qquad \text{Eq. 10}$$

Where F_A is the force applied by the manipulator. Expanding and simplifying using equations 3 though 6 yields: (equation 11)

$$m_1\ddot{z}_1 = F_A + \frac{m_2 gzx}{l^2} + \frac{m_2\ddot{z}_1 z^2}{l^2} - \frac{m_2\dot{z}^2 z}{x^2} \qquad \text{Eq. 11}$$

Solving for the acceleration of the connector and simplifying: (equation 12)

$$\ddot{z}_1 = \frac{F_A}{m_1 + \frac{m_2 z^2}{l^2}} + \frac{m_2 gzx}{m_1 l^2 - m_2 z^2} - \frac{m_2\dot{z}^2 z}{m_1 x^2 - \frac{m_2 z^2 x^2}{l^2}} \qquad \text{Eq. 12}$$

Applying the small angle assumption where $x/l \approx 1$ yields: (equation 13)

$$\ddot{z}_1 = \frac{F_A}{m_1 + \frac{m_2 z^2}{l^2}} + \frac{m_2 gzx}{m_1 l^2 - m_2 z^2} - \frac{m_2\dot{z}^2 z}{m_1 x^2 - m_2 z^2} \qquad \text{Eq. 13}$$

If m_1 is greater than or approximately equal to m_2, the term $m_2 z^2$ becomes negligible, leading to: (equation 14)

$$\ddot{z}_1 = \frac{F_A}{m_1} + \frac{m_2 gz}{m_1 l} - \frac{m_2\dot{z}^2 z}{m_1 x^2} \qquad \text{Eq. 14}$$

The final terms on equations 2 and 14 are the last remaining non-linear terms in the equations of motion. If the acceleration and subsequently the velocity remains small, these terms also approach zero.

Thus, the equations of motion for a pendulum can be represented as shown in equations 15 and 16 if it: 1) has a driven attachment point that moves along the z

axis, 2) exhibits damping, 3) swings through small angles, 4) has a connector mass, m_1, that is greater than or approximately equal to the bob mass, m_2, and 5) accelerates slowly.

$$\ddot{z}_1 = \frac{F_A}{m_1} + \frac{m_2 g z}{m_1 l} \qquad \text{Eq. 15}$$

$$\ddot{z}_2 = -\frac{b\dot{z}}{m_2 l^2} - \frac{gz}{l} \qquad \text{Eq. 16}$$

A pendulum under the given assumptions can be approximated by a simple fourth order adaptive observer and may be represented as a mass-spring-damper system evolving along a line.

11.4 Experimental Setup

11.4.1 Configuration

The pendulum experimental configuration is shown in figure 11.4. Experiments are performed using a five degree of freedom manipulator operating in a one dimensional space. The receptacle is attached to an adjustable receptacle mount which is attached to the world frame.

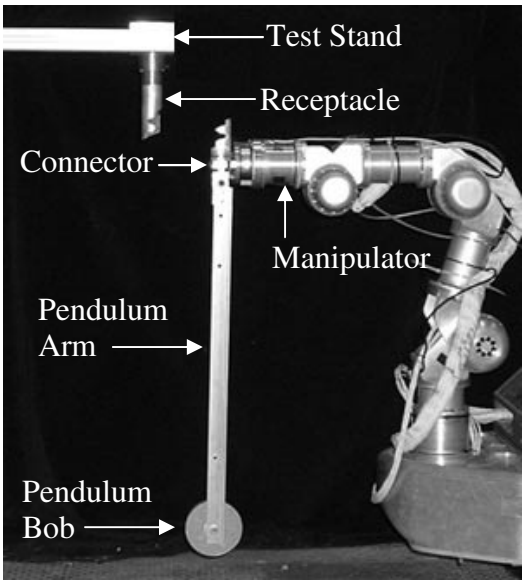

Figure 11.4 – Pendulum experimental configuration.

11.4.2 Bias Source

The bias source for these experiments is a 0.95 kilogram bob attached to a rigid 0.57 m pendulum arm. The pendulum is attached to the connector at one end and allowed to swing freely. The amplitude of the oscillation is modified with every

test. The mass of the connector and associated hardware is approximately 0.5 kilograms.

11.4.3 Identification

Identification of the spatial-temporal domain pendulum requires the characterization of model parameters and the identification of the pendulum state. A simple fourth order adaptive observer [13] is implemented for this purpose. The adaptive observer is represented in a canonical form that simplifies the implementation of the observer. Equations 17 to 23 describe the adaptive observer.

$$\begin{bmatrix} \dot{\hat{y}} \\ \dot{\hat{x}} \end{bmatrix} = \begin{bmatrix} \hat{a}^T \\ r \quad F^T \end{bmatrix} \cdot \begin{bmatrix} \hat{y} \\ \hat{x} \end{bmatrix} + \begin{bmatrix} 1 \\ 0 \end{bmatrix} \left(\hat{b}^T \cdot \hat{\omega} - \lambda \cdot er \right) \quad \text{Eq. 17}$$

$$\hat{a}_1 = -\gamma_1 \cdot y \cdot er \quad \text{Eq. 18}$$

$$\hat{a}_i = -\gamma_i \cdot x_i \cdot er \quad \text{Eq. 19}$$

$$\hat{b}_1 = -\delta_1 \cdot u \cdot er \quad \text{Eq. 20}$$

$$\hat{b}_i = -\delta_i \cdot \hat{\omega}_i \cdot er \quad \text{Eq. 21}$$

$$\dot{\hat{\bar{\omega}}} = F^T \cdot \hat{\bar{\omega}} + r \cdot u \quad \text{Eq. 22}$$

$$\hat{\omega} = \left(u, \hat{\bar{\omega}}^T \right)^T \quad \text{Eq. 23}$$

Where in an N^{th} order system:

the hat symbol indicates an estimate,

u is the scalar input corresponding to applied force,

y is the scalar output corresponding to connector position,

x is the internal state of the observer and is and (N-1) vector,

a and b are parameter vectors that are each (N) vectors,

γ, λ and δ are adaptive gains,

r is an (N-1) vector,

F is an (N-1)x(N-1) stable matrix and the pair (r^T, F) is observable.

This observer is globally asymptotically stable, guaranteeing that the system converges as time approaches infinity. A sinusoidal input is added to the transport vector to realize parameter convergence during transport.

11.4.4 Issues

As is discussed in experiment 1, the sensor used in this setup is constrained by a relatively slow control bandwidth of 50 Hz and an analog output sensor that is particularly susceptible to external sources of noise.

11.5 Results

11.5.1 Simulation

A simulation of the pendulum is created to show that a single-input single-output fourth order adaptive observer is capable of emulating pendulum motion at small angles. Equations 7 and 13 are used to calculate the forces applied to the connector and bob respectively.

The values are set such that they emulate the real system as well as possible. The masses m_1 and m_2 are set to 0.5 kg and 0.95 kg respectively, l is 0.57 m, and b is set to 0.01 such that it is essentially negligible.

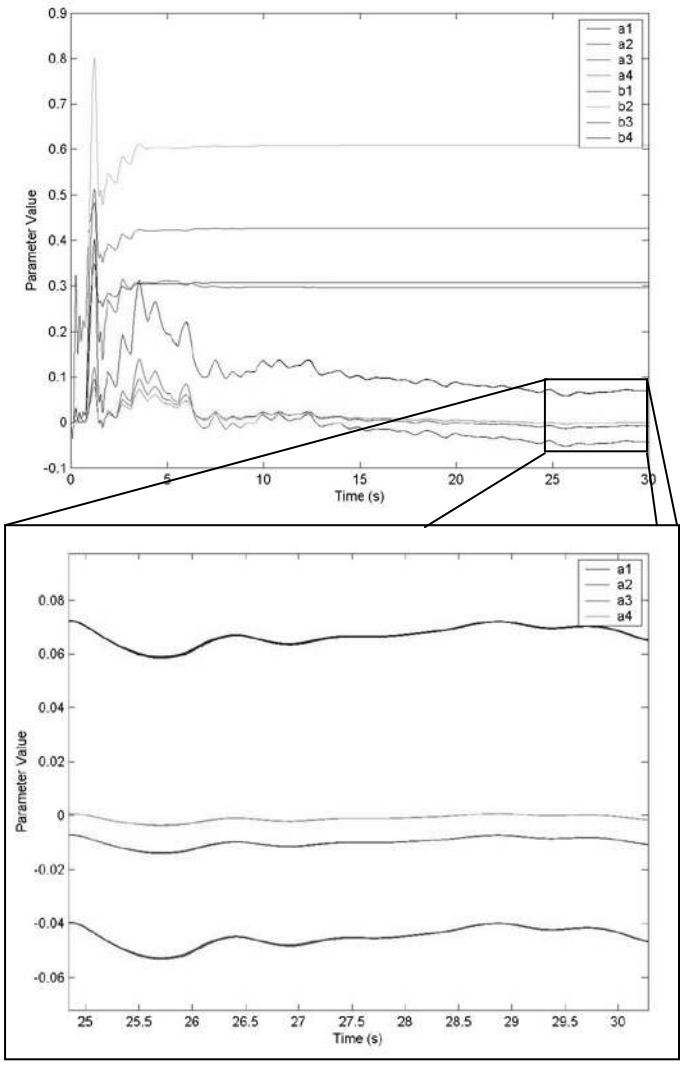

Figure 11.5 – Simulated parameter estimates.

Figure 11.5 illustrates the parameter estimates of the system as a function of time. The position estimation error is shown in figure 11.6. The parameter values are nearly constant at 30 seconds, with small adjustments still being made for the low frequency components of the signal. After eight seconds the position estimation error remains below ± 0.0003 m. These graphs show that the fourth order adaptive observer is capable of emulating pendulum motion for small angles.

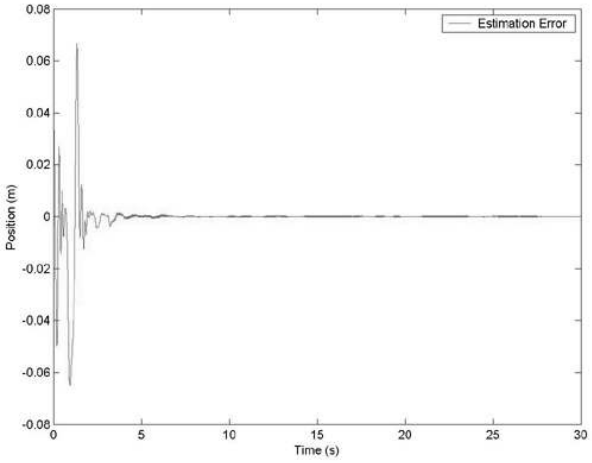

Figure 11.6 – Simulated position estimation error.

11.5.2 Experiment Failure

The same adaptive observer is implemented on the real manipulator and pendulum. Although the parameters converge to approximately constant values in a time frame comparable to that of the simulation, they proceed to oscillate in the vicinity of their respective values (Figure 11.8). Figure 11.7 illustrates the actual output, estimated output and error of a pendulum experiment after convergence of the observer. Failure of the system to settle and accurately emulate the position is attributed to two aspects of the experimental setup: sensor noise and sensor bandwidth.

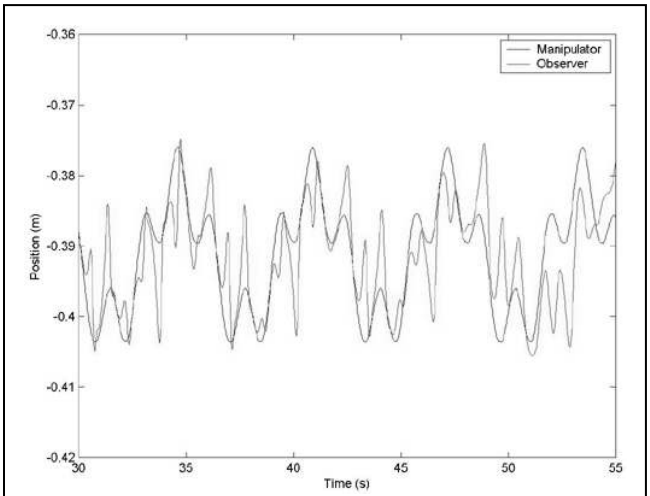

Figure 11.7 – Actual system position and adaptive observer's estimate of position.

Excessive sensor noise obscures

the force input. The adaptive observer can not distinguish between signal and noise thus it attempts to determine parameter and state values that account for every spike and trough in a data stream. The magnitude of the sensor noise is sufficient to prevent emulation of fine motions like those in the experiment.

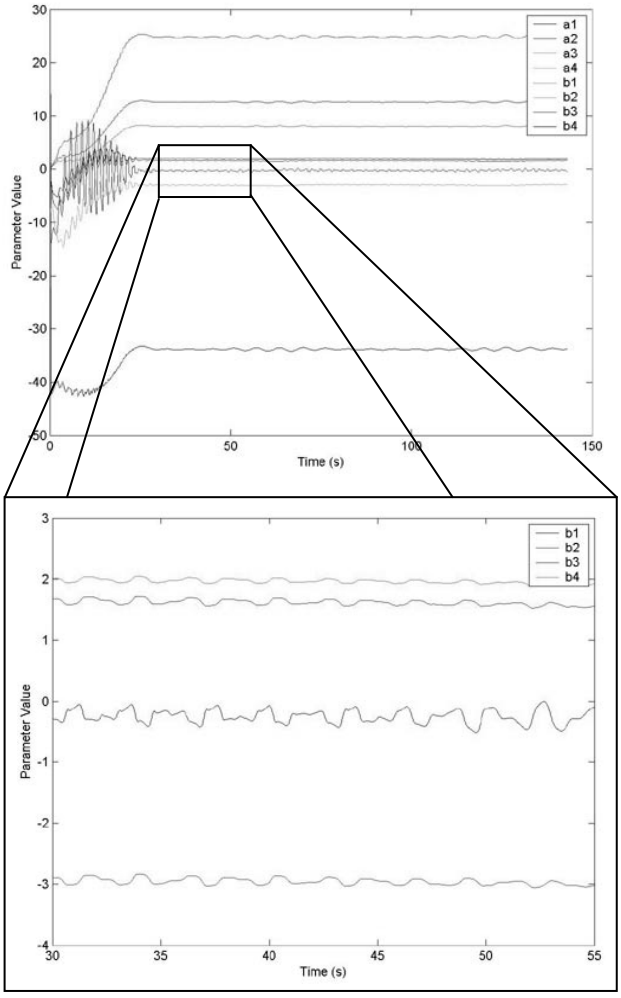

Figure 11.8 – Parameter estimates of the real system oscillate in the vicinity of their true values .

The relatively low sensing bandwidth, which limits the observer update frequency, prevents the accurate emulation of some signals. The theoretical minimum sampling frequency must be twice that of the highest frequency component of the sensed signal. (Nyquist) Sampling frequencies on the order of ten times the highest frequency component are generally accepted as sufficient. Thus, an integrator with a 50 Hz bandwidth should be able to emulate signals on the order of 5 Hz. In general, adaptive observers require the ability to emulate signals approximately ten times faster than the highest frequency component of an input in order to efficiently converge. Thus given a 50 Hz sensing and control bandwidth, a 5 Hz signal may be accurately emulated and a 0.5 Hz signal may be accurately learned.

The highest frequency components of the signals considered in this experiment are on the order of 0.7 Hz, exceeding (although barely) the 0.5 Hz goal. It is believed that the 50 Hz bandwidth of the system in conjunction with sensor noise account for the adaptive observer's failure to converge.

11.5.3 Obstacles to Realization

The failure of the adaptive observer to converge is a result of the experimental equipment available. A sensor with less noise and a faster update frequency would likely enable the timely convergence of the adaptive observer. However, this would not have resulted in the successful completion of this experiment.

Two significant obstacles must be overcome if the adaptive observer approach to bias compensation is to be realized. The determination of forces from a state model is a significant challenge that does not yet have a sufficient solution. Also, the rate of parameter convergence must increase for this approach to become useful.

Adaptive observers simultaneously identify the parameters and the state of dynamic systems. The observer takes the forces applied by the manipulator as input and adapts based on the output motion of the connector. When the system parameters are stable and no longer change, adaptation ends and the position and velocity response of the system may be emulated by providing the input force. This research seeks the opposite capability, to emulate the forces that generate the known motion of the system.

One approach to achieving this capability is to assume that the mass of the manipulated component is much less than that of the adjacent mass in the chain. For example, in the case of the pendulum, the mass of the connector must be much less than the mass of the bob. If this assumption holds then the forces applied to the manipulator (and conversely by the manipulator) may be approximated as a function of the state of the adjacent mass. For example, if the

adjacent mass is connected to the manipulated mass by a spring and damper, knowing the position and velocity with respect to the manipulated mass enables estimation of the bias wrench.

This assumption imposes a significant constraint on biased components and in most situations will not be the case. It also conflicts with the requirement for linear representation presented in the Model section of this chapter which states that m_1 should be greater than or approximately equal to m_2. Thus this approach is extremely limited in its applicability and an alternative must be found if the adaptive observer approach to bias compensation is to become a reality.

Another complication associated with this approach is the determination of the state of the adjacent mass. Adaptive observers learn the parameters and state of a system in a representation other than that of the real system. These representations share the same input and output as the real system but the internal states are different. Thus, transforming the internal states of the observer to the real system's representation is necessary. Determining this transformation requires the solution of a set of simultaneous equations. There exist circumstances in which the number of unknowns exceeds the number of equations, preventing the determination of the transformation and, subsequently, the state of the adjacent mass in the real representation.

For the bias compensation approach to be practically useful the time necessary to achieve parameter convergence must be small enough that other approaches are less desirable. Approaches like the active damping of vibration or slow manipulation to avoid excitation are viable alternatives if the bias compensation approach is too time consuming.

Examining the results of the simulation presented illustrates that the simplest system, a single input single output fourth order system with no measurement noise, exhibits convergence times on the order of 30 seconds. Such

convergence rates already approach the limits of usefulness for real world application. But in real applications convergence rates are significantly longer due to sensor noise, multiple inputs/outputs and systems with more than two masses.

The combination of incomplete state vectors, unrealistically restrictive assumptions and excessively long parameter modeling durations indicates that the adaptive observer approach is not the best solution for emulating spatial-temporal biases. Alternative approaches should be pursued.

11.6 Traditional Approach

The traditional approach tests performed for experiment 3 are considered directly applicable to this experiment and are not repeated.

Chapter 12

Contributions and Conclusions

The research presented in this dissertation makes four major contributions to the discipline of autonomous robotic assembly.

1. This research contributes a method for force guided assembly under bias that enables assemblies that would otherwise be impossible.
2. This research formulates the bias number, B, which enables quantitative characterization of the extent to which a system is biased.
3. This research shows that simple bias models are useful for emulating complex systems for assembly under bias.
4. This research presents a methodology that can realize meaningful reductions in the forces required for assembly under bias when compared to forces incurred during uncompensated assembly.

This research also leads to two significant conclusions regarding autonomous robotic assembly under bias.

1. Multiple obstacles must be overcome in order to realize adaptive observation for the emulation of spatial-temporal domain biases.
2. The performance of force guided assembly under bias is dependent on connector dimensions.

12.1 Contributions

This research contributes a method for force guided assembly under bias that enables assemblies that would otherwise be impossible.

Force guided assembly utilizes contact wrenches to determine contact state and to issue control commands. When a component experiences bias the manipulator senses the sum of the forces from bias and contact. For example, the forces sensed when pumping gas not only stem from the insertion of the nozzle into the car but also the stretching and flexure of the hose. The inability to distinguish the forces from contact prevents accurate determination of contact state. Traditional approaches to force guided assembly can not gently connect components in the presence of bias.

Bias compensated force guided assembly models the contribution of biases prior to contact. In the example, a model is generated that accurately predicts the forces from the stretching of the hose. During contact bias wrenches are emulated and subtracted from the sensed wrench providing an estimate of contact wrenches. This estimate is then used to determine contact state and issue control commands.

This research creates the bias number, B, which enables quantitative characterization of the extent to which a system is biased.

Not all systems are biased to the same degree. Consider, for example, plugging a heavy power cable and a light cord into respective receptacles. One cable is massive, stiff, and stretched taught when near the receptacle, the other is lightweight, flexible and slack. The biases (and the mating forces) generated by these sources are very different. In the case of the lightweight cable, the biases may be low enough that compensation isn't necessary but the biases from the stiffer, heavier cable almost certainly call for compensation.

The need for bias compensation is determined by evaluating the bias number. This quantitative measure of biased systems is based on the magnitude of bias change and the physical constraints of the connector. Values greater than or equal to unity indicate that bias compensation is necessary. Rearranged, the bias number yields the minimum necessary force, the lowest force that may be applied to reliably distinguish contact from bias.

This research shows that simple bias models are useful for emulating complex systems for assembly under bias.

Gentle assembly of biased systems does not require models that perfectly emulate bias. The equation for bias number shows that larger emulation errors may be compensated for by larger assembly forces. Thus, the more gentle the desired assembly, the more accurate the models must be.

Establishing the force and torque requirements of an assembly enables the determination of acceptable force and torque error. This provides a clear limit to how well a model must emulate a real system.

Consider the cable model presented in experiment 1. A two tier approach is adopted in which gross force estimates are fine tuned by locally accurate linear

models of error. In cases where slightly larger contact forces are acceptable, the gross estimate tier may be sufficient to perform force guided assembly.

This research presents a methodology that can realize meaningful reductions in the forces required for assembly under bias when compared to forces incurred during uncompensated assembly.

The effects of bias may be overcome by exerting enough force to disambiguate the effects of bias from contact forces. Consider for example plugging an extension cord into a socket, the plug experiences biases (though possibly small) from the cord. If forcefully pushing the plug into the socket creates forces that are ten times larger than the largest biases expected from the cord, then the mating forces are likely from contact.

This same concept is applied to the biased systems examined in this work. The amount of force needed to perform assembly without bias compensation is determined and compared to the force needed with compensation. This work shows that reductions in force in excess of 90% are easily obtained.

12.2 Conclusions

Multiple obstacles must be overcome in order to realize adaptive observation for the emulation of spatial-temporal domain biases.

Connecting a vibrating beam to a structure using force guided assembly requires the emulation of bias forces. In cases where manipulator motion has an appreciable effect on the motion of the beam the parameters and state must be learned. This research has shown that there are obstacles to implementing adaptive observation for the emulation of spatial-temporal domain biases. Incomplete state vectors, unrealistically restrictive assumptions and excessively long parameter modeling durations all contribute to this conclusion.

1. Incomplete State Vectors

Physical systems are most naturally represented such that the positions and velocities of the masses of that system constitute its states. Adaptive observers learn the parameters and states of a system in a less convenient representation which is governed by the form of the adaptive observer. These representations share the same input and output but the internal states are different. The approach presented in this research advocates the transformation of the internal states of the adaptive observer to the representation where positions and velocities constitute the individual states. This transformation is performed with the goal of emulating forces based on the positions and velocities of the internal components. Determining this transformation is not always possible and, consequently, either is the emulation of bias using this approach.

2. Unrealistically Restrictive Assumptions

When emulating the forces from bias, the force applied to the connector can be estimated by the state of the adjacent mass if the mass of the connector is small relative to that of the adjacent mass. This assumption places significant constraints on the hardware that this approach may be used on and in some cases directly conflicts with assumptions regarding linearity. In many cases this assumption is not true and this approach is not applicable.

3. Parameter Modeling Durations

Simulations illustrate that simple systems, for example a single input single output fourth order system with no measurement noise, exhibit convergence times in excess of 30 seconds. Such convergence rates approach the limits of usefulness for real world application. Actual implementation convergence rates

are significantly longer due to sensor noise, multiple inputs/outputs and more complex systems.

The performance of force guided assembly under bias is dependant on connector dimensions.

The forces and torques applied at contact during assembly are dependant on the magnitude of the modeling error and the dimensions of the connector. As the distances between connector contact points become smaller, the force needed to impart the same contact torque increases. Thus, larger connectors with wider contact point spacing yield gentler assembly than a smaller connector used for the same task.

Scientific and Technical References

[1] Anderson, B.D.O. “Multivariable adaptive identification.” Technical Report EE7402, University of Newcastle, Australia, 1974.

[2] Arimoto, S., Liu, Y.H., Naniwa, T. *Model-Based Adaptive Control for Geometrically Constrained Robots*. IEEE Int. Conf. On Robotics and Automation. 1993.

[3] Åström, K. and Wittenmark, B. *Adaptive Control.* Addison Wesley, Reading, MA. 1989.

[4] Austin, D. and McCarragher, B. *Experiments in Force Controlled Assembly using a Discrete Event Framework*. IEEE Int. Conf. On Int. Robots and Systems. 1997.

[5] Buckham, B. and Nahon, M. *Dynamics Simulation of Low Tension Tethers.* Oceans ’99 MTS/IEEE. Volume 2, 1999.

[6] Elmer, FJ. *Equations of Motion of Damped and Driven Pendula*. http://monet.physik.unibas.ch/~elmer/pendulum/eqm2.htm#(periodic%20force). 1998.

[7] Inoue, A., Iwai, A., Ishitobi, M. and Tokumaru, H. *Adaptive Observer with Exponential Rate of Convergence for Multi-Input Multi-Output Systems.* Int. Federation of Automatic Control, 9th Triennial World Congress, 1984.

[8] Jenkins, C.H.M. “Gossamer Spacecraft: membrane and Inflatable Structures Technology for Space Applications.” AIAA Reston, Va. 2001.

[9] Kang, S., Kim, M., Lee, C.W., and Lee, K-I. *Adaptive Accommodation control for Complex Assembly: Theory and Experiment*. IEEE Int. Conf. On Robotics and Automation. 1999.

[10] Kazanzides, P., Zuhars, J., Mittelstadt, B., and Taylor, R.H. *Force Sensing and Control for a Surgical Robot.* IEEE Int. Conf. On Robotics and Automation. 1992.

[11] Kresselmier, G. *Adaptive Observer with Exponential Rate of Convergence.* IEEE Trans. On Automatic Control. Vol. AC-22, No.1, Feb. 1977.

[12] Lardner, T. and Archer, R. *Mechanics of Solids: An Introduction.* McGraw-Hill, New York, NY 1994.

[13] Luders, G., and Narendra, K. *An Adaptive Observer and Identifier for a Linear System.* IEEE Trans. On Automatic Control, October 1973.

[14] Luders, G., and Narendra, K. *A New Canonical Form for an Adaptive Observer.* IEEE Trans. On Automatic Control, April 1974.

[15] Luenberger, D.G. *Introduction to Dynamic Systems Theory, Models, and Applications*. John Wiley & Sons. New York. 1979.

[16] Marquart, D. *Journal of the Society for Industrial and Applied Mathematics.* Vol. 11. 1963.

[17] McCarragher, B.J. and Austin, D.J. *Model Adaptive Hybrid Dynamic Control for Constrained Motion Systems.* IEEE Trans. On Automatic Control. Vol.43, No.4, 1998

[18] Meitinger, T., Pfeiffer, F. *Automated Assembly with Compliant Mating Parts.* IEEE Int. Conf. On Robotics and Automation. Vol. 2, 1994.

[19] Mitchell, T. *Machine Learning.* McGraw-Hill. New York, NY 1997.

[20] Morrow, J.D.; Nelson, B.J.; Khosla, P.K. *Vision and Force Driven Sensorimotor Primitives for Robotic Assembly Skills.* IEEE Int. Conf. On Int. Robots and Systems. 1995.

[21] Narendra, K.S. and Annaswamy A.M. *Stable Adaptive Systems*. Prentice Hall, Englewood cliffs, NJ. 1989.

[22] Newman, W.S.; Branicky, M.S.; Podgurski, H.A.; Chhatpar, S.; Ling Huang, Swaminathan, J.; Hao Zhang. *Force-responsive robotic assembly of transmission components*. IEEE Int. Conf. on Robotics and Automation. Vol. 3, 1999.

[23] Newman, W.S.; Zhao, Y.; Pao, Y.-H. *Interpretation of force and moment signals for compliant peg-in-hole assembly.* IEEE Int. Conf. on Robotics and Automation. Vol. 1, 2001.

[24] Rao, S. *Mechanical Vibrations.* Addison-Wesley, New York, NY 1995.

[25] Riley, W. and Sturges, L. *Engineering Mechanics Dynamics.* John Wiley and Sons, New York, NY 1993.

[26] Schimmels, J.M., and Peshkin, M.A. *Admittance Matrix Design for Force-Guided Assembly.* IEEE Int. Conf. Of Robotics and Automation. Vol.8 No.2. 1992.

[27] Slotine, J-J. and Li, W. Applied Nonlinear Control. Prentice Hall, Englewood cliffs, NJ. 1991.

[28] Staritz, P., Skaff, S., Urmson, C., Whittaker, W. “Skyworker: A Robot for Assembly, Inspection, and Maintenance of Large Scale Orbital Facilities.” ICRA, 2001.

[29] Whittaker, W., Staritz, P., Ambrose, R., Kennedy, B., Fredrickson, S., Parrish, J. and Urmson, C. “Robotic Assembly of Space Solar Power Facilities.” J. Aerospace Engrg. ASCE, April, 2001.

[30] Whittaker, W., Urmson, C., Staritz, P., Kennedy, B. and Ambrose. R. “Robotics for Assembly, Inspection, and Maintenance of Space Macrofacilities.” AIAA Space 2000 Conference and Exposition, AIAA-2000-5288, September, 2000.

[31] Whittaker, W., Urmson,C. and Staritz,P. "Assembly, Inspection and Maintenance (AIM) of Space Facilities." Presentation at Space Solar Power Technical Interchange Meeting. April 6, 2000.

[32] Whitcomb, L.; Arimoto, S.; Naniwa, T.; Ozaki, F. *Adaptive model-based hybrid control of geometrically constrained robot arms.* IEEE Trans. on Robotics and Automation. Vol.13 1997.

[33] Whitcomb, L.; Arimoto, S.; Naniwa, T.; Ozaki, F. *Experiments in adaptive model-based force control.* Proc. IEEE Int. Conf. On Robotics and Automation. Vol.2 1995.

[34] Will, P.M. and Grossman, D.D. *An Experimental System for Computer Controller Mechanical Assembly.* IEEE Transactions on Computers. Vol. C-24. No. 9 1975.

[35] Yukawa, T., Uchiyama, M., Inoka, H. *Handling of a Constrained Flexible Object by a Robot.* IEEE Int. Conf. On Robotics and Automation. 1995.

[36] Zheng, Y., Pei, R., Chen, C. *Strategies for Automatic Assembly of Deformable Objects.* Proc. IEEE Int. Conf. On Robotics and Automation. 1991.

Appendix 1

Derivation of Overlap Force

This appendix shows the derivation of the force needed to cause overlap of the error bounds of two adjacent contact points. Figure A1.1 shows the error bounds for two contacts that are distances d_1 and d_2 from the force/torque sensor.

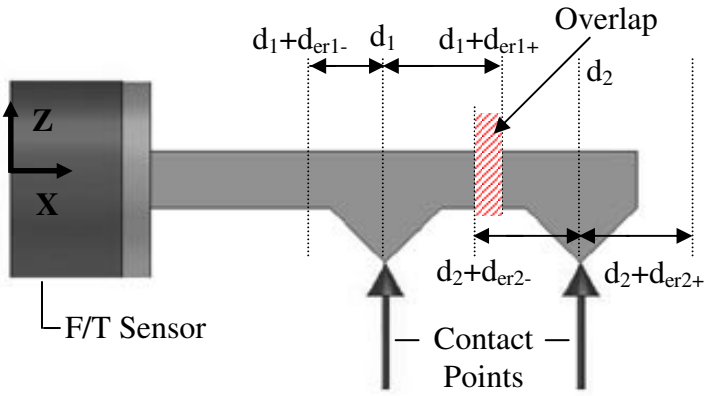

Figure A1.1 – The error bounds for two contact points d_1 and d_2.

Given that the positions of the error bounds are:

$$d_{eb1} = d_1 + d_{er+}$$
$$d_{eb2} = d_2 + d_{er2-}$$

The position at which d_{eb1} and d_{eb2} are equal is the point of overlap. Thus:

$$d_1 + d_{er1+} = d_2 + d_{er2-} \qquad \text{Eq. A.1}$$

Rearranging equation A.1 yields:

$$d_2 - d_1 = d_{er1+} - d_{er2-} \qquad \text{Eq. A.2}$$

Substituting the equations for d_{er1+} and d_{er2-} from equations 4 and 5 of Chapter 5:

$$d_2 - d_1 = \frac{\tau_{er} - F_{er} \cdot d_1}{F + F_{er}} + \frac{\tau_{er} - F_{er} \cdot d_2}{F - F_{er}} \qquad \text{Eq. A.3}$$

$$d_2 - d_1 = \frac{(\tau_{er} - F_{er} \cdot d_1)(F - F_{er})}{(F + F_{er})(F - F_{er})} + \frac{(\tau_{er} - F_{er} \cdot d_2)(F + F_{er})}{(F + F_{er})(F - F_{er})} \qquad \text{Eq. A4}$$

$$d_2 - d_1 = \frac{\left(\tau_{er} \cdot F - \tau_{er} \cdot F_{er} - F_{er} \cdot d_1 \cdot F + {F_{er}}^2 \cdot d_1\right) + \left(\tau_{er} \cdot F + \tau_{er} \cdot F_{er} - F_{er} \cdot d_2 \cdot F - {F_{er}}^2 \cdot d_2\right)}{(F + F_{er})(F - F_{er})} \qquad \text{Eq. A5}$$

$$d_2 - d_1 = \frac{\left(2 \cdot \tau_{er} \cdot F - F_{er} \cdot F \cdot (d_1 + d_2) + {F_{er}}^2 \cdot (d_1 - d_2)\right)}{\left(F^2 - {F_{er}}^2\right)} \qquad \text{Eq. A6}$$

$$(d_2 - d_1)\left(F^2 - {F_{er}}^2\right) = \left(2 \cdot \tau_{er} \cdot F - F_{er} \cdot F \cdot (d_1 + d_2) + {F_{er}}^2 \cdot (d_1 - d_2)\right) \qquad \text{Eq. A7}$$

$$\left(d_2 \cdot F^2 - d_2 \cdot {F_{er}}^2 - d_1 \cdot F^2 + d_1 \cdot {F_{er}}^2\right) = \left(2 \cdot \tau_{er} \cdot F - F_{er} \cdot F \cdot (d_1 + d_2) + {F_{er}}^2 \cdot (d_1 - d_2)\right) \qquad \text{Eq. A8}$$

$$(d_2 - d_1) \cdot F^2 = \left(2 \cdot \tau_{er} \cdot F - F_{er} \cdot F \cdot (d_1 + d_2)\right) \qquad \text{Eq. A9}$$

$$(d_2 - d_1) \cdot F = \left(2 \cdot \tau_{er} - F_{er} \cdot (d_1 + d_2)\right) \qquad \text{Eq. A10}$$

$$F = \frac{\left(\tau_{er} - F_{er} \cdot \frac{(d_1 + d_2)}{2}\right)}{\frac{(d_2 - d_1)}{2}} \qquad \text{Eq. A11}$$

Where :

$\frac{(d_1 + d_2)}{2}$ is the midpoint between the two force application points, the sensor to center distance (d_{sc}), and

$\frac{(d_2 - d_1)}{2}$ is the distance from the contact to the midpoint, the center distance (d_{cd}).

Thus the equation to determine the force at which the error bounds from two adjacent points overlap is:

$$F = \frac{\tau_{er} - F_{er} \cdot d_{sc}}{d_{cd}} \qquad \text{Eq. A12}$$

Appendix 2

Sample Cable Error Map

This appendix shows an error map for the cable bias source. A portion of this map is found in Chapter 7 – Experiment 1. Details regarding the model used to emulate the cable, experimental configuration and the bias source may be found in Chapter 7. The bias source for these maps is configured as illustrated in figure 7.3, with the 13 mm fiberoptic cable as the flexural element.

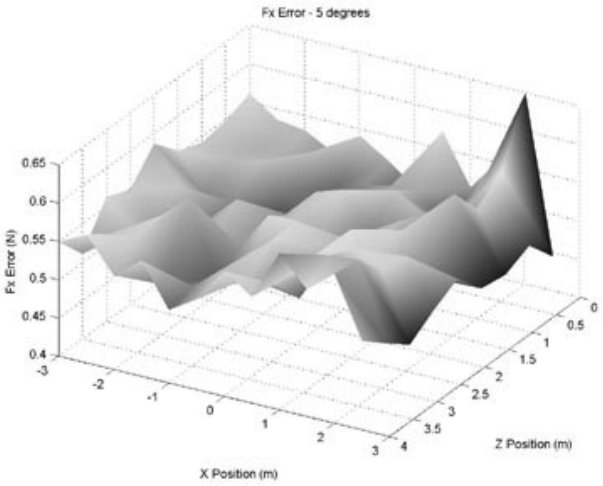

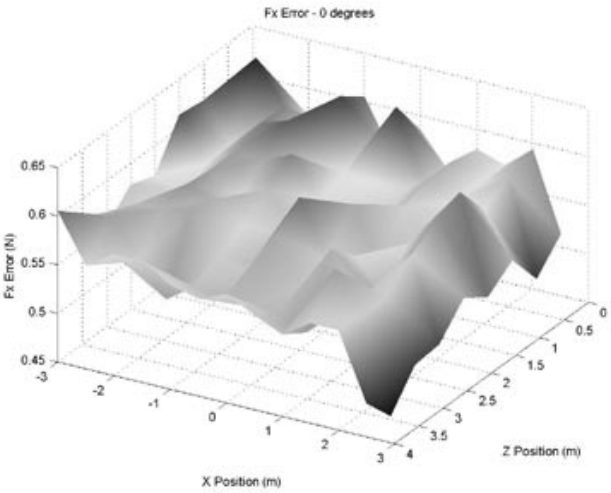

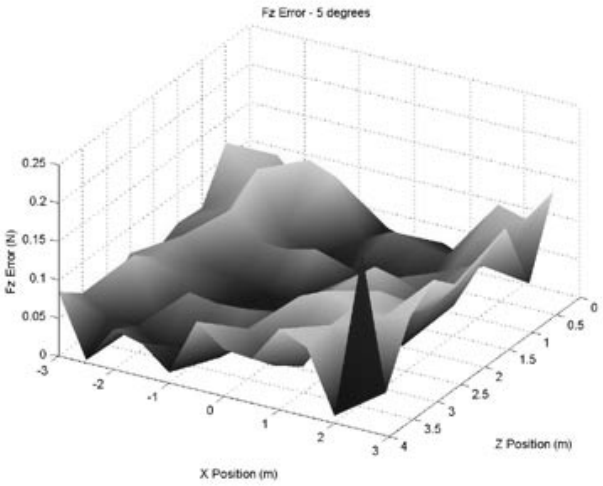

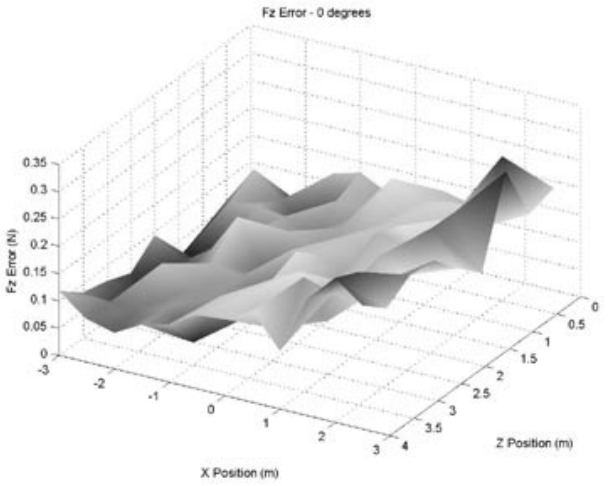

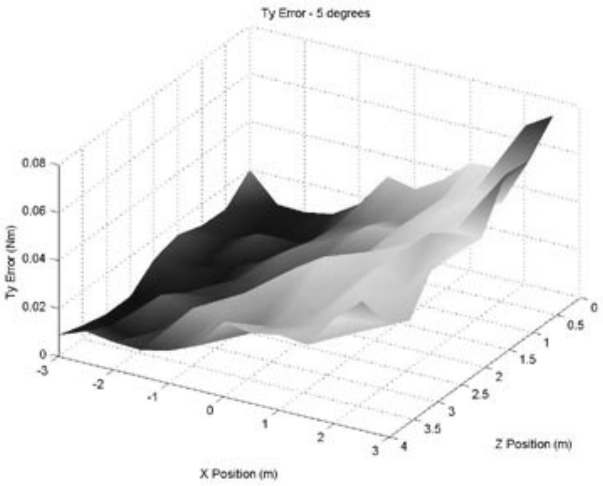

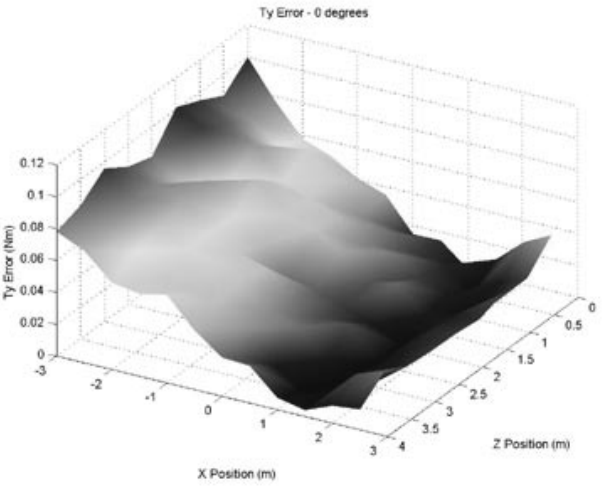

F_x, F_z and T_y at 5 degrees from the learning orientation.

F_x, F_z and T_y at 0 degrees from the learning orientation.

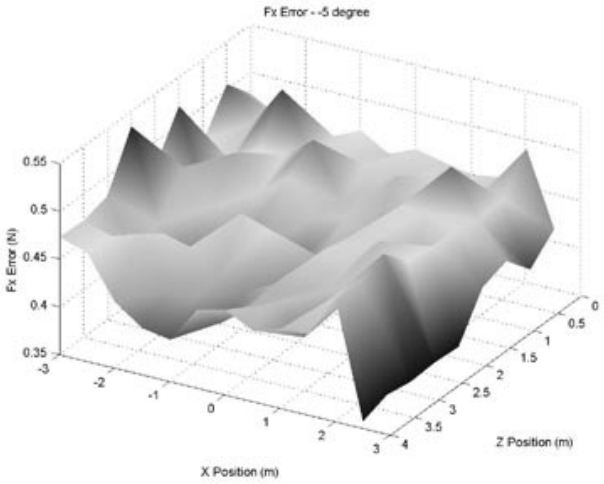

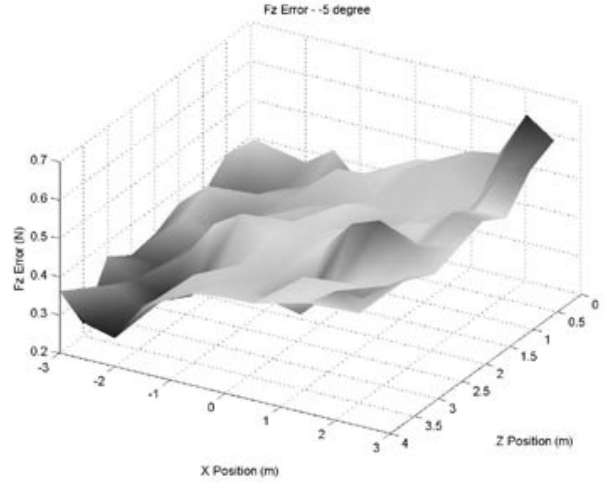

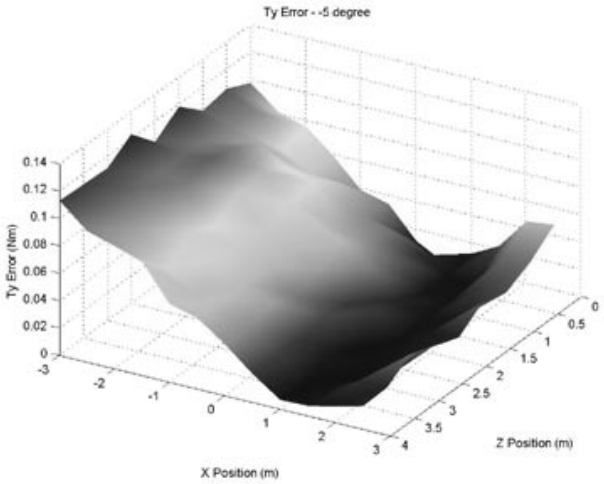

F_x, F_z and T_y at -5 degrees from the learning orientation.

Appendix 3

Bending Beam Error Map

This appendix shows an error map for the bending beam bias source using the linear model. A portion of this map is found in Chapter 8 – Experiment 2. Details regarding the model used to emulate the cable, experimental configuration and the bias source may be found in Chapter 8. The bias source for these maps is configured as illustrated in figure 8.1, with the distance between the contact point and the force application point equal to 1.52 meters and the initial deflection in the z axis equal to 0.25 meters.

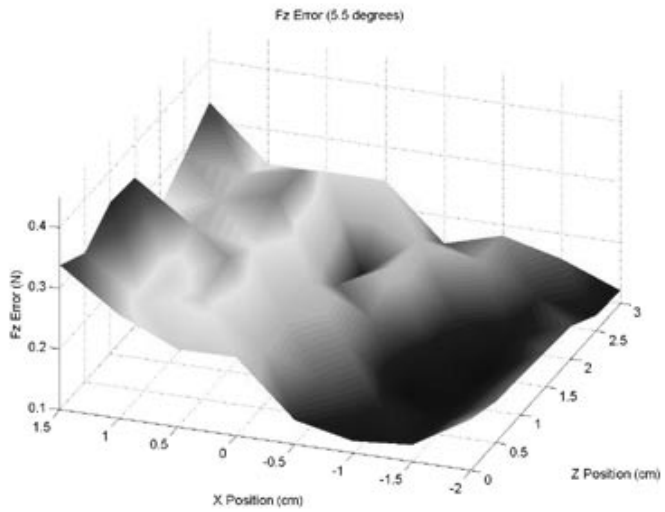

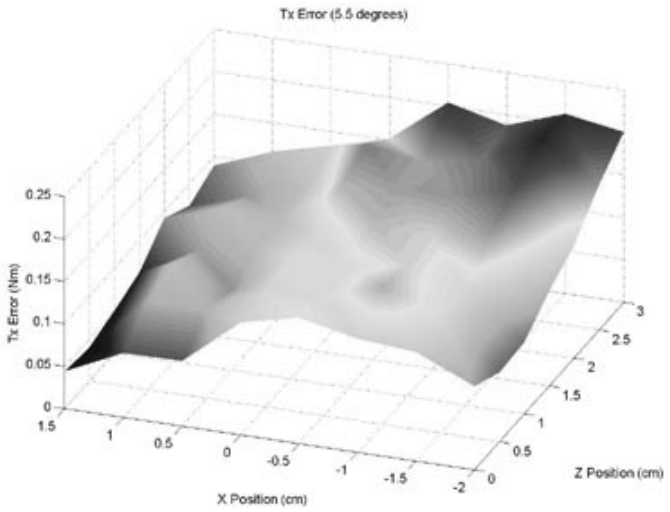

F_z and T_y at 5.5 degrees from the learning orientation.

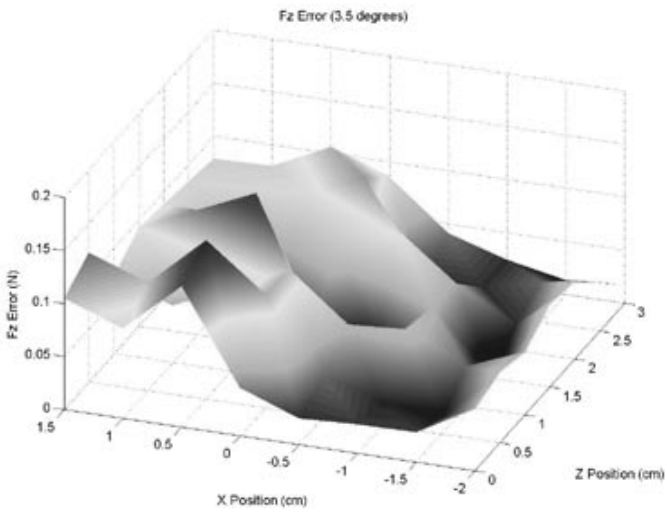

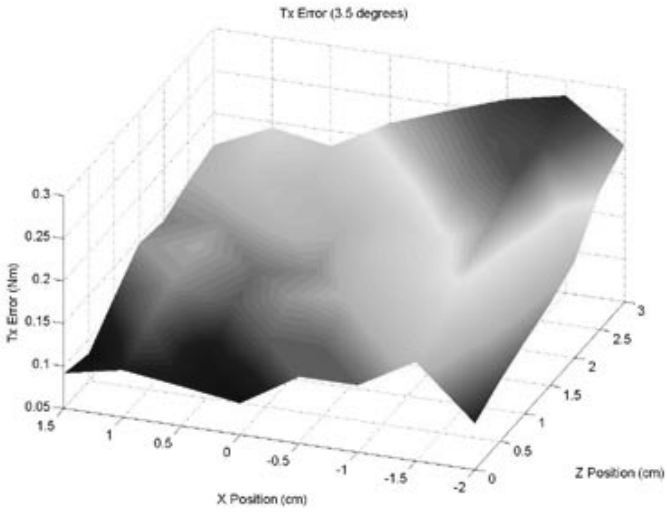

F_z and T_y at 3.5 degrees from the learning orientation.

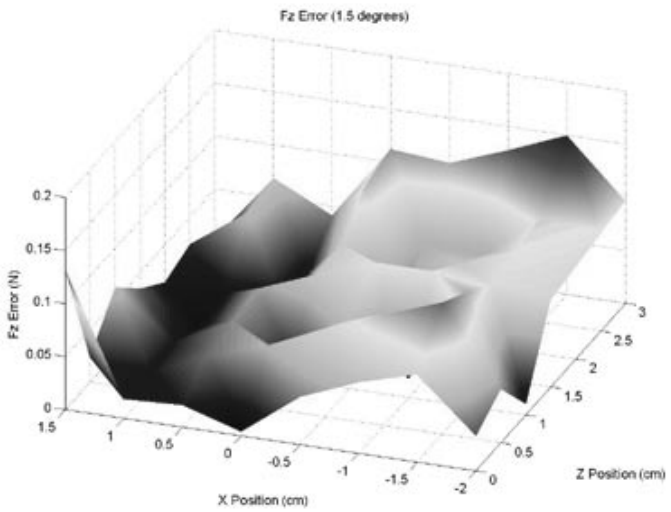

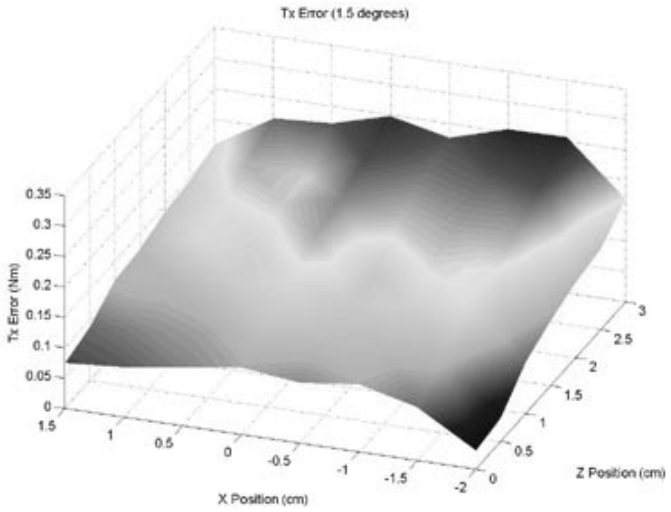

F_z and T_y at 1.5 degrees from the learning orientation.

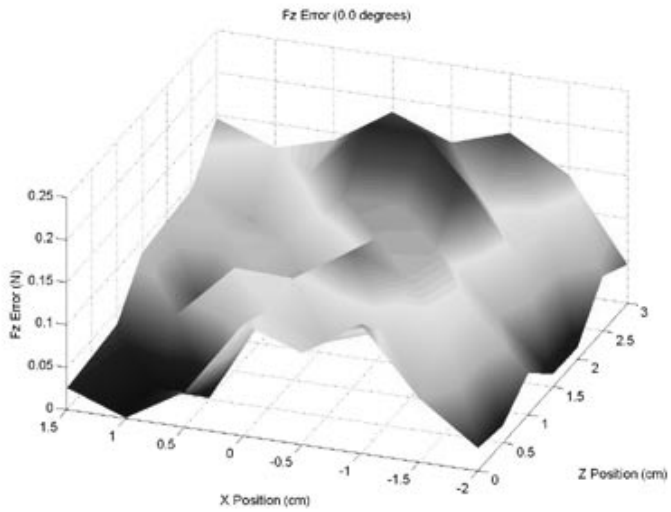

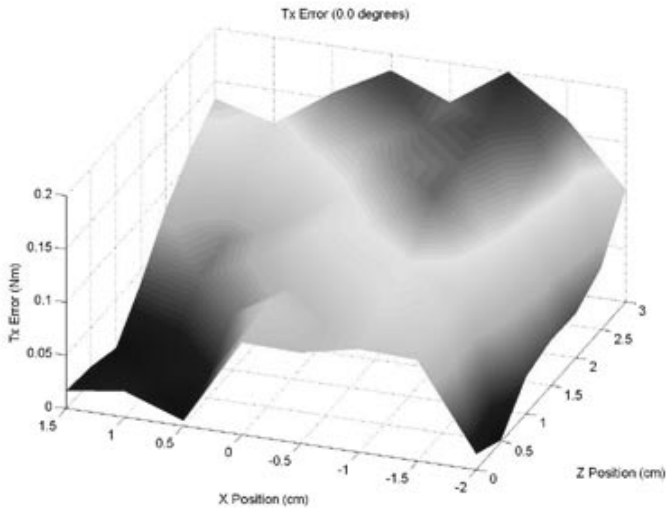

F_z and T_y at 0.0 degrees from the learning orientation.

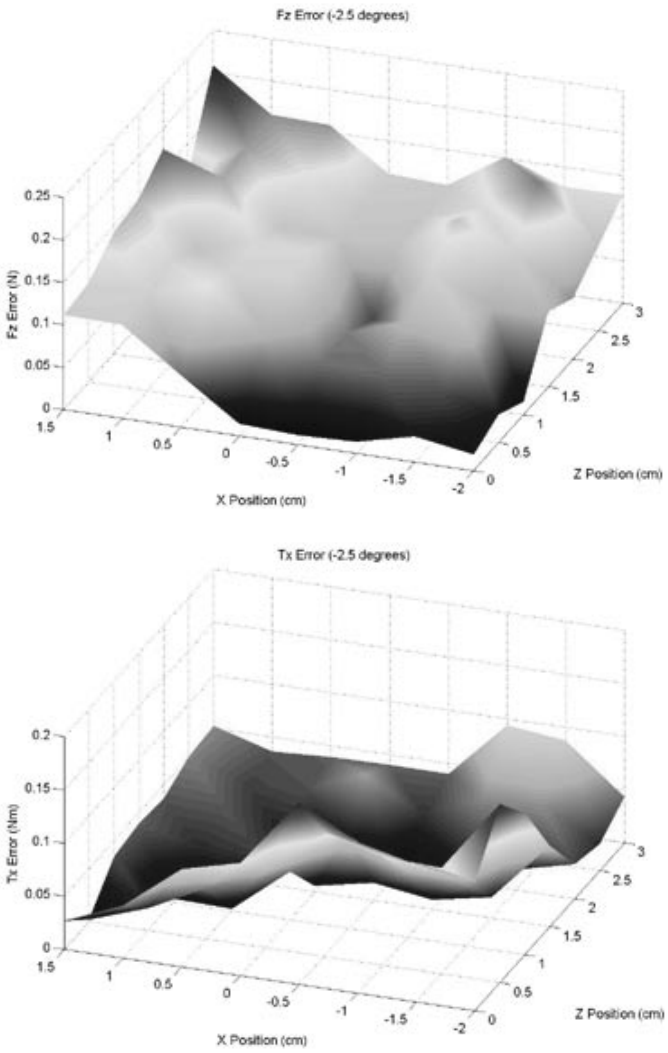

F_z and T_y at -2.5 degrees from the learning orientation.

Appendix 4

Lessons Learned and Future Work

Beyond the methods, experiments, results and conclusions, this research generated perspectives. The research revealed lessons that are not immediately obvious or intuitive. Several paths for future research have also become clear. The goal of this appendix is to guide future research and help avoid pitfalls that may otherwise consume time and energy.

Lessons learned

Lessons learned in adaptive observers, connector design and the limitations of force/torque sensors are discussed in this section.

Adaptive Observers

This research embarked to apply adaptive observers to various systems without appreciable success. Single-input single-output and multi-input multi-output systems of different orders were examined. Several lessons were derived from this experience:

Convergence Time

The viability and applicability of the approach advocated in this work decreases as the time required for parameter convergence increases. The speed at which adaptive observers converge is directly linked to the richness of the input signal. There are two aspects of an input signal that are of interest. One is how persistently exciting it is, this is discussed in one of the following sections. The other is the period of the lowest mode of a system. Convergence of an adaptive system that is characterizing an oscillation requires on the order of ten or more periods to attain convergence, thus if the lowest order period is N seconds, convergence can be expected to take at least 10•N seconds.

Effects of High Adaptive Gains

The adaptive gains in an adaptive observer are an example of variables that may be manipulated by the designer. The rate of adaptation of system parameters is determined by the adaptive gains. Increasing the adaptive gains beyond certain thresholds causes instability in the adaptive process and parameter estimates diverge. However, maintaining high gains that are below the point of instability does not ensure correct operation of an adaptive observer. When gains are set too high, adaptive observers can change the parameters to fit the local behavior of the signal being learned. Thus, it may appear as though an observer has converged but in reality it is constantly changing parameter estimates to fit the local behavior.

Testing for this condition is simple. By holding current parameter values constant and continuing to estimate output state, output estimates will quickly diverge.

Persistence of Excitation for Continuous Systems

The application of a persistently exciting signal to a discrete plant being modeled by an adaptive observer ensures fast convergence of parameters to their correct values. However, attempting to achieving persistence of excitation for continuous systems can result in protracted convergence times. Consider, for example, a

bending beam. This continuous system has an infinite number of modes. In a particular assembly operation, designers may only be interested in the first N modes of a system, thus an adaptive observer of a suitable order is chosen. The process of trying to persistently excite those N modes inevitably leads to the excitation of higher modes. The presence of higher modes in the signal may be considered noise and prevents the timely and accurate convergence of a model. Thus applying a persistently exciting signal to a continuous system with the goal of promoting accurate and fast convergence actually impedes convergence.

Noise sensitivity

The presence of noise in an input signal of an adaptive observer has a significant and detrimental effect on parameter and estimate convergence. The magnitude of this effect was greater than expected. In the cases examined, using an analog output force/torque sensor, the noise prevented accurate estimation of connector position in all cases.

Connector Design

Examination of the equation for minimum necessary force shows that the dimensions of a connector have an effect on the minimum force needed for unambiguous detection of contact location. These dimensions, including distance from sensor to the center of contact and the center distance, have opposing effects when increased. Increasing the distance to the sensor increases the minimum necessary force while increasing the center distance decreases it. Determining the relative effect of each of these distances is dependant on the particular force and torque errors anticipated. Thus, general rules for connector design are not established but the adoption of a particular set of connector dimensions should be conducted with anticipated errors in mind.

Limitations of Force / Torque Sensors

Force/torque sensors suffer from a number of limitations that must be overcome before they may be effectively applied for force guided assembly under bias. Sensitivity to

external strains is one such limitation. This sensitivity was clearly illustrated during the course of this research.

The manipulators used to perform the bending beam and independent pendulum assembly tasks have seven degrees of freedom. The final degree of freedom is a harmonic drive with the flexspline oriented in the distal direction. An aluminum plate is attached to the flexspline and a sensor is mounted to the plate. Nominal operation of harmonic drives involves flexure of the flexspline. This flexure induces stresses in the aluminum plate and consequently the sensor. The resultant effect of this flexure is the sensing of forces and torques that are not actually applied to the end effector.

Future Work

There are many paths future research in bias compensation may take. Three topics that emerged from this dissertation are the application of bias compensation to spatial/temporal domain bias sources, development of the bias number for the three dimensional case, and application to and understanding of this approach for the statically indeterminate case.

Application to Spatial/Temporal Domain Bias Sources

This work reveals some of the difficulties associated with identifying and emulating wrenches from bias sources that belong to the spatial/temporal domain. Future work should explore alternative approaches to bias emulation that bypass the theoretical and practical limitations encountered in this work.

Bias Number for the Three Dimensional Case

Although the planar derivation of the bias number may be applied to three dimensional connectors (as shown in section 5.5) this document does not explore the development and application of the bias number to the general three dimensional case. Future work should

include the derivation of the bias number for three dimensions and an effort to understand what distinguishes the three dimensional case from the planar case.

Statically Indeterminate Case

The limitations of the experimental setups used in this dissertation prevent the experimental application of this approach to cases in which bias sources are statically indeterminate. Future work should explore the requirements for applying the proposed approach to the statically indeterminate case and seek to better understand the application of the technology to realistic assembly scenarios.